



HAL
open science

Marine biogeochemical emissions and aerosol formation

Maija Peltola

► **To cite this version:**

Maija Peltola. Marine biogeochemical emissions and aerosol formation. Earth Sciences. Université Clermont Auvergne, 2021. English. NNT : 2021UCFAC100 . tel-03771545

HAL Id: tel-03771545

<https://theses.hal.science/tel-03771545>

Submitted on 7 Sep 2022

HAL is a multi-disciplinary open access archive for the deposit and dissemination of scientific research documents, whether they are published or not. The documents may come from teaching and research institutions in France or abroad, or from public or private research centers.

L'archive ouverte pluridisciplinaire **HAL**, est destinée au dépôt et à la diffusion de documents scientifiques de niveau recherche, publiés ou non, émanant des établissements d'enseignement et de recherche français ou étrangers, des laboratoires publics ou privés.



Laboratoire de météorologie physique
LaMP

UCA
UNIVERSITÉ
Clermont
Auvergne



PhD Thesis

Laboratoire de Météorologie Physique

University of Clermont Auvergne

Doctoral School of Fundamental Sciences

Speciality: Physics and chemistry of the atmosphere and climate

Defended on the 6th of December 2021, by:

Maija PELTOLA

Marine biogeochemical emissions and aerosol formation

Supervised by:

Karine SELLEGRI Research director, LaMP CNRS	Primary supervisor
Mike HARVEY Principal Scientist, NIWA	Co-supervisor
Cliff LAW Principal Scientist, NIWA	Co-supervisor
Clémence ROSE Researcher, LaMP CNRS	Co-supervisor

PhD committee:

Colin O'DOWD Professor, NUIG	Reviewer
Julia SCHMALE Assistant professor, EPFL ENAC IIE EERL	Reviewer
Eija ASMI Senior Research Scientist, FMI	Examiner
Andrea FLOSSMANN WOBROCK Professor, LaMP CNRS	President of jury

Acknowledgements

This PhD would not have been possible without the help of numerous people. First, I want to thank my primary supervisor Karine Sellegri, without whom I would not have started this thesis journey. I am grateful to you for this very unique opportunity and for your continuous support, enthusiasm and persistence over these PhD years. I am also very grateful for having had Clémence Rose as one of my co-supervisors. I really appreciate all the conversations we have had and all the advice and support from you. This thesis would not have been the same without the opportunity to do research in New Zealand and I want to thank Mike Harvey and Cliff Law for welcoming me at NIWA and acting as co-supervisors of my thesis. I really enjoyed working at NIWA and your expertise and practical help was invaluable.

I also want to thank my thesis committee. I was very honoured to have Colin O'Dowd and Julia Schmale review my thesis and Eija Asmi and Andrea Flossman-Wobrock in my jury. I would like to thank you all for taking the time for reading my work and the interesting discussions that we got to have in my defence.

One of the best parts of doing your PhD in two countries is getting to meet a lot of amazing people from different parts of the world. From France, I am grateful for the company of my fellow PhD students and other people in the building 8 student office and the other staff at LaMP for a lot of technical help (esp. David, Jean-Marc, Paolo, Laetitia and Mickael) as well as company during lunch and coffee breaks. I'm also glad for the international friends I made in France (Denise, Kruthika, French class folks).

From New Zealand, I would especially like to thank Neill Barr for your supportive attitude and all your work with the ASITs, they would not have been possible without you. I am also very grateful for the help of the NIWA site services, the Baring Head team, the marine biogeochemistry group and RV Tangaroa crew for making my work in New Zealand possible. My time in New Zealand would not have been the same without all the amazing people. I was very lucky to be surrounded by a strong student community of some brilliant ninewites and I am grateful for our countless lunch breaks and fun nights out as well as having you as my second family over the holidays. I was also fortunate to share this Sea2Cloud work experience with Jon and have him as my company on our numerous field trips to Baring Head. I'm thankful for your company, all our discussions and chances to vent. In addition, I'm very happy for getting to know Sinead as my favourite flatmate and beyond grateful for having Ben support me in both good and tough times over my last PhD year.

Apart from all the people I got to work with in NZ and France, I must thank the people at Aerodyne for always being ready to help with my instrument and software issues. I am also thankful to many people in Finland. Deciding to leave Finland and pursue my PhD abroad was not an easy decision, but the strong science background I got to develop in Helsinki before my PhD made me confident in surviving this experience. I am grateful for both that and for getting help in science questions during my PhD from knowledgeable Finns like Matti. I'm also grateful for my old friends in Finland for making my visits back home more fun. Furthermore, I want to thank Minna for our long friendship and for your support. Our weekend trips were some of the highlights of my time in France.

Finally, I would like to say a big kiitos to my parents Päivi and Raimo and my sister Liisa and brother Mikko with their families. I was very lucky to grow up surrounded by books in a family that values learning and always trusted me to make it in whatever adventures I decided to pursue. I appreciate you being so supportive of me on this PhD journey.

Abstract

Understanding aerosol formation and having ambient aerosol data is crucial for accurate climate modelling because aerosols have both direct and indirect climate effects. Even though the majority of the Earth is covered by oceans and the radiative budget over oceans is sensitive to changes in aerosol concentrations, most aerosol measurements are from continental sites. In this thesis, I study the formation of marine aerosols extensively using both laboratory and field measurements. With the laboratory studies we could study aerosol formation directly from sea surface emissions and connect this information to seawater properties. The long-term field measurements allowed studying the importance of these processes in ambient air. The lab studies used real seawater in tanks and isolated the air above the water to study aerosol formation from emissions from the sea surface directly. In these studies we used both coastal and open ocean seawater collected around New Zealand and measured aerosol number concentrations down to 1 nm. The results from these experiments identified eukaryotic nanoplankton as a potential plankton group responsible for emitting particle precursor species. Long-term field measurements conducted at Baring Head, in coastal New Zealand, were used to study aerosol formation in the real marine atmosphere. The results from this work showed that while aerosol formation can be observed in clean marine air masses, it is weaker than particle formation over land and should be studied with different criteria than continental particle formation. Analysing the chemical composition of ambient ions showed that different chemical species were responsible for aerosol formation over land and oceans with organic compounds and sulfuric acid likely important over land and iodine oxides and sulfur species likely important in open ocean air masses. The work done in this thesis is highly valuable, because marine aerosol measurements are scarce even though they are important for constraining climate models.

Key words: aerosol formation, marine aerosols, nucleation, new particle formation, chemical precursors, marine biology

Résumé

Comprendre la formation des aérosols et disposer de données sur les aérosols ambiants est crucial pour la modélisation du climat futur, car les aérosols ont à la fois des effets directs et indirects sur le climat. Bien que la surface de la Terre soit couverte en majorité par les océans, et que le bilan radiatif au-dessus des océans soit sensible aux changements de concentrations des aérosols, la plupart des mesures d'aérosols ont été obtenues au-dessus des continents. Dans cette thèse, j'étudie la formation d'aérosols marins, en utilisant à la fois des mesures en atmosphère ambiante sur le terrain et lors d'expériences menées en conditions naturelles. Les expériences en conditions naturelles nous ont permis d'étudier la formation d'aérosols par nucléation directement à partir des émissions issues d'un volume d'eau de mer isolé et donc de relier les mécanismes de formation de l'aérosol aux propriétés de l'eau de mer. Les mesures de terrain à long terme ont permis d'étudier l'importance de ces processus dans l'air ambiant. Pour les expériences de terrain, nous avons étudié d'une part les émissions issues de l'eau de mer échantillonnée en zone côtière et d'autre part les émissions de l'eau de mer échantillonnée en conditions hauturières au large de la Nouvelle-Zélande. Pour chaque campagne de mesures, la distribution en taille de l'aérosol a été mesurée dès les plus petites tailles (à partir de 1 nm). Les résultats de ces expériences ont permis d'identifier que le nanoplancton eucaryote présent dans l'eau de mer était majoritairement responsable de l'émission d'espèces précurseurs de particules. Les mesures ambiantes effectuées à Baring Head sur la côte néo-zélandaise, sur plusieurs mois ont quant à elles, permis de montrer que si la formation d'aérosols peut être observée dans les masses d'air marines, elle est plus faible que la formation de particules sur terre et devrait être étudiée avec des critères différents de ceux pour caractériser les événements de formation de particules continentales. L'analyse de la composition chimique des ions ambiants à Baring Head a montré que différentes espèces chimiques étaient responsables de la formation d'aérosols sur les terres et les océans. Les composés organiques et l'acide sulfurique semblent importants dans la nucléation observée dans les masses d'air ayant eu un contact avec la terre, alors que les oxydes d'iode et les espèces soufrées semblent d'avantage être impliquées dans les événements de formation de nouvelles particules en milieu océanique hauturier. Le travail effectué dans cette thèse apporte des informations nouvelles sur la formation de nouvelles particules dans un milieu relativement peu documenté, qui pourraient être utiles pour contraindre les modèles climatiques.

Mots-clés : Formation des aérosols, aérosols marines, nucléation, formation de nouvelles particules, précurseurs chimiques, biologie marine

Contents

1	Introduction	1
1.1	Motivation	1
1.2	Marine aerosols	3
1.2.1	Sulfur species	4
1.2.2	Iodine	5
1.2.3	Organics	5
1.3	Goals of this work	6
2	Methods	8
2.1	Measurements	8
2.1.1	Aerosols	8
2.1.2	Chemical composition of ambient ions and neutral molecular clusters . . .	9
2.1.3	Gases	9
2.1.4	Radon	10
2.1.5	Chemical properties of water	10
2.1.6	Plankton measurements	10
2.1.7	Surface tension measurements	11
2.2	Data analysis	11
2.2.1	Aerosol data	11
2.2.2	New particle formation event classification	11
2.2.3	Growth rates	12
2.2.4	Formation rates	12
2.2.5	Air masses	13
3	ME3 mesocosm experiment	14
3.1	Experimental setup	14
3.1.1	Air measurements	15
3.1.2	Sea water properties	15
3.1.3	Modelling of iodine sea-air fluxes and iodine oxide particles	15
3.1.4	Data processing	16
3.2	Results and discussion	16
3.2.1	Aerosol number concentrations	16
3.2.2	Factors explaining aerosol concentrations	19
3.2.3	Connection to chemistry	19
3.2.4	Connection to biology	23
3.3	Conclusions	25
4	Air-Sea Interaction Tanks	27
4.1	Experimental setup	27
4.1.1	Tank design	27
4.1.2	Experiments on board RV Tangaroa	30

4.1.3	Additional experiments	32
4.2	Results and discussion	33
4.2.1	Experiments on board RV Tangaroa	34
4.2.2	Chemical species in the ASIT headspaces	35
4.2.3	Connecting particle formation to seawater properties	42
4.2.4	Additional experiments	43
4.3	Conclusions	46
5	New particle formation and aerosols in ambient air	48
5.1	Measurement setup	48
5.1.1	Aerosol measurements	49
5.1.2	Ancillary data	50
5.2	Data analysis	51
5.3	Results	51
5.3.1	New particle formation events	52
5.3.2	Aerosol concentrations	57
5.3.3	Growth rates	59
5.3.4	Formation rates	61
5.3.5	Marine new particle formation	61
5.4	Conclusions	67
6	Chemical composition of ambient ions and their connection to new particle formation	69
6.1	Measurement setup	69
6.2	Detected species	69
6.2.1	Identifying relevant compounds	70
6.2.2	General comparison of marine and land-influenced air masses	73
6.3	Diurnal cycles	73
6.4	Seasonal cycles	77
6.5	Geographical source regions	79
6.6	New particle formation precursor species	81
6.6.1	Correlations between chemical species and aerosol data	81
6.6.2	Land-influenced new particle formation	83
6.6.3	Marine new particle formation	87
6.7	Conclusions	89
7	Conclusions	90
	Bibliography	93

Chapter 1

Introduction

1.1 Motivation

One of the largest single uncertainties in predicting future climate is the role of aerosols and their interactions with climate (Stocker et al., 2013). Aerosols are liquid or solid particles that are light enough to float in the atmosphere. They are important for the climate because they can interact with radiation both directly and indirectly. The direct effects include absorbing and reflecting radiation while indirect effects refer to the capability of aerosols to act as cloud condensation nuclei (CCN). All cloud droplets form by water condensing onto aerosol particles and this is why the abundance, size and chemical properties of aerosol particles influence the formation and properties of clouds (see e.g., Kerminen et al., 2012). Recently, it was reported that variations in CCN concentrations can explain up to 75% of the variability in the radiative cooling effect of clouds in given meteorological conditions (Rosenfeld et al., 2019).

The sizes of aerosol particles range by several orders of magnitude from nanometer scale molecular clusters to coarse particles of dozens of micrometers. The chemical composition of aerosols can vary greatly depending on their sources and processing in the atmosphere during transport. Aerosol particles can be divided to primary and secondary aerosols. Primary aerosols are emitted directly into the atmosphere. This includes for example dust, sea spray and biomass burning emissions. Secondary aerosols form in the atmosphere by gas-to-particle conversion. The first step of gas-to-particle conversion is the initial formation of particles by nucleation, also known as new particle formation (NPF). Freshly nucleated particles are in the nanometre size scale and in order to be able to act as cloud condensation nuclei, they have to grow larger past several dozens or even hundred nanometres. This happens by the condensation of different low-volatility chemical species onto the aerosol surface. The occurrence of particle nucleation and growth episodes is also known as new particle formation (NPF).

According to modelling studies, half of the aerosol particles that can act as CCN are formed in the atmosphere from vapours (Merikanto et al., 2009; Gordon et al., 2017). NPF has been observed in various environments (Kulmala et al., 2004; Nieminen et al., 2018; Kerminen et al., 2018), but most of the observations are from continental sites even though the oceans cover over 70% of the Earth and remote marine aerosol measurements are highly valuable for constraining climate models (L. A. Regayre et al., 2020). Secondary aerosol formation from marine sources has been studied since the late 1980's when the famous CLAW hypothesis (Charlson et al., 1987) was first proposed. The idea in the hypothesis was that dimethyl sulfide (DMS) produced by phytoplankton can get oxidised to sulfuric acid which can then nucleate and form new aerosol particles. If these particles grow to large enough sizes, they can then act as CCN, influencing the formation and properties of clouds. This again has an impact on the climate and climatic conditions have an influence on the marine phytoplankton. Marine CCN concentrations are especially important since particle concentrations in marine air are typically lower than in continental air, meaning that cloud formation is more limited by CCN availability. The oceans

are also a very vast and relatively dark surface, while clouds reflect radiation effectively. This makes understanding the cloud cover over oceans especially important for the radiative balance.

The CLAW hypothesis has been debated since its publication (Quinn and Bates, 2011) and it is evident that marine aerosol formation processes are not as straight forward as originally proposed and as highlighted earlier, extensive marine aerosol measurements are scarce. While most of the human population and thus sources of anthropogenic pollution are in the Northern Hemisphere, four fifths of the Southern Hemisphere is covered by oceans. Southern Hemisphere aerosol and cloud properties can thus be used to study natural aerosols and even estimate the pre-industrial aerosol concentrations (e.g. I. L. McCoy et al., 2020).

Most previous marine aerosol measurements in the Southern Hemisphere are from ship or flight campaigns (see Table 1 in Schmale et al., 2019). The benefit of these campaigns is the ability to sample marine air in different locations over open ocean, but the drawback is the short duration of the measurements. The longest field measurements that have captured aerosol concentrations in background marine air in the Southern Hemisphere have been performed at Cape Grimm, in Australia. The station at Cape Grim has been running since 1970's for baseline measurements of different climatically relevant atmospheric parameters and the most recent aerosol number concentration measurements at Cape Grim start from 3 nm (e.g. Gras and M. Keywood, 2017).

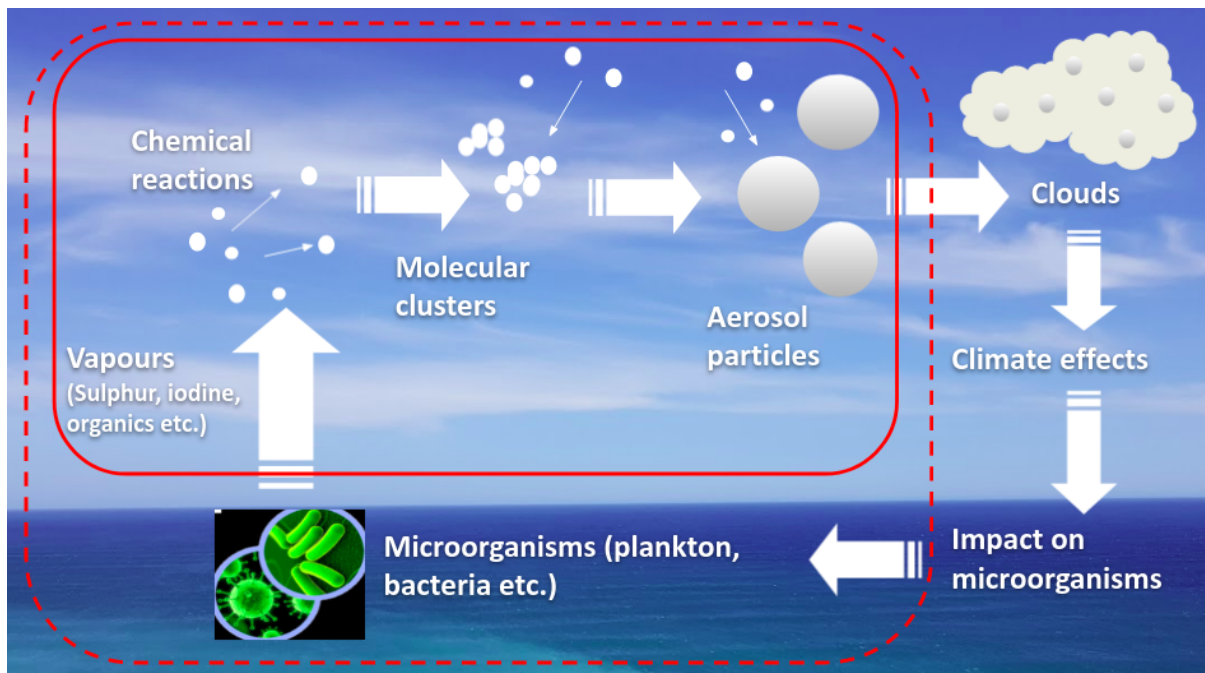


Figure 1.1: Illustration of the CLAW feedback loop, with the focus of this thesis circled with a dashed red line and key measurements circled with a solid red line.

This thesis studies the formation of aerosol particles from marine sources with both laboratory and field studies to better understand the processes leading to new particle formation in marine conditions. Figure 1.1 illustrates the CLAW feedback loop and the key research areas of this thesis. We measured the first steps of the feedback loop starting from chemical species emitted from the sea surface to their oxidation products and aerosol particles in different size ranges. In the laboratory work we also measured the chemical and biological properties of seawater to understand how they are connected to aerosol formation. All the measurements were conducted in New Zealand and for the laboratory experiments we used both coastal New Zealand seawater and seawater collected from the open ocean east of New Zealand. The long term ambient measurements were performed at Baring Head, in coastal New Zealand, because

the site allows sampling air masses that have travelled to New Zealand from the Southern Ocean region. Baring Head is approximately 2500 km from Cape Grim and previous aerosol measurements there have focused on filter samples (e.g. Allen et al., 1997; Sievering et al., 2004; Li et al., 2018; Li et al., 2021b). This means low time resolution and not being able to study aerosol properties and formation in detail. The measurements done during this thesis are a clear advancement to the previous work done in the area, because we were able to bring over new instrumentation that can measure particle number concentrations starting already from 1 nm and the chemical composition of ambient ions which can be used to study the chemical species responsible for particle formation. This chapter explains the progress made in research so far and outlines the goals of this research.

1.2 Marine aerosols

Marine aerosols can form both through the production of sea spray aerosol when waves break and through new particle formation from different chemical species emitted from the sea surface. Quinn et al. (2017) showed that on global level only 30% of marine CCN are sea spray aerosol. Several field measurements have supported the importance of secondary marine aerosols since then. For example Fossum et al. (2018) observed that only 8-51% of the CCN around the Southern Ocean were from primary sources when wind speeds were below 16 m/s. Sanchez et al. (2018) showed that in the North Atlantic, a major fraction of CCN is comprised of secondary sulphates from biogenic sources, with new sulphate particles forming in the free troposphere. Croft et al. (2021) proposed that particle formation and growth over the North West Atlantic Ocean was important for the CCN concentrations and had significant cooling effects through both direct and indirect effects. A mesocosm study comparing the sea spray and secondary aerosol formation pathways also showed that secondary marine aerosols dominate over sea spray production (Mayer et al., 2020).

On the other hand, the concentrations of sea spray aerosols influence the amount of new particles formed by acting as a sink for particle forming vapours. Fossum et al. (2020) studied the connection of different marine aerosol types on the cloud droplet number concentration and showed that number of activated cloud droplets is inversely proportional to sea spray aerosol concentrations. This is because high sea spray concentrations suppress the formation of new particles and decrease the total CCN concentrations. The relations between different aerosol components are important and this has to be kept in mind when working with aerosol data.

One of the factors making the interpretation of marine aerosol data more complicated is the effect of meteorological conditions and mixing of the atmosphere. One important question is where the particle formation takes place. The chemical species that can participate in NPF are originally emitted from the sea surface and they are diluted into the mixed boundary layer, which is the lowermost part of the atmosphere. Typical marine boundary layer heights around the Southern Ocean are below 1 km (see e.g. Alexander and Protat, 2019). Above the boundary layer, there is free troposphere (FT). The transport of particles and gases from the boundary layer to the FT is relatively slow. Clouds can transport particle precursor species into the FT because they increase convective transport. The same is not true for particles, because clouds act as a sink for aerosol particles.

Modelling work by H. Korhonen et al. (2008) showed that marine nucleation is more likely to occur in the FT than within the mixed boundary layer, because the pre-existing particle population in the FT is lower. Some of the recent work addressing the altitude dependence of marine new particle formation has shown that over the Atlantic, the initial steps of particle formation are most likely to happen in the free troposphere or in the upper decoupled layer of the boundary layer. Sanchez et al. (2018) showed that in the North Atlantic, a major fraction of CCN is comprised of secondary sulphates from biogenic sources, with new sulphate particles nucleating in the free troposphere. Zheng et al. (2021), on the other hand, showed that new

particle formation is likely to occur in the upper decoupled part of the marine boundary layer after the passage of a cold front. The upper decoupled layer is associated with low particle concentrations, high concentrations of aerosol precursor species, cold air temperatures and high actinic fluxes close to the scattered clouds. All of these factors favour particle formation. Particle formation occurring after the passage of cold fronts has been observed also at Cape Grim, in Australia (Gras et al., 2009). The importance of meteorological conditions was also highlighted by Wollesen de Jonge et al. (2021), who combined DMS oxidation chamber measurement results with modelling and observed that clear particle formation occurred in the model after a rain event which decreased the condensation sink formed by the pre-existing particles.

All of these factors are important to remember when studying marine new particle formation. Since one of the goals of this work is to understand what chemical species are important for aerosol formation, the next subsection focus on the different chemical species groups that have been expected to form aerosols in marine conditions in the past.

1.2.1 Sulfur species

Dimethyl sulfide is the largest natural source of sulfur (Bates et al., 1992) and many studies have focused on its emissions, reaction products, and aerosol yields. The most commonly know oxidation products of DMS are methane sulfonic acid (MSA) and SO_2 , with SO_2 further oxidising into sulfuric acid (SA). The relative yields of SA and MSA vary depending on conditions such as temperature, NO_x , and halogen concentrations (Nicovich et al., 2006; Stark et al., 2007; Breider et al., 2010; Mardyukov and Schreiner, 2018). Recent chamber experiments studying DMS oxidation found that the yield of MSA was typically higher than that of sulfate (Rosati et al., 2021). Field work studying the relationships of DMS, MSA and non-sea-salt sulfate in the Southern Ocean showed that explaining the factors controlling DMS to MSA oxidation is complicated (J. Yan et al., 2020b) and that the uptake of MSA to aerosol phase depends on the chemical composition of pre-existing particles (J. Yan et al., 2020a). One of the factors complicating the understanding of DMS oxidation processes is that MSA can also be formed in aqueous phase, that is, in aerosol liquid water of cloud droplets. Some work has showed that aqueous phase formation of MSA could even be more important than its gas phase formation (Hoffmann et al., 2016; Baccarini et al., 2021).

It is also possible that not all pathways of DMS oxidation are yet known. Recent work has pointed out new climatically relevant DMS oxidation products, such as hydroperoxy thioformate (HPMTF, $\text{HOOCH}_2\text{SCHO}$, Veres et al., 2020) and methane sulfonamide (MSAM, $\text{CH}_5\text{NO}_2\text{S}$, Edtbauer et al., 2020). Veres et al. (2020) suggested that HPTMF could participate in aerosol formation, but some recent modelling work has indicated that the formation of HPMTF would rather be a sink of sulfur and reduce the formation of secondary aerosol rather than increase it (Wollesen de Jonge et al., 2021).

Until recently, the effect of MSA on secondary aerosol formation has not been taken into account in global models. Hodshire et al., 2019 modelled the effect of MSA on aerosol concentrations and climate. They showed that while the effect of taking MSA into account is small for direct radiative effects, including it can increase the number of CCN sized particles and thus be important for aerosol indirect radiative effects. In addition to uncertainty created by the variable relative yields of SO_2 and MSA from DMS oxidation in literature, one drawback in their work was the lack of knowledge on the effective equilibrium vapour pressure of MSA. This information is needed to know if MSA can participate in the first steps of particle formation and to know how readily MSA condenses onto particles. More work is thus clearly needed to fully understand new particle formation from MSA.

Another key element complicating the understanding of marine aerosol formation from DMS and other sources is its different connections to biology. DMS is emitted into the atmosphere by different phytoplankton species and the plankton populations have already shifted due to climate change (Jonkers et al., 2019). Some lab studies have already tried to understand how changes

in climate conditions could alter the emissions of DMS (Avgoustidi et al., 2012; Archer et al., 2013; A. D. Saint-Macary et al., 2021). Further studies have also aimed to model the impact of changing DMS emissions on climate (Six et al., 2013; Woodhouse et al., 2013; Schwinger et al., 2017; S. Wang et al., 2018), but if the aerosol yields from DMS are not fully known, the modelling results are likely to be uncertain too.

1.2.2 Iodine

More recent work has shown that DMS is not the only chemical species responsible for NPF in marine conditions. The capability of iodine to form new particles was shown already almost 20 years ago (C. D. O’Dowd et al., 2002). A lot of advances have been made since and recent work has been able to track the formation mechanisms of iodine particles in detail (He et al., 2021; Gomez Martin et al., 2020). According to chamber experiments performed by He et al. (2021), iodine new particle formation is driven by HIO_3 , while HIO_2 is important for stabilising HIO_3 clusters during the first steps of nucleation. They also show that HIO_3 can form in the presence of ozone and water vapour even in cloudy conditions.

Iodine can be emitted to the atmosphere in different forms as a result of both biological processes and sea surface chemistry (Carpenter et al., 2021). It has been shown to be emitted in especially high concentrations by macroalgae at coastal sites (McFiggans et al., 2004; Sellegri et al., 2005; Carpenter et al., 2000). This is why much of the work studying iodine particle formation has focused on the effect of coastal sources of iodine (Grose et al., 2007; Furneaux et al., 2010; Sipilä et al., 2016). However, iodine particle formation has been observed also over sea ice (Baccarini et al., 2020 and some evidence of it happening over open ocean exists as well (Sellegri et al., 2016). He et al. (2021) showed that iodine particle formation can happen in various environments and iodine in aerosols (Gomez Martin et al., 2021) and iodine oxides (Takashima et al., 2021) have been observed globally.

Even though a lot of progress has been made in unravelling the processes leading to iodine oxide particle formation, real atmospheric conditions are complicated and the presence of other chemical species can influence these processes. For example, a new modelling study suggested that MSA could stabilise iodic acid, leading to higher particle formation rates when both MSA and iodic acid are available compared to iodic acid alone (Ning et al., 2021). Field work in coastal China has shown that there nucleation can involve both iodine and organic species (Wan et al., 2020).

1.2.3 Organics

Another important group of chemical species that can be important for marine new particle formation is different organic species. A ship measurement campaign east of New Zealand has observed secondary organic aerosol (SOA) in sunny conditions over plankton bloom regions (Law et al., 2017; L. Cravigan, 2019). The importance of SOA has been also examined in several studies around the Arctic (Willis et al., 2017; Tremblay et al., 2019; Croft et al., 2019; Beck et al., 2021b) and many other environments with marine influence.

Potentially relevant organic species include for example monoterpenes ($\text{C}_{10}\text{H}_{16}$), isoprene (C_5H_8) and different organic acids. The role of isoprene in marine SOA formation was first proposed by Meskhidze and Nenes (2006). While the emissions of monoterpenes and isoprene are typically connected directly to biological activities (Shaw et al., 2010), isoprene can be produced also abiotically by photosensitized reactions at the sea surface microlayer (Ciuraru et al., 2015). Like other biogenic emissions, marine isoprene emissions are influenced by temperature and light conditions (Meskhidze et al., 2015; Dani et al., 2017). S. R. Arnold et al. (2009) combined isoprene emissions from different phytoplankton cultures with satellite data and estimated the global marine emissions of isoprene to be important for marine SOA. Field work in Australia, at Cape Grimm, has shown that isoprene and monoterpene derived SOA had higher concentrations

during the summer and this component was connected to marine biological activity (Cui et al., 2019). However, this accounted for less than 1 % of the total organic aerosol mass at the site.

Another possible source of marine SOA is fatty acids (FA). Fatty acids are produced by phytoplankton and their amount and composition can depend not only on plankton group but also on the environmental conditions (e.g. R. Bermudez et al., 2015; J. R. Bermudez et al., 2016; Peltomaa et al., 2019). The photochemical reactions of FAs on the seawater surface can form volatile organic compounds (VOC) that can further produce SOA (Bernard et al., 2016; Alpert et al., 2017). The formation of VOCs from FAs is enhanced in the presence of photosensitisers such as humic acid (Alpert et al., 2017).

While the emissions of isoprene and monoterpenes are typically directly connected to biological activity, dead cells can also produce VOCs and the VOC fluxes from dead cells can be even higher than emissions from living cells (Brüggemann et al., 2017). This was connected to cell lysis producing several chemical compounds that can be further transformed into FAs. Similar results have been seen by S. R. Schneider et al. (2019) who used a monoculture of *Thalassiosira pseudonana* to create an artificial sea surface microlayer. Their results showed an increase in SOA production when the culture was older, indicating the role of cell lysis. According to a modelling study, taking into account the abiotic organic sources could increase the mass of organic aerosol clearly on global level (Brüggemann et al., 2018).

While organic compounds, sulfur species, and iodine oxides can all be important for marine aerosol formation, many studies focus only on one chemical species. This is problematic, because the real atmosphere can contain all of these species. For example, recently Beck et al. (2021b) showed that in the Arctic sulfur species and organics are important for particle formation during the summer while during the winter iodic acid is important for nucleation. They also showed that different species can contribute to nucleation and growth. This highlights the importance of long term field measurements for determining the roles of different precursor species in new particle formation and the seasonal variations of these processes.

1.3 Goals of this work

As the previous research shows, more information is needed to fully understand the processes controlling marine aerosol formation. The aim of this thesis was to study aerosol formation from marine biogeochemical emissions. We study marine aerosol formation with both mesocosm and ambient air measurements. The mesocosm studies are used to study new particle formation directly from sea surface emissions. By sampling the seawater simultaneously with the air, we can connect aerosol formation to seawater chemical properties and abundances of different phytoplankton species. This research is especially valuable because, while previous studies have measured the fluxes of single species, such as DMS from plankton cultures, using real seawater and measuring both chemical species emitted from the sea surface and aerosols formed from these species is rare.

The ambient measurements enable studying how significant these processes are in real atmospheric conditions. We performed measurement at a coastal New Zealand site for a total period of 10 months. This is very valuable, because long term coastal aerosol measurements, especially from the Southern Hemisphere are very rare. Moreover, not only did we measure the aerosol number size distributions, but we also measured the chemical composition of ambient ions. This way we could characterise the chemical species present in the atmosphere and connect this information to the aerosol data to understand which chemical species drive new particle formation.

The key questions that I aim to answer in this thesis are: 1) does nucleation happen in marine boundary layer 2) what chemical species are responsible for marine nucleation, and 3) what biological species are responsible for emitting these chemical species. The next chapter summarises the methods used in this thesis, Chapter 3 shows the results of the first mesocosm

experiment where we connect particle formation to different plankton species and Chapter 4 describes the more advanced mesocosm studies in which we also studied the chemical species responsible for particle formation. In Chapter 5 we explain the ambient measurements and study the aerosol properties and nucleation and growth at the Baring Head coastal site. Chapter 6 takes the work from Chapter 5 one step further by connecting its results to the chemical composition of ambient ions to understand which chemical species are responsible for particle formation. The last chapter draws together the final conclusions of this work.

Chapter 2

Methods

This chapter explains the main measurement techniques and data analysis methods used in this thesis.

2.1 Measurements

2.1.1 Aerosols

As the focus of this thesis is on aerosol formation, let us first go through the different instruments used in this work for aerosol measurements. To measure aerosol number size distribution, we used Scanning Mobility Particle Sizers (SMPS, see e.g., S. C. Wang and Flagan, 1990). The SMPS works by first charging the particles with an x-ray source so that they follow an equilibrium charge distribution. Then the particles go through a Differential Mobility Analyser (DMA) which selects one size range of particles at a time based on their electrical mobility. From the DMA the particles are lead to a Condensation Particle Counter (CPC) which grows the particles by condensing butanol onto them and the counts them optically. The main SMPS measurements in this work measured the size distribution of particles between 10-500 nm in 25 size bins with approximately 13 min time resolution.

In addition to the SMPS, most of our measurements included a second CPC ran in parallel with SMPS. The second CPC was used to obtain the total particle number concentration with a better time resolution. It was also used for the quality control of the SMPS measurements by checking that the two instruments showed similar concentrations. Most of the CPCs that we used had a lower detection limit of 10 nm, which means that they are able to detect at least 50 % of 10 nm sized particles. Particles larger than 10 nm are more likely to be detected and particles smaller than 10 less likely to be detected.

Particle Size Magnifier (PSM, Vanhanen et al., 2011) was used to detect the number concentration of particles in smaller size ranges, starting from 1 nm. By detecting particles in this size range we can study the very first steps of nucleation. The PSM functions by first growing the particles with diethylene glycol (DEG) to size of 90 nm. Then the particles are directed to a CPC which further grows the particles to optically detectable sizes and counts them. The saturation flow rate of the PSM can be varied to alter the smallest size range at which the particles can be detected. The higher the saturation flow is, the smaller the sizes that can be detected. Here we used the instrument either fixed to one supersaturation flow rate or in stepping mode where the saturation flow rate varies between two values. The stepping mode can be used to estimate the number concentration of the smallest particles by calculating the difference between particle concentrations observed at the different saturation flow rates. The instrument settings should be optimised for give condition to avoid homogeneous nucleation of DEG which would lead to overestimation of particle concentrations (Sulo et al., 2021). On the other hand, if the saturation flow rate is too low, particles are not detected and the concentra-

tions are underestimated. The detectable sizes depend also on particle chemical composition and charge (Kangasluoma et al., 2016).

Additional particle size distribution measurements were done with Neutral cluster and Air Ion Spectrometer (NAIS, S. Mirme and A. Mirme, 2013; H. E. Manninen et al., 2016). It can measure the size distribution of both ions and particles below 42 nm. In ion mode the instrument measures only ambient ions whereas in particle mode the air is charged with corona discharge sources. In offset mode, the air is ionised and then the ions are removed with an ion trap. This is done to obtain the background of the instrument. Due to the high flow rates required by the instrument, the NAIS was only used for ambient measurements. The data was inspected visually following guidelines by H. E. Manninen et al. (2016).

2.1.2 Chemical composition of ambient ions and neutral molecular clusters

Some of the key measurement of this thesis were done with Atmospheric Pressure Interface Time of Flight mass spectrometer (APi-TOF, Junninen et al., 2010). It can be used to determine the chemical composition of ions in ambient ions. It draws in ambient air and gradually decreases the pressure of the air first with a scroll pump and then a turbo pump. The ions are kept in the air flow by guiding them with quadrupole magnets and an ion lens. Once the pressure has reached -5×10^{-6} mbar or below, the ions are pulsed to a multichannel plate and their time of flight is determined. The time of flight can then be transformed into a mass to charge ratio. Assuming unit charge we can then identify the chemical composition of ions. When we look at only ions, we have to remember that the ion concentrations are driven by not only the availability of different chemical species, but also by the available charge. The likelihood of compounds to obtain charge is largely driven by their proton affinities (C. Yan et al., 2018).

For the long term-field measurements we used the instrument as such without chemical ionisation. For the ship measurements we also used it with an Eisele type chemical ionisation inlet with nitric acid. The function of the inlet is to form nitrate ions which then interact with the sample air and charge its molecules. For a full description of the inlet, see Jokinen et al. (2012). The advantage of chemical ionisation is that we can measure the total concentrations of some chemical species. For example nitrate chemical ionisation is suitable for measuring the total concentrations of sulfuric acid. The down side is that nitrate ions are selective and do not charge all chemical species as effectively. This is why other ions such as iodide and bromide can also be used (see for example, Lopez-Hilfiker et al., 2016; M. Wang et al., 2021). The benefits of using APi-TOF without chemical ionisation include the fact that the signal is not influenced by the choice of the ionising chemical species and that the detection limit is several orders of magnitude lower than with the CI-inlet (see Beck et al., 2021a).

The APi-TOF is very sensitive to the voltages used in the quadrupoles and other charged parts. If too hard voltages are used, the clusters can fragment as studied in detail by for example Passananti et al. (2019). Optimising the voltages for wanted purposes is thus important when using this instrument. The CI-inlet with nitric acid was used to optimise the voltages of the instrument for all the work done in this thesis. With the CI inlet we can create stable concentrations of known ions that can be used to experiment with the effect of different voltage settings. We chose to optimise sensitivity over mass resolution because we worked with marine air, which is typically characterised by low concentrations of pollutants.

2.1.3 Gases

Gas sampling was conducted with 1/4 inch Teflon inlets. Sulphur dioxide was measured with Thermo Scientific Model 43i SO₂ Analyzer. Due to technical limitations the instrument was not calibrated during this work, but its zero level was corrected based on data. Ozone was measured with Thermo Scientific Model 49i Ozone Analyzer. This instrument was calibrated with an ozone generator. A proton transfer mass spectrometer (PTR-MS, Ionicon Analytik,

Innsbruck, Austria) was used during to measure the concentrations of different volatile organic compounds during the ship campaign.

2.1.4 Radon

Radon measurements from Baring Head were used to identify when the air masses had been in contact with land. The measurements were done with ANSTO designed high-sensitivity site background radon detector (Ansto, Australia www.ansto.gov.au, Chambers et al., 2014).

2.1.5 Chemical properties of water

Chlorophyll-a

Chlorophyll-a was collected onto 25 mm grade GF/F glass microfiber filters by pouring one litre of water through the filter. The filters were then snap frozen and stored at -80 °C. To analyse the samples, they were mixed with 6 ml of acetone and left in a -20 °C over night to extract the chlorophyll from the filters. After the wait the samples were centrifuged to remove particulate matter in the sample. Then they were analysed with a Turner Design fluorometer before and after adding hydrochloric acid. For full method description, see Arar and G. B. Collins (1997).

Chromphoric Dissolved Organic Carbon

Chromphoric Dissolved Organic Carbon (CDOM) water samples were collected through 25 mm 0.2 µm polycarbonate filters and stored briefly in 60 ml Nalgene bottles. The filtered samles were then analysed with Ocean Optics DT-MINI UV/VIS light source, Liquid Waveguide Capillary Cell (LWCC), and USB4000 spectrophotometer.

Dimethyl sulfide

Dimethyl sulfide (DMS) and dimethylsulfoniopropionate (DMSP) concentrations in water were determined by Agilent Technology 6850 Gas Chromatography coupled with an Agilent 355 sulfur detector. The measurements are described in more detail in A. D. Saint-Macary et al. (2021).

Fatty acids

Particulate fatty acid samples were collected by filtering 3 or 4 l of seawater onto a 0.7 µm filter. The samples were analysed by Cawthron Institute following method AOAC 963.22 OMA.

Iodine

Iodide content in samples was determined by Liquid Chromatography coupled to Mass Spectrometry (LC-MS) in an Agilent 1290 Infinity II LC system coupled to an Agilent 6470 triple quadrupole mass spectrometer (Agilent Technologies, Santa Clara, CA, USA), following the method developed by Hernáiz-Izquierdo et al. (2019).

2.1.6 Plankton measurements

Flow cytometry

Flow cytometry with BD FACS Calibur instrument was used to determine number concentrations of eukaryotic nanoplankton (cell size 2-20 µm) and eukaryotic and prokaryotic picophytoplankton (cells < 2 µm) following the procedure described by Hall and K. Safi (2001).

Microscopy

For phytoplankton with cells larger than 5 μm , the composition of the plankton community was determined with optical microscopy. For this, we took 1 l water samples. These samples were stored using Lugols solution and analysed as described in K. A. Safi et al. (2007). In addition to identifying the main species, we use the plankton divisions to group similar plankton species.

2.1.7 Surface tension measurements

Surface tension of daily samples was measured using a SITA DynoTester bubble lifetime-based analyzer. Seawater samples were first frozen to investigate the relation of surface tension to temperature over a large temperature range. Surface tension was then measured three times for each seawater temperature over the range 3-15°C. For each temperature, the difference to ideal seawater was calculated using the relationship to temperature and salinity reported in Nayar et al. (2014).

2.2 Data analysis

2.2.1 Aerosol data

We combined information from PSM, CPC, and SMPS in order to obtain particle number concentrations in different size ranges. For sub-10 nm particles we used PSM data, for total number concentration of particles with diameters above 10 nm CPC data and for large size ranges SMPS data. All the number concentrations are denoted with N and the size range in nanometers, for example N1-3 for 1-3 nm particles and N10 for particles with diameters above 10 nm.

SMPS data were also used to calculate the condensation sink (CS) formed by the particle population as in Kulmala et al. (2001). This basically represents the surface area of aerosols and describes their ability to act as a sink for condensable vapours. For the calculation we used sulphuric acid as the condensing species.

2.2.2 New particle formation event classification

The particle size distribution measurements from Baring Head were classified manually based on whether new particle formation was observed or not. We used the classification criteria by Dal Maso et al. (2005). The classification was primarily based on SMPS data but NAIS data was included in the surface plot below 10 nm when it existed. If SMPS data was missing for part of the day, the day was not classified with this method. In this method, particle number size distributions for each day are inspected visually and days are divided into Class I, Class II, undefined and non-event days. Class I and Class II days are days when new particle formation is clear with the difference that during Class I the new particle mode is clear and determination of growth rates is possible, whereas during Class II events the mode diameter or concentration varies. On non-event days there is no new particle formation and on undefined days there is a new mode of particles under 25 nm that lasts over an hour, but does not grow.

To obtain further information about the events, we also performed event classification based on the method developed by Dada et al. (2018) using NAIS data when it was available. This method is more quantitative than the method of Dal Maso et al. (2005) and gives us information about the size range of the events as well as event start and end times. The method is based on comparing the daytime ion and particle concentrations to background concentrations during the night. It uses the concentration of ions in 2-4 nm to detect the first steps of particle formation and the particle concentration in 7-25 nm to determine if the particles grow further or if there is a transported event that started somewhere else and is only observed at the station once the particles have grown. Here, we only used the particle concentration between 7-15

nm, because our instrument did not work properly for sizes above 15 nm. Even below that, the detection limit seemed high, meaning that the concentrations can be somewhat underestimated. Because of this and because the typical particle concentrations at Baring Head are lower than at Hyytiälä, we modified the Dada et al. (2018) algorithm parameters to take this into account. The algorithm has relative and absolute threshold values for both the ions and particles. The relative thresholds refer to comparing the daytime concentrations to background nighttime concentrations and absolute thresholds are fixed values that the daytime concentrations have to exceed in order for the day to be considered as an event. The relative ion and particle limits that are determined based on the background remained the same, but the absolute thresholds for ion and particle concentrations were lowered. For ions we used 3 instead of 20 cm^{-3} and for particles we used 100 instead of 3000 cm^{-3} . Despite the instrument issues and the different environment, we consider the method reliable, because a comparison to the manual method (see the Chapter 5) seemed good.

2.2.3 Growth rates

Aerosol particle typically form log normal modes, for which one can determine the mean diameter of the mode. If this mean mode diameter increases as a function of time, the particles are growing. The main process growing the particles is condensation of vapours on the surface of the particles. The rate at which the particle diameter grows is relative to the concentration of these condensable species which is why the particle diameter growth rates can be used to study the for example which chemical species grow small freshly formed particles to climatically relevant sizes.

We used the SMPS data and an automatic growth rate calculation method developed by Paasonen et al. (2018) to determine growth rates in particle size ranges. To use the same criteria as Paasonen et al. (2018), we first interpolated the SMPS data to 10 minute time resolution. The method first looks for peaks in the concentration data for each time point to determine the mean mode diameter. These peak concentration points are then grouped based on the diameter at which the peak is observed so that different particle modes are not mixed. The algorithm then goes through each mode and looks for periods where the diameter of the peak is growing. If the growth is monotonic enough and lasts for at least 2 hours, a growth rate is determined as the slope of a linear fitting to the peak points. This slope and the diameter of the growing particles is then saved along with the start and end times of the observed growth period.

To further analyse the growth rates, we turn this information into hourly time series. In the analysis the growth rates are separated into nucleation (< 25 nm), Aitken (25-100 nm) and accumulation (> 100 nm) modes based on the size of the growing particles because different processes can affect growth in different size ranges.

2.2.4 Formation rates

Particle formation rate is the rate at which particles at a chosen size are formed and it tells us about the intensity of particle formation. In ambient air, this can be calculated when we know the change in particle concentration over time and losses due to coagulation to pre-existing particle population and growth out of the wanted size range. We calculated formation rates for Baring Head data for 10 nm particles in order to compare them to different sites previously analysed by Nieminen et al. (2018). The formation rate is defined as

$$J_{10} = \frac{dN_{10-25}}{dt} + CoagS \times N_{10-25} + \frac{GR}{\Delta d_p} N_{10-25}, \quad (2.1)$$

where $\frac{dN_{10-25}}{dt}$ is the change of concentration in 10-25 nm, CoagS is the coagulation sink calculated for 15 nm particles and the last term defines the growth losses out of the size range. For

the growth term, we used manually calculated growth rates that use mode fitting method by Hussein et al., 2008 to be consistent with previous work.

2.2.5 Air masses

In order to study marine air masses, we separated marine air masses from land-influenced air using air mass back trajectories, radon concentrations and wind direction. To differentiate between land-influenced and marine air mass back trajectories, we used landmask code (<https://se.mathworks.com/matlabcentral/fileexchange/48661-landmask>), last accessed 13 May 2021) to define how long the air mass back trajectories had spent over land. Only times for which the back trajectories had spent 100 % of time over the sea were classified as marine. Due to the one hour time resolution of the back trajectories and spatial resolution of the land data, this method occasionally classifies back trajectories coming from the north as 100 % marine even though they have to pass over land. This is problematic especially since the area north of the station contains urban areas of Wellington which act as pollution sources as discussed by for example by Bruyn et al. (2002). This is why we also used radon and wind data to separate marine and terrestrially influenced air masses.

Radon (Radon-222) has been previously used at Cape Grim in Australia to identify time periods when air has not been in contact with land for several days (e.g. Molloy et al., 2009). This is based on radon being emitted from land around 100 times faster than from the sea and having a half-life of 3.8 days. The radon limit traditionally used at Cape Grim is 100 mBq m⁻³ and since the environment is similar to Baring Head, we used the same value to separate between marine and land-influenced air.

Finally, since we observed some points with radon below 100 mBq m⁻³ coming from the direction of Wellington city, we also used wind direction to eliminate these data. Wind direction values accepted for marine air are 120–220°, since this range has been previously used for Baring Head by Bruyn et al. (2002). Combining all these criteria we can compare marine air masses that have not been in touch with land during several days with air masses that have been influenced by land.

In addition to separating between marine and land-influenced air masses, we use the altitude of the back trajectories to estimate whether the marine air masses have been in the marine boundary layer or in the free troposphere. Previous work at Cape Grim has shown that the marine boundary layer is typically mixed up to altitudes of 500–1000 m (Bigg et al., 1984). This is why we decided to use an altitude limit of 500 m to separate between air masses that have likely been within the MBL and air masses that could have come from the free troposphere.

Air masses were also used to identify regions that favoured new particle formation, similarly to the work by Rose et al. (2015a). This was done by combining the air mass back trajectories with the number concentration of negative ions in 2-4 nm. For each time step, we attributed the concentration of ions measured at Baring Head to the full back trajectory path. Then, for a given grid cell, we averaged the resulting concentration by the number of back trajectories that pass through the 1x1° grid cell, which provided a map of the ion concentration occurring when air masses are coming from different grid cells. Only cells that had at least 10 back trajectories passing through them were accepted.

Chapter 3

ME3 mesocosm experiment

The first laboratory experiments used in this thesis were performed in November 2017, as a part of the Mesocosm experiment 3 (ME3), which was part of the CARIM (Coastal Acidification: Rate, Impacts & Management) project. The primary goal of this project was to study the effect of ocean acidification and warming on primary production and food quality in coastal New Zealand waters, but we used the opportunity to study aerosol formation from seawater emissions in different conditions. This chapter describes the experimental setup used in this experiment and the obtained results.

3.1 Experimental setup

Our measurement setup consisted of three mesocosms that were part of the Mesocosm Experiment 3 (ME3) that has been described earlier by A. D. Saint-Macary et al. (2021). While we use only three mesocosms, this campaign used a total of nine mesocosms in three different temperature and pH conditions to study the effect of coastal acidification over 21 days. Each of the mesocosms were 3.7 m long cylinders with a diameter of 1.2 m. The bottom parts of the mesocosms were filled with 4200 l of seawater collected from the Evans Bay area in Wellington, New Zealand. The volume of the headspace of each mesocosm was 170 l and the headspace was continuously flushed with particle filtered air. We chose not to scrub gases entering the mesocosm headspace to allow natural oxidants in. While filtering some gas-phase components, the particle filters may have let in some other gas-phase species than oxidants already present in the ambient air, and thus not immediately emitted at the mesocosm seawater-air interface. Regarding this drawback in the measurement set-up, the significant correlations that we will show between seawater properties and the particle concentrations formed within the mesocosm headspace indicate that the main precursors to particles measured in this study do originate from the mesocosm seawater and not the ambient air.

Nutrients were added to all mesocosms daily to mimic the conditions of a plankton bloom. The mesocosms were kept in different conditions with one serving as a control mesocosm (M_7) in ambient conditions, one having its temperature increased by 2.6 °C and pH lowered by 0.33 (M_8) and one with temperature increased by 4.5 °C and the pH was lowered by 0.5 (M_9). The idea of this setup was to mimic the conditions of future climate scenarios and the temperature and pH changes were determined based on work by Law et al. (2018). Due to the mesocosm with the highest temperature leaking water, we are not considering this mesocosm as representative of future climate conditions. The differences in the mesocosms do, however, allow us to study the effects of different seawater compositions on aerosol production. The impact of climate change on the biogeochemical properties of the seawater from the complete study including all the available mesocosms is the topic of other studies (e.g. A. D. Saint-Macary et al., 2021).

To study the formation of new particles from the emissions of biological species in the seawater of the mesocosms, we measured the number concentrations of aerosol particles in

different size ranges in the headspaces of the mesocosms. All the mesocosms used in this study were connected to a switching valve that directed air to the aerosol instrumentation. The valve was switching from one mesocosm to the other every 20 minutes. In between every measurement cycle the valve was also connected to ambient air for 20 minutes.

The headspace of each of the mesocosms was flushed with a 9 lpm circular flow that entered the mesocosm 5 cm above the seawater surface. The air used for flushing was filtered from particles with a HEPA filter, which means that all the particles observed within the mesocosm headspace should have formed within the mesocosm headspace. The headspace can be considered an ideally mixed continuous stirred-tank reactor, which means that the distribution of the residence time of air in the headspace is exponential. This means that even though the average residence time of air in the headspace is only 19 min, part of the air can stay in the headspace longer with 5% of the particles left after 82 min. This can allow the particles to grow to larger sizes as explained by e.g. Sellegri et al., 2005. From the headspace, air was pulled to the aerosol instrumentation and an ozone analyser at 3.5 lpm flow rate through 3.8 m long 1/4 inch tubing. There was thus a 5.5 lpm excess air flow exiting the headspace to limit contaminated air from entering the headspace through possible leaks. However, as the mesocosm headspaces were not completely airtight, a specific procedure was applied to the data set to take into account and correct for potential intrusion of external air (see Section 3.1.4 for data processing).

3.1.1 Air measurements

The aerosol instrumentation consisted of a TSI model 3010 Condensational Particle Counter (CPC) and a model A11 Particle Size Magnifier (PSM). The CPC was used to measure the number concentrations of particles with diameters larger than 10 nm. The PSM was used in stepping mode which means that its saturation flow rate was varied so that every other 60 seconds it was 1 lpm and every other 60 seconds it was 0.1 lpm. Here, we assume that these saturation flow rates correspond to particles with diameters of 1 and 3 nm, respectively. The values obtained from the PSM were corrected for the instrument's detection efficiency and diffusion losses in the inlets. From these measurements we derived the number concentrations of particles with diameters between 1 and 3 nm (N1-3), 3 and 10 nm (N3-10) and larger than 10 nm (N10). These aerosol data are available for 19 days of the experiment. Given that the aerosol growth rates in a similar experiment varied between 2.9 and 9.5 nm/h Sellegri et al., 2016, in the 19 minute average residence time the particles should not grow past 10 nm, but our conditions are different and as mentioned previously, the residence time follows an exponential function which means that part of the particles have more time to grow and can thus reach larger sizes.

3.1.2 Sea water properties

For ME3 the measured seawater properties used include DMS, iodide, particulate fatty acids, CDOM, and total Chlorophyll-a (Chl-a) concentrations and flow cytometry and microscopy measurements to characterise the plankton population. See Chapter 2.1 for more details on these measurements.

3.1.3 Modelling of iodine sea-air fluxes and iodine oxide particles

Previous laboratory studies have established that sea-air fluxes of inorganic iodine species (primarily I₂ and HOI) depend on the iodide concentration in the seawater, the gas phase ozone concentration and the wind speed (Carpenter et al., 2013; MacDonald et al., 2014). These studies developed empirical equations based on the above parameters, the inclusion of which helped to model the observations of reactive iodine species in the field in the past (Lawler et al., 2014). In order to test whether emissions of inorganic iodine species could account for the number

and size of particles observed during the current study, we performed model simulations using a box model based on the Tropospheric HALogen chemistry Model (THAMO) (A. Mahajan et al., 2010; Saiz-Lopez et al., 2008). The sea-air fluxes of I₂ and HOI were computed using the observed ozone and iodide concentrations and a constrained wind speed of 1 m s⁻¹ (the wind speed inside the mesocosms). Further details of the model set-up, chemistry and rates of particle coagulation and growth are available in past works (A. S. Mahajan, 2009; A. Mahajan et al., 2010; Sellegri et al., 2016). We model the size and number of particles formed in different scenarios mimicking the mesocosms, covering a range of iodide and ozone concentrations observed through the study.

3.1.4 Data processing

It should be noted that as the mesocosms were not entirely leak proof, there is a possibility of small contamination from outside air. To take this into account, we investigated the diurnal variation of the ratio of N₁₀ in the mesocosm headspace (N_{10_{mesocosm}}) to N₁₀ in ambient air (N_{10_{ambient}}). The diurnal variation of the ratio of N_{10_{mesocosm}} to N_{10_{ambient}} shows a minimum between 4 am and 6 am for most of the days and we assumed that the level of maximum contamination from ambient air can be calculated during this period of time when the source of N₁₀ within the mesocosms headspace seems the lowest. The average ratio of N_{10_{mesocosm}} to N_{10_{ambient}} was $7.4 \pm 4.1\%$ during this period of time. We thus subtracted this percentage of the ambient air concentrations of N₁₋₃, N₃₋₁₀, and N₁₀ from the mesocosm headspace concentrations of N₁₋₃, N₃₋₁₀ and N₁₀, similar to the subtraction of a blank value. This subtraction occasionally led to negative concentrations. In order to get rid of the nonphysical negative values found in the data set, the median of the negative values for a given day was subtracted from the aerosol concentrations of that day and this was used as an error estimate.

3.2 Results and discussion

3.2.1 Aerosol number concentrations

On the first three days of the experiment, when we can assume that the biological populations have not yet changed due to the differences in the temperature and pH conditions, the daily median concentrations of N₁₋₃ and N₃₋₁₀ were below 500 cm⁻³ in all three mesocosms (Fig. 3.1). After this, the concentrations rose in all the mesocosms and had their first peak between days 10–14 and a second peak around days 19 and 20. Over the whole measurement campaign the median N₁₋₃ concentrations were 474 cm⁻³ (range between 25th and 75th percentiles 200–1020 cm⁻³) for M₇, 570 cm⁻³ (240–1270 cm⁻³) for M₈ and 730 cm⁻³ (320–1700 cm⁻³) for M₉. While the concentrations are in similar ranges for all three mesocosms, the treated mesocosms had on average higher particle concentrations.

Observing particles in the sub-3 nm size range inside the mesocosm headspace with concentrations significantly higher than 10% of the ambient air concentrations indicates that nucleation is happening inside the mesocosms headspace from precursors emitted from the seawater. The day to day variations indicate that the concentrations of aerosol precursors are varying, possibly due to the changes in the biological and chemical properties of the seawater. The differences between mesocosms indicate that warmer and more acidic conditions seem to favour the emission of new particle formation precursors. Also for N₃₋₁₀ the concentrations were in general higher in the treated mesocosms with median N₃₋₁₀ over the whole measurement period being 240 cm⁻³ (120–580 cm⁻³) for M₇, 370 cm⁻³ (150–960 cm⁻³) for M₈ and 400 cm⁻³ (180–1120 cm⁻³) for M₉. N₁₀ had a slightly different time evolution than the smaller particles, and it shows a peak in concentrations in all mesocosms already on day 7, but after that the trends in concentrations are more similar to those of the smaller particles. Even though the time evolution of N₁₀ does not follow exactly the same pattern as N₁₋₃ and N₃₋₁₀, its median values

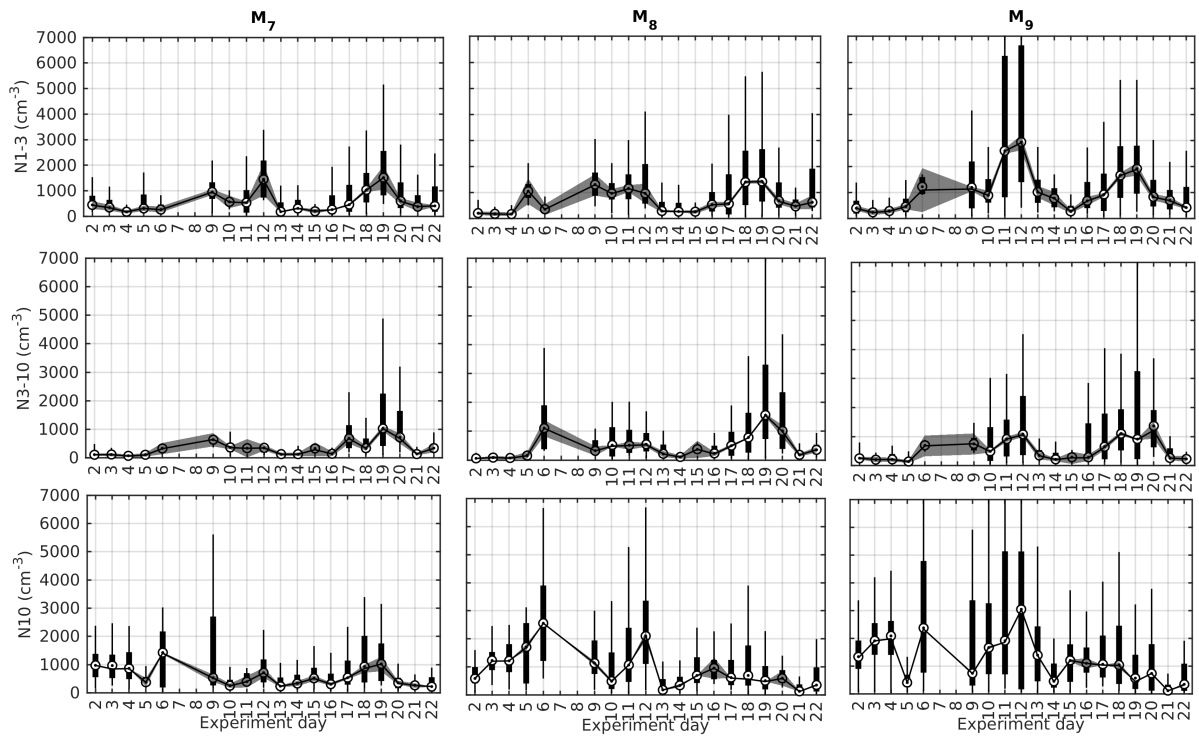


Figure 3.1: Time evolution of aerosol particle number concentrations in different size ranges in the different mesocosms. N1-3 stands for 1-3 nm particles, N3-10 for 3-10 nm particles and N10 for particles with diameters above 10 nm. Circles indicate the median values for a given day, boxes show the 25th and 75th percentile of the data and whiskers include 99.3% of the data. The grey shaded area describes the uncertainty of the values as described in the data processing section

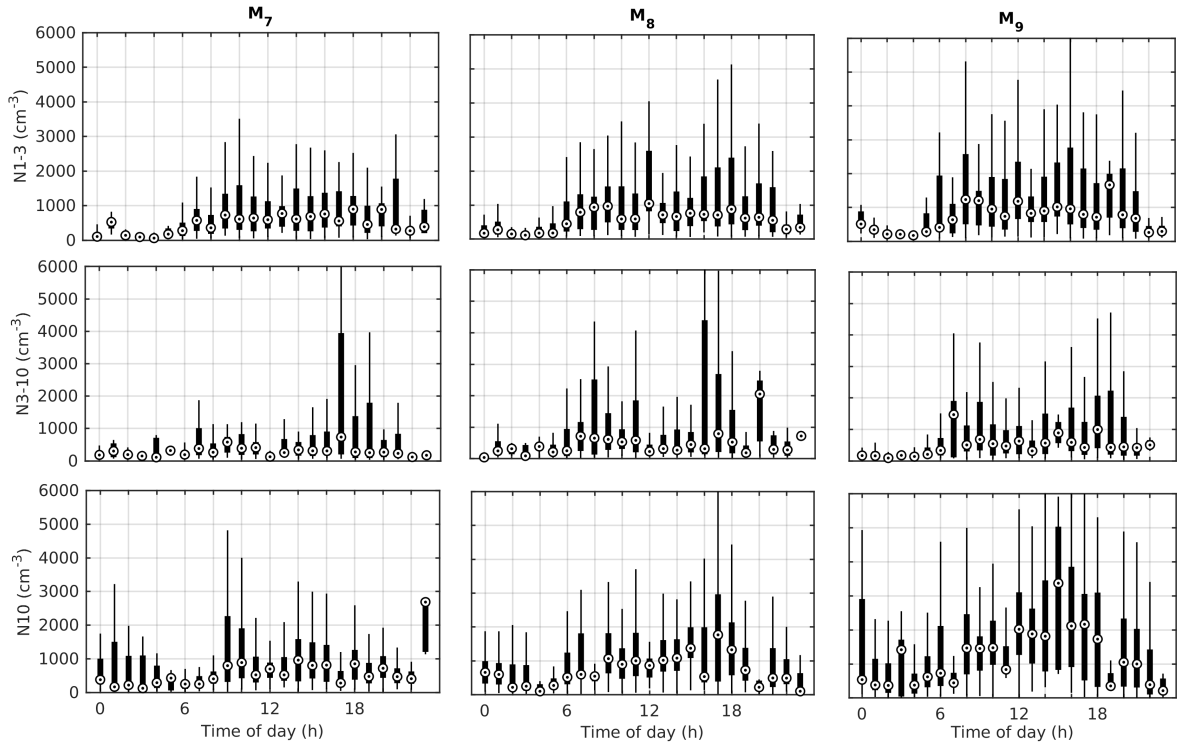


Figure 3.2: Diurnal cycles of aerosol number concentrations in different size ranges in the different mesocosms. N1-3 stands for 1-3 nm particles, N3-10 for 3-10 nm particles and N10 for particles with diameters above 10 nm. Circles indicate the median values for a given day, boxes show the 25th and 75th percentile of the data and whiskers include 99.3% of the data.

are also higher for the treated mesocosms with particle concentrations of 500 (240–1080), 740 (320–1470) and 1090 (360–2270) cm^{-3} for mesocosms M_7 , M_8 and M_9 , respectively.

Figure 3.2 shows that in the sub-10 nm size ranges the number concentrations follow a clear diurnal cycle. During the night between 22–06 LT the median hourly concentrations stay below 600 cm^{-3} while during the day the medians reach values as high as 2000 cm^{-3} . The daytime concentrations show a bi-modal behaviour for all size classes, with one peak of concentrations appearing between 8–13 LT and a second peak between 18–21 LT. Surprisingly, the N10 concentration has an additional third peak at night (0–4 LT). A similar diurnal variation of cluster particles formed in a mesocosm headspace has already been reported by Sellegri et al. (2016), with two daytime maxima, one in the morning and the other in the late afternoon. The diurnal cycle of cluster mode particles could be at least partly explained by solar radiation, because radiation can produce oxidisers, trigger photosensitized reactions and create stress to the plankton which could increase the production of different chemical species by the plankton. However, the diurnal cycle of particle concentrations does not fully follow that of radiation and other parameters have to be involved. In particular, the N10 concentration has an additional third peak at night (0–4 LT). The fact that only particles larger than 10 nm show a peak, without sub-10 nm particle concentrations increasing can only be explained by losses of smaller clusters being higher in the sampling lines than for the larger particles. For small enough concentrations this would lead to a complete loss of cluster mode particles in the lines, preventing for any losses correction. Similar issues have been observed in ambient measurements where instrument sampling through a longer inlet lost particles in smallest size ranges while another instrument with shorter inlet was able to observe them (Kremser et al., 2020). In order to explain the variations in aerosol concentrations, next we will compare the aerosol concentrations to sunlight and different chemical and biological variables.

3.2.2 Factors explaining aerosol concentrations

As a diurnal cycle was seen for the aerosol concentrations and radiation is known to be important for photochemical processes, let us first see if photosynthetically active radiation levels can explain part of the variations in particle concentrations. The number concentrations in all size bins and all mesocosms show a positive correlation with photosynthetically active radiation (Fig. 3.3). Even though all the number concentrations correlate positively with radiation, radiation data explains only a minor fraction of the variability in the number concentrations (correlation coefficients between 0.23 and 0.4, $p < 0.05$). This means that other factors have to play a role in aerosol production and that is why next we will investigate its relation to different chemical and biological variables.

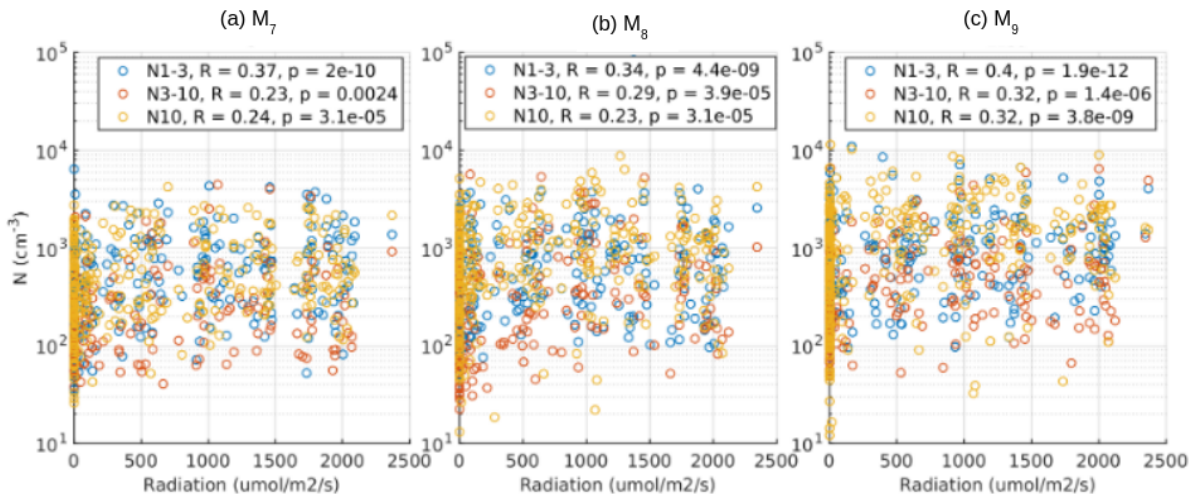


Figure 3.3: Particle number concentrations in different size ranges in different mesocosms as a function of radiation.

3.2.3 Connection to chemistry

During the ME3 campaign the only measured gas phase chemical compound was ozone and as it was also measured more often than once a day, it was the first chemical species we explored. Ozone is important for aerosol formation because it can act as an oxidiser and react with different chemical species producing aerosol precursor vapours (e.g. Rose et al., 2018). Ozone concentration is itself strongly linked to solar radiation and often has a clear diurnal cycle. In marine air masses boundary layer ozone concentration often has a minimum in the daytime and a maximum during the nighttime as during the day ozone is destroyed in photochemical reactions close to the sea surface and during the night more ozone enters the boundary layer from the free troposphere (see e.g. Ayers et al., 1992). This cycle was observed also during our campaign in ambient air (Fig. 3.4).

In the mesocosms the diurnal cycles were very different from the ambient air and the values were generally very low and below 15 ppbv, indicating that ozone is likely reacting with species in or emitted from seawater. Contrary to ambient air, in the mesocosms the nighttime concentrations were even lower than the daytime concentrations, meaning that ozone was likely completely consumed in the mesocosms during nighttime. The fact that ozone concentrations were higher in the mesocosms during the day than during the night could also mean that during the day ozone was either less reacting than during the night, or also produced within the mesocosm headspace. Given that the ozone concentrations were low during the whole campaign, ozone was possibly a limiting factor for particle formation within the mesocosms. One thing

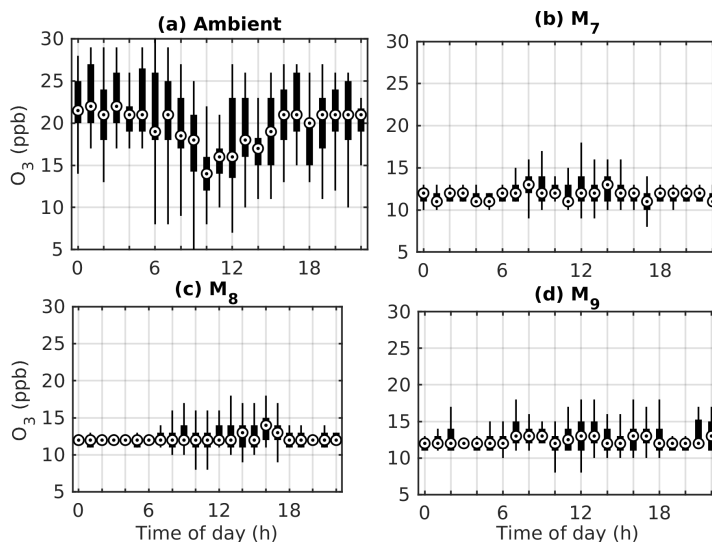


Figure 3.4: Daily cycle of ozone in the ambient air (a) and the different mesocosms (b-d). Circles indicate the median values for a given day, boxes show the 25th and 75th percentile of the data and whiskers include 99.3% of the data.

that has to be taken into account when looking at ozone, is that ozone could have been also lost in the walls of the inlet lines and the mesocosm headspaces. This could partly be responsible for the low ozone values observed in the mesocosms, but as losses should be constant in time within the lines and walls, it can not explain the different diurnal variability of ozone within the mesocosm headspace compared to ambient air.

Figure 3.5 shows the connection of particle formation to different chemical species by comparing Pearson’s correlation coefficients between the particle concentrations and the chemical species. As the seawater samples were taken only once a day in the morning and aerosol concentrations showed clear diurnal cycles, we compare the concentrations of different species to the aerosol concentration medians taken over the morning (6–12 LT), afternoon (16–21 LT), and nighttime (0–4 LT) of each day. To increase the number of comparable data points and explore processes, results from all the three mesocosms have been combined when calculating the correlation coefficients. Because ozone concentrations in the mesocosms headspaces are the result of reactions with chemical species, we chose to rather investigate the relationship with ozone entering the mesocosms headspace, i.e. ambient air ozone. Both N1–3 and N3–10 have negative correlations with entering ozone during the morning. The negative correlations between ambient ozone and sub 10 nm particles could result from the fact that UV-radiation is responsible for both ozone destruction in ambient air and photo-oxidation of cluster precursors within the mesocosm headspace. This would indicate that the oxidation processes responsible for the production of the morning peak cluster precursors are linked to OH radical chemistry rather than ozone chemistry. On, the contrary, the nighttime N10 concentrations are correlated to nighttime ozone, which indicates that ozone chemistry would contribute to aerosol formation and growth at night when no radiation is available. We did not find any correlation of nighttime N1-3 or N3-10 with ozone, presumably because growth is fast and cluster concentrations are also easily lost in sampling lines compared to particles larger than 10 nm.

Next we look into the chemical properties of the seawater for further links to new particle formation. Since previous work has shown that seawater DMS (DMS_{sw}) and iodide are playing a role in NPF in marine environments, we studied if the seawater concentrations of these species are related to aerosol concentrations. First three rows of Figure 3.5 show that the morning aerosol concentrations do not show significant correlations with DMS_{sw} . This is not surprising as the time scale over which seawater DMS transforms to gas phase precursors and then to aerosol

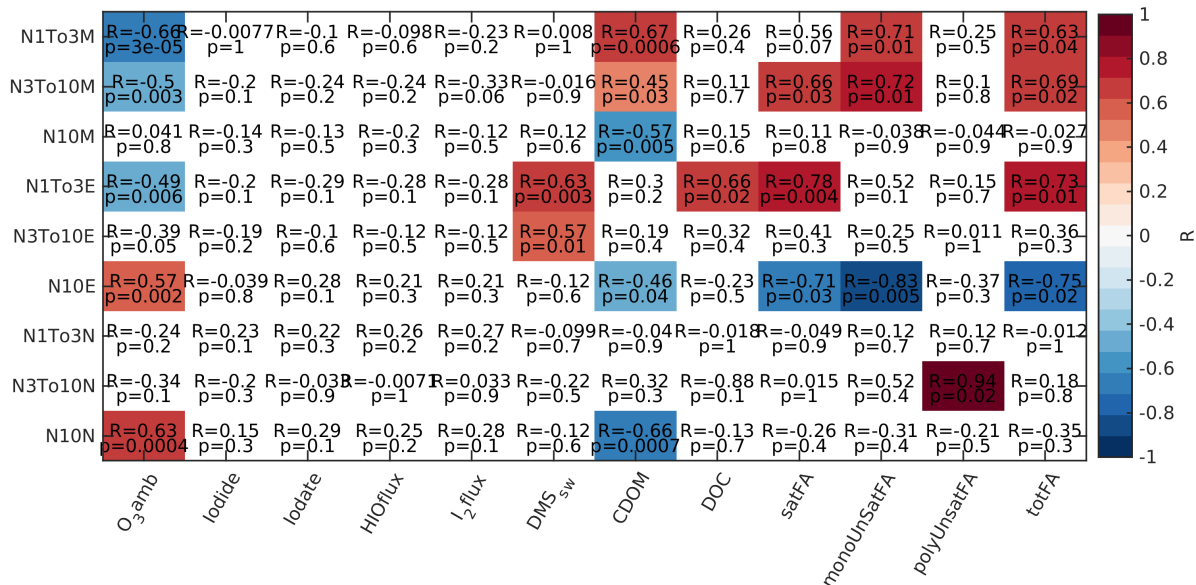


Figure 3.5: Correlations of particle number concentrations (N1-3, N3-10 and N10) in different size ranges during different times of the day (M = morning (6-12 h), E evening (16-21 h), N = night (0-4 h)) with ozone and chemical properties of water. Each square corresponds to the correlation coefficient between the variables on the x- and y-axes and the colour indicates the strength of the correlations with the square being white if p-value was above 0.05.

phase is expected to be longer than the residence time of air in the mesocosms. However, we do find a correlation of the afternoon peak of N1-3 and N3-10 particle concentrations and DMS in the seawater (Fig. 3.5 fourth and fifth row). A recent study by Veres et al. (2020) is revealing a new DMS OH oxidation pathway leading to hydroperoxymethyl thioformate (HPMTF) and suggests that HPMTF is linked to NPF. The presence of HPMTF at altitudes below 2 km indicates that the reaction is faster than the conventional oxidation pathway. On the other hand, Wollesen de Jonge et al. (2021) saw modelled that formation of HPMTF would rather be a sink of sulfur and reduce the formation of secondary aerosol rather than increase it. In our data set, none of the particle concentrations are linked to DMS during nighttime, which is consistent with the absence of an efficient oxidation pathway of DMS involving ozone. We do not explain why the morning sub-10 nm particle concentrations would not be connected to DMS while the evening concentrations are.

No significant correlations can be seen between seawater iodide or iodate and N's of any of the morning, evening or nighttime peaks. The emissions of iodine from seawater to gas phase are also complex and depend on various variables, including ozone. Therefore, we checked how the concentrations of modelled gas phase iodine species (I₂ and HOI) fluxes, correlate with N's. When comparing the I₂ and HOI fluxes with N's during different times of the day, no significant correlations were observed either. The lack of correlations with the modelled gas phase iodine species fluxes indicates that other chemical species were likely involved in particle formation and growth.

We used the model also to study what levels of particles could have been produced from seawater iodine in the mesocosm conditions. The results indicate that the model can reproduce sufficient particles in the size range of 1–3 nm as observed in the experiments (100-6000 particles cm⁻³) at inorganic iodine fluxes that are expected for the range of observed iodide (40–70 nM) and ozone (15-30 ppbv) concentrations. The model also suggests that there is a threshold of inorganic iodine fluxes below which new particle formation would not occur. A combination of seawater iodide greater than 40 nM and gas phase ozone mixing ratios larger than 15 ppbv are necessary to sustain a flux of I₂ and HOI large enough to result in coagulation rates fast enough

to cause iodine oxide particle formation. Similar observations have also been made in the field, where results suggested that iodine oxide levels in the atmosphere need to be > 8 pptv to lead to CCN (>20 nm) sized particles composed primarily of iodine compounds (A. Mahajan et al., 2010). Also in a previous mesocosm nucleation study, it was shown that a threshold of iodine concentrations was observed below which particle cluster formation was a tenfold lower than above this threshold (Sellegrì et al., 2016), confirmed by a modelling exercise defining a gas-phase total iodine threshold of 0.8 pptv. Since ozone concentrations in the mesocosms headspaces did not reach higher values than 15 ppbv, iodine is not expected to play a determining role in the formation of clusters observed in the present experiments, and other precursors should be involved.

In addition to sulphur species and iodine, organic compounds may be involved in NPF. Brean et al. (2021) evidenced that amines could be, in association with sulfuric acid, at the origin of open ocean NPF events. During the evening, N1-3 is correlated to DMS_{sw} , but actually also correlates positively with DOC. Mungall et al. (2017) observed during a ship campaign in the Arctic that emissions of oxidised VOCs (OVOC) correlated with seawater DOC, so the correlation between DOC and N1-3 could also be explained by OVOCs formed from DOC and the OVOCs further forming SOA. Recent studies have shown that fatty acids on the sea surface can be a source of new particles in sunny conditions (Bernard et al., 2016; Alpert et al., 2017). During our mesocosm experiment we only had access to particulate fatty acids. Relationships between particulate and dissolved fatty acids reported in the literature usually show that the polyunsaturated fatty acids are usually depleted in the dissolved phase compared to the particulate phase (Goutx and Saliot, 1980; Kattner and Brockmann, 1990). This was attributed to decomposition by photolytic and oxidising splitting of the DOC (Goutx and Saliot, 1980) and phytoplankton decay phases (Kattner and Brockmann, 1990). In Figure 3.5, we compare the particle concentrations to particulate saturated and unsaturated fatty acids present in the seawater. The evening N1-3 concentrations are correlated to the total fatty acid concentrations, and among these, particularly the saturated fatty acids, that would support the findings by Bernard et al. (2016) and Alpert et al. (2017). When looking at the morning peak values, correlations can be found between both N1-3 and N3-10 particle concentrations and total particulate fatty acid concentration in the seawater, with contributions from both its saturated and monounsaturated fractions. We found that the particulate saturated fatty acids concentrations correlated to surface tension decrease ($R = 0.66$, $p < 0.01$), indicating that they have surface active properties and hence may be enriched in the surface microlayer (SML), directly photo-oxidized. It has been shown by Freney et al. (2021) that a class of sea spray organic matter, containing a mixed signature of amino acids and fatty acids, was connected to DOC enrichment in the SML from Mediterranean seawater.

For the evening peak, N10 are found anti-correlated with fatty acids. One possible explanation for the observed anti-correlation is that an enriched SML can play the role of a screen for the transfer across the air sea interface of more volatile dissolved VOCs. Experimental studies have indeed revealed substantial suppression of the bulk gas transfer velocity of various gases by surfactants in the laboratory (see e.g., Mesarchaki et al., 2015) and in the field (see e.g., Salter et al., 2011) and the SML has been shown to suppress the emissions of inorganic species from the bulk seawater (Tinel et al., 0000). These dissolved VOCs are likely too volatile to play a role in the formation of clusters, but condensable enough for growing already formed clusters. The fact that N10 correlates with ambient ozone at night, indicates that ozonolysis is the most likely process for the formation of vapours contributing to the growth of the particles to larger sizes at night.

To summarise, we find a relationship between sub-10 nm particles concentrations formed in the morning and particulate fatty acids in the seawater during this experiment, with indications that these particles are rather formed via photochemistry than ozonolysis. Ozone is showing a strong depletion during these hours of the day and it is hence likely playing a minor role. In the

early evening, our hypothesis is that small clusters are formed from several compounds, including the oxidation of the dissolved organic matter present in the seawater, again formed from reactions with saturated fatty acids. At the seawater interface possibly both photo-oxidation and ozonolysis are involved in the evening formation of new clusters. These clusters are however prevented from growing to sizes larger than 10 nm by the presence of these fatty acids in the SML that form a screen preventing more volatile dissolved VOC from volatilising. At night, ozonolysis is the process forming vapours that contribute to the new particle growth. At night clusters are not detected as they are formed in lesser quantities than during the day.

3.2.4 Connection to biology

In order to study which plankton species or groups could be responsible for producing particle forming chemical species, we compared the aerosol number concentrations also to biological populations in the seawater. The evolution of the plankton population during the experiment can be divided into three phases based on chlorophyll-a (Chl-a) data (Fig. 3.6). During the first eight days, the population adjusted to the new conditions, then during the next seven days the Chl-a biomass stayed rather constant and for the rest of the experiment it increased. The biomass was dominated by diatoms and the most abundant diatom was *Cylindrotheca closterium* (see, A. D. Saint-Macary et al., 2021). Other abundant plankton species during the experiment were *Pseudo-nitzschia*, *Skeletonema* and *Protoperdinium bipes*.

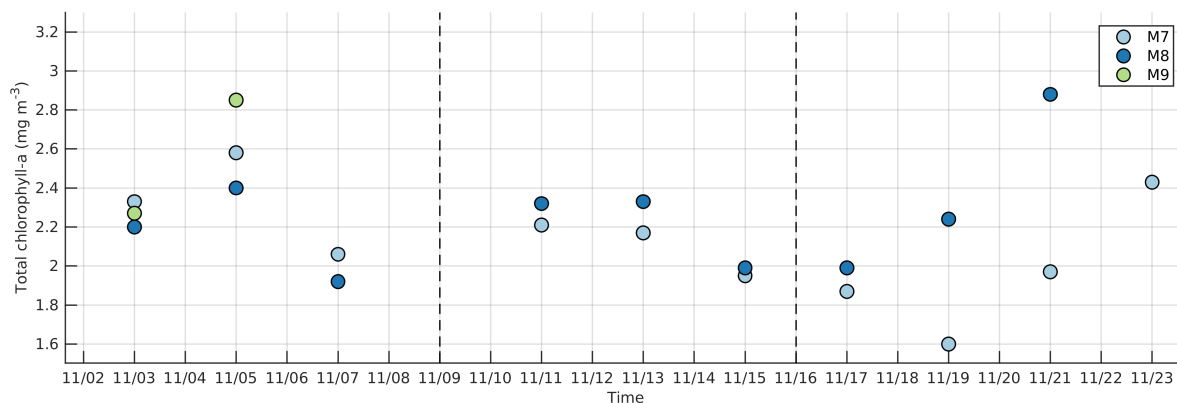


Figure 3.6: Time evolution of total chlorophyll-a during the experiment in the three mesocosms. The vertical lines mark the phases of the experiment.

Figure 3.7 summarises the correlations that the morning, evening and night medians of aerosol concentrations have with different plankton classes, heterotrophic bacteria and Chlorophyll-a. For the plankton species and divisions we used carbon content instead of cell number to get a better image of the total biomass of each group. We can see that, among all biological species analysed, morning and evening N1–3 have positive correlations with the eukaryotic nanoplankton cell abundance, indicating that species in the eukaryotic nanoplankton group could be emitting vapours or producing organic components that could be oxidised and participate in particle formation. The anticorrelation between N1–3 and micro-organisms of the pico size (eukaryotic and prokaryotic) is likely the result of the competition between nanophytoplankton and picophytoplankton across the experiment. The eukaryotic nanophytoplankton cell abundance is also correlated with particulate saturated fatty acids concentrations in the seawater ($R = 0.71$, $p = 0.01$). The same plankton group has been earlier identified as a producer of CCN from sea spray aerosol, via its role in producing an organic class with a fatty acid signature and also surface active properties particularly linked to the SML (Sellegrì et al., 2021). Among the nanophytoplankton group, a relationship with the diatom *Cylindrotheca closterium* suggests

that this group is particularly responsible for production of monounsaturated fatty acids in the morning.

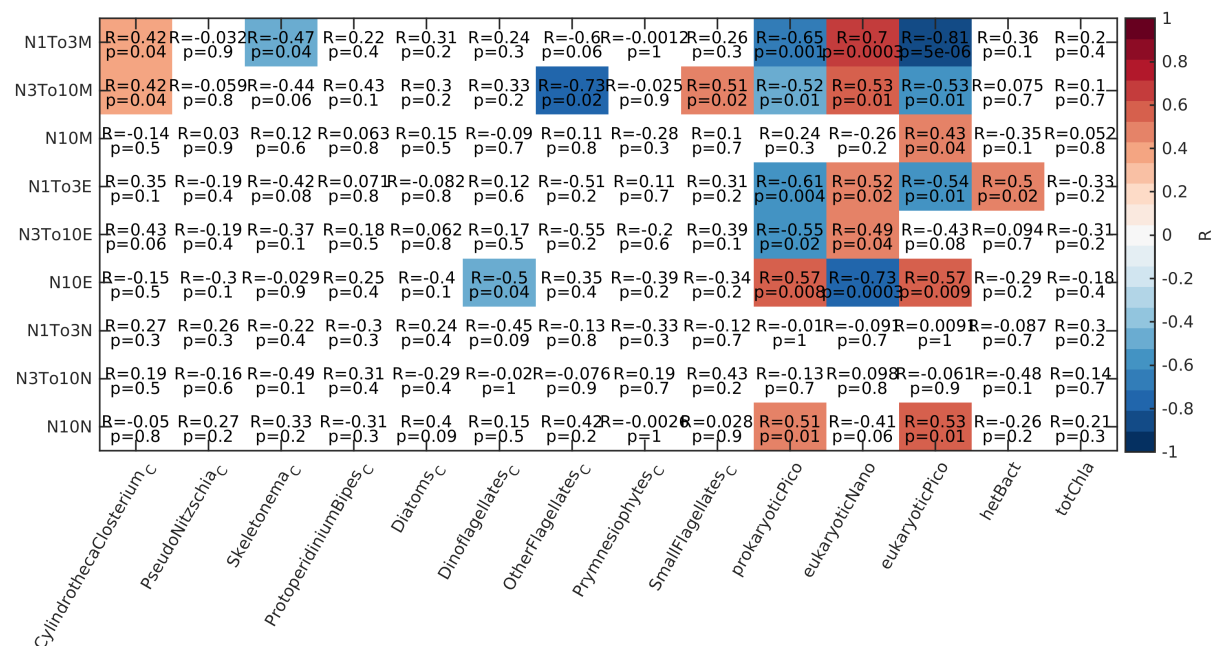


Figure 3.7: Correlation coefficients of aerosol number concentration (N) in different size classes with carbon content of different plankton species and divisions, plankton groups and heterotrophic bacteria and Chl-a when using the median of the morning (M), evening (E) and night (N) values for N's. Each square presents the correlation coefficient between the variables at x- and y-axes. The colour indicates the strength of correlation and statistically insignificant values ($p > 0.05$) are white.

When looking at the correlations of morning N3–10 concentrations with the biological variables, the positive correlation between N3–10 and eukaryotic nanoplankton is weaker than between N1–3 and eukaryotic nanoplankton. Instead, N3–10 has a positive correlation with small flagellates that was not significant for N1–3. This suggests that different phytoplankton groups may contribute differently to the formation of clusters and their early growth with the emission of different precursors of slightly different volatilities.

The correlations between biology and particles larger than 10 nm in diameter differs from those of N1–3 and N3–10, even though in the morning N10 is weakly correlated to N1–3 and N3–10 from which the particles have grown (correlations coefficients for N10 0.42 with N1–3 and 0.30 with N3–10, $p < 0.05$). N10 has a positive correlation with eukaryotic picoplankton. Eukaryotic picoplankton may emit species that are oxidised to higher volatility classes compared to the ones emitted by the nanoplankton class, and thus participate to the growth of clusters rather than their initial formation.

For the evening peaks, we find primarily the same relationship between number concentration in different particle size classes and biology as for the morning concentrations. This would indicate that the difference between morning and evening peaks lies in the oxidation mechanisms rather than in the nature of the emissions. Another possibility is that emissions differ from the same species between morning and evening, due to a change in the type of stress, such as UV light, that the species experience across the day. At night, the rapid growth of sub-10 nm particles to larger sizes is again correlated to the presence of picophytoplankton.

When interpreting these results, one has to keep in mind that the mesocosm environment differs from the ambient environment in many ways. First, the emissions from seawater are mixed into a smaller volume of air than they would be if they were mixed in the marine boundary

layer which can be hundreds of meters or even some kilometres high and thus the concentrations of potential aerosol precursors can be elevated. On the other hand, the time that the seawater has to interact with air is shorter and the lack of wind would minimise air-sea exchanges and the result of these opposite effects on VOC fluxes to the atmosphere is not clear. Second, as the air in the mesocosm headspace is constantly flushed and the air coming into the mesocosm is filtered from particles, the pre-existing particle population that acts as a sink for the condensing vapours is lower in the mesocosm headspace compared to the ambient air. On the other hand, the mesocosm walls can act as an additional sink for both condensing species, oxidisers and particles. Again, it is not clear whether these conflicting effects are resulting in an increase or decrease of nucleation rates compared to the ambient atmosphere. It should be also noted that in the real atmosphere the time scales are longer, which means that there is time for more complex processes and for the particles to grow.

The results of this experiment cannot thus be directly generalised into the ambient atmosphere but they do give us hints of the role of biological species in the formation of marine aerosols. The differences in correlations during different times indicate that the aerosol forming processes are not straight forward and more measurements are needed to fully understand the role of different species in NPF in the South-West Pacific Ocean area.

3.3 Conclusions

When predicting the future climate, we need to know how increasing temperatures and ocean acidification will affect marine biology and consequently the aerosol production from marine sources. In this chapter, we studied the formation of aerosol particles from seawater emissions and examined the relationship of particle formation with different biological species and chemical properties of seawater. We used three mesocosms with one of them serving as a control mesocosm and the two other ones having altered temperature and pH. We measured aerosol particle number concentrations down to 1 nm and observed that their formation has a clear diurnal cycle with low nighttime and high daytime concentrations. Three peaks of particles were detected in the diurnal variations: one in the morning and one in the evening for all particle sizes and one smaller peak of particles larger than 10 nm during the night. The particle concentrations varied over the duration of the experiment and highest daily median particle concentrations were observed in the treated mesocosms.

We detected a positive correlation between the concentrations of 1–3 nm particles and the concentration of eukaryotic nanoplankton in the morning and afternoon, indicating that this type of plankton could be a possible emitter of aerosol precursor vapours. Analysis with seawater chemical properties showed indications that fatty acids or other organic compounds in the water could be a possible source of particle forming vapours. On the other hand, the concentration of particles with diameters above 10 nm showed a positive correlation with eukaryotic picoplankton for evening and nighttime concentrations. The fact that different species correlated with under and over 10 nm sized particle concentrations could mean that the phytoplankton groups influencing formation and growth of particles were different. Ozone concentrations were connected to the concentration of over 10 nm particles indicating a role of ozone in the growth of the particles. Comparison to seawater inorganic iodine-related content and fluxes did not directly explain the sources of aerosol particles, and we identified that ozone was likely a limiting factor for iodine chemistry responsible for nucleation in this ozone-poor environment.

Interpreting the impact of future environmental changes, such as temperature increase and ocean acidification, on new particle formation process is to be taken with caution, as one of the three mesocosms had water leakages. Seeing differences in particle concentrations between the different mesocosms does however indicate that environmental changes could have an influence on particle formation. When interpreting these results one has to keep in mind that the mesocosm environment differs from the ambient environment in many ways. First, the emissions

from the seawater are mixed into a smaller volume of air than they would be if they were diluted in the marine boundary layer and thus the concentrations of potential aerosol precursors can be higher. On the other hand, the lack of wind in the mesocosms would minimise air-sea exchanges and the result of these two opposite effects on VOC fluxes to the atmosphere is not clear. Second, as the air in the mesocosm headspace is constantly flushed and the air coming into the mesocosms is filtered from particles, the pre-existing particle population that acts as a sink for the condensing vapours is likely lower in the mesocosm headspace compared to the ambient air. On the other hand, the mesocosm walls can act as an additional sink for both condensing species, oxidisers and particles. Again, it is not clear whether these conflicting effects are resulting in an increase or a decrease of particle formation compared to the ambient atmosphere. It should be also noted that in the real atmosphere the timescales are longer, which means that there is time for more complex processes and for particles to grow. Additionally, some particle formation precursor gases may have entered the mesocosm headspaces from ambient air. However, the level of concentrations measured within the mesocosm headspaces, the differences in concentrations between control and treatment mesocosms, and the correlations to biological and chemical compounds of the mesocosm seawater indicate that the main precursors to particles measured in this study do originate from the mesocosm seawater. The results of this experiment cannot thus be directly generalised into the ambient atmosphere but they do provide hints of the role of marine biogeochemical influences on formation of marine aerosols. The differences in correlations during different times of the day indicate that the aerosol forming processes are not straight forward and more research is needed to fully understand these processes. The next chapter introduces more advanced experiments to understand these phenomena. For that work, we used tanks specifically designed to study air-sea interactions and had more instrumentation available.

Chapter 4

Air-Sea Interaction Tanks

Since the ME3 campaign had many limitations, during this thesis we built two so-called Air-Sea Interaction Tanks (ASIT) that were specifically designed to study air-sea interactions and new particle formation from marine emissions. The Air-Sea Interaction Tanks had almost 5 times larger headspaces than the tanks of ME3. This way we could increase the average residence time of air in the headspace, allowing more time for chemical reactions and the use of more instrumentation with higher total flow rate. The instruments that we used with the ASITs were able to measure both aerosol concentrations and the chemical composition of volatile organic compounds and molecular clusters. Especially the instruments measuring the chemical composition of molecular clusters require higher flow rates which would not have been possible with smaller headspace.

Another benefit that the ASIT experiments had compared to the ME3 experiment is that we were able to take the tanks out to sea on board RV Tangaroa, which allowed using open ocean seawater from different locations rather than only coastal seawater. One difference compared to the ME3 experiment was also that now we added extra ozone to one of the tanks. This was done to study the effect of ozone on chemical reactions in the headspace and seawater surface. One of the reasons this was interesting is that in the ME3 experiment we observed ozone depletion in the mesocosms. This chapter describes the ASIT design, the experimental setups used and gives an overview of the results obtained with the ASITs.

4.1 Experimental setup

This section describes the design of the Air-Sea Interaction Tanks (ASIT) and the experimental setups used with them. Compared to the ME3 experiment in which the tanks were originally designed for only biological experiments, the ASITs were specifically made for studying sea-atmosphere interactions. The ASITs were made during my thesis and I participated in designing and building the tanks and tested them myself.

4.1.1 Tank design

Figure 4.1 shows the basic structure of the ASITs. We built 2 tanks that each had a total volume of 2000 l. The volume was chosen because it was the largest practical volume available. The tanks both consisted of the 2000 l containers made out of plastic, a lid, baffles, support structure and inlets for needed water and air flows. The idea of the baffles at the bottom of the tank was to prevent the water from moving too much during the time on the ship, since we wanted to avoid sea spray generation. The red support structure was made of the same material as the lid and it both kept the baffles in place and supported the weight of the lid. The lid had a hatch (shown in grey in the top left sketch of Figure 4.1) that allowed for sea surface sampling.

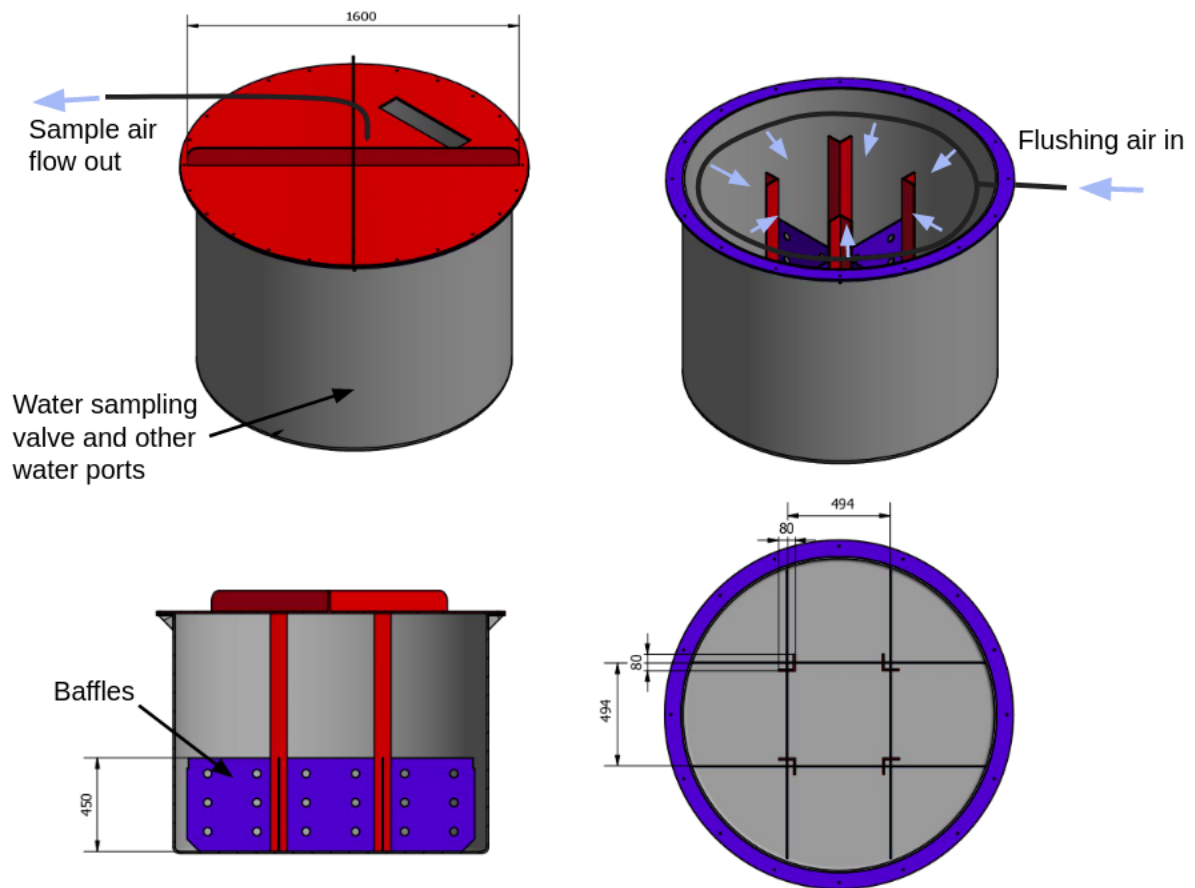


Figure 4.1: The design of the Air-Sea-Interaction Tanks. Figure modified from a figure by from Neill Barr and Thermoplastic Engineering Limited. The measures are in millimetres.

The lid was made of Poly (methyl methacrylate) (PMMA) and it was not UV-transparent to allow a fraction of sunlight including UV which is important for atmospheric chemistry to pass through the lid. The level of light was monitored with several different sensors. Both tanks had four light sensors, one at each corner, in order to compare the levels of light in the two tanks. Additionally we measured UV-A and UV-B at one spot outside the tanks and had one light sensor inside each tank to estimate the amount of light that passes the lid.

The bottom half of each tank was filled with seawater leaving the upper 1000 l for air. In order to avoid contamination from the plastic walls of the tank, the walls were covered with a teflon film that was attached to the wall with double-sided tape and squeezed at the top between the tank and the lid. The teflon only covered the top part of the walls as the bottom was always under water. No contamination of the seawater with the plastic part of the tank that it was in contact with was observed, as the seawater dissolved VOC content in the ASITs matched the VOC content of seawater sampled away from the ship using a work boat (Rocco et al., 2021).

The seawater was sampled through a tap at the side of the tank. The water connections also included a cooling system to keep the water from heating above ambient seawater temperature. The cooling system consisted of two metal pipes that ran through the tank walls, at the same level as the water tap. The pipes had cold water running through them and the temperature of this water was controlled with a thermostat. At land we did not use the baffles but instead we mixed the water by taking water from one side of the tank and pushing it in on the other side so that the plankton wouldn't get settled at the bottom of the tank. At sea this additional mixing was not used since the movements of the ship moved the water and the experiments were relatively slow.

The air sampling was through a 1/4" stainless steel bulkhead fitting that was connected to 3/8" stainless steel tubing. The inlet was placed on top of the tank close to the intersection of the two supporting structures of the lid. The length of the tube inside the tank was approximately 10 cm. This was a compromise between minimising inlet length and ensuring that we sample well mixed air rather than the air just next to the lid.

For the in-going flushing air we used another 1/4" stainless steel bulkhead fitting that went through the side of the tank close to the top. Inside the tank, the fitting was connected with a T to 1/4" teflon tubing that circulated the whole tank as illustrated on the top right figure of Fig. 4.1. In this teflon tubing, we drilled small holes at even spaces through which the flushing air entered the tank. The holes were facing down to ensure that the air gets mixed as evenly as possible.

The air going into the tanks was pushed there by pumps. For most of the experiment the used flow rate was 25 lpm. This was slightly higher than the flow going from the tanks to the instruments. This was done to ensure that no air other than the flushing air would enter the tanks in case there was a leak. To compensate for this excess flow, the hatch had a valve which was kept open to let the excess flow out. The valve was connected to a particle filter to assure that if there was a problem with the flows and the direction of the flow turned inwards, we would still not get any aerosol contamination. To make sure that the tank would not break in case the pressure inside the tank dropped or increased radically, the hatch had pressure relief valves to both directions.

For one of the tanks, we also added ozone. This was done through a simple stainless steel bulkhead fitting going through the wall of the tank opposite to the fitting of the general flushing air. It was not connected to the circular flow system due to pressure handling issues with the generator. When additional ozone was used, the flow rate of flushing air coming from the pump was lowered to 17.5 lpm and the flow rate coming from the ozone generator was 7.5 lpm with an ozone concentration of 100 ppb.

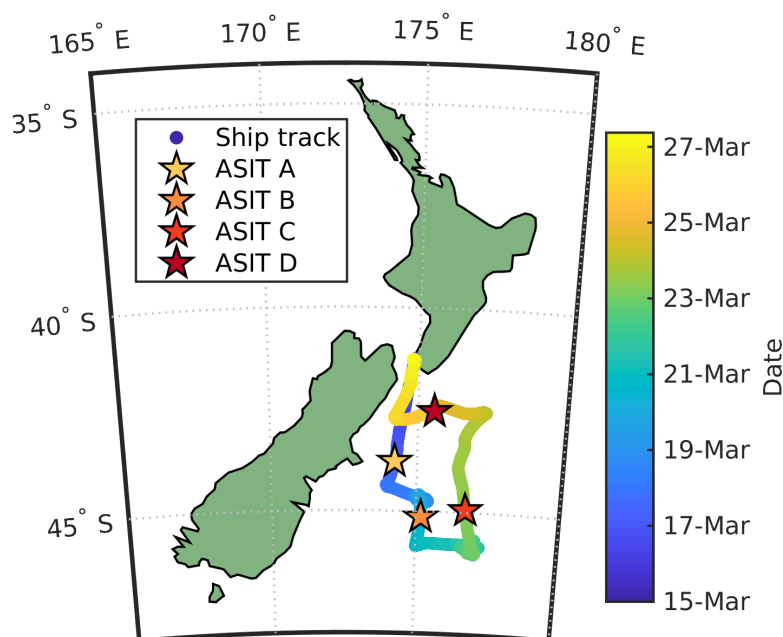


Figure 4.2: The track of the ship coloured by time with the start locations of the ASIT experiments marked with stars.

4.1.2 Experiments on board RV Tangaroa

The primary experiments with the ASITs were done during the Sea2Cloud voyage on board NIWA’s RV Tangaroa in March 2020. One of the main objectives of doing experiments on board Tangaroa was to obtain open ocean seawater with different biological populations from different locations. The ASITs were filled by pumping in seawater simultaneously to both tanks. They were flushed with new seawater overnight to assure that the water was well mixed. Before the start of an experiment, the flushing was stopped so that each tank contained 2000 l of water. At the end of each experiment the tanks were emptied and cleaned with a weak acid and rinsed with tap water.

The locations of ASIT water filling were decided based on satellite chlorophyll data. We aimed primarily for biologically active areas and wanted to obtain different types of plankton populations in order to study the effect of chemical emissions from different plankton species. The cruise focused on the Chatham Rise area which is known to be biologically active. By moving around the area we were able to collect frontal, subantarctic and subtropical seawater. Originally more experiments were planned, but the voyage was shortened due to New Zealand going into lockdown due to the pandemic. Figure 4.2 shows the locations at which we started the different experiments, named here ASIT A, B, C and D. The tanks were filled during the hours before those points.

Figure 4.3 shows how the tanks and all the instrumentation was placed during the Sea2Cloud voyage. The tanks were outside on the trawl deck of the ship and the main container with the instruments was on the bow side of the tanks. A separate smaller container on the stern side was used to house the flushing pumps that were used to avoid overheating the containers. After each pump we used a moisture trap and a particle filter to reduce moisture and remove possible aerosol particles from the air going into the tanks. To monitor the contamination level of the air entering the tanks, we used a third similar pump as a background air measure.

The instrumentation used during the ship measurements included aerosol instrumentation, SO₂, ozone, VOCs and chemical composition of molecular clusters as well as light and tempera-

ture sensors. The used light sensors were described briefly earlier. The aerosol instrumentation included model A11 PSM, a model 3760A CPC and an SMPS. The PSM was run in stepping mode with saturation flow rates switching between 0.1 and 1 lpm every 60 s. With these saturation flow rates we can measure roughly 3 nm and 1 nm sized particles and the difference between the values observed at the two flow rates was used to calculate the number concentration of 1-3 nm particles. Out of gases, we measured SO₂ with Thermo Scientific Model 43i SO₂ Analyzer, ozone with Thermo Scientific Model 49i Ozone Analyzer and volatile organic compounds with PTR-MS. The chemical composition of molecular clusters was measured with two APi-TOFs, one run with nitrate chemical ionisation using Eisele type chemical ionisation inlet and one run without chemical ionisation. The instruments are described in more detail in the methods chapter. The flow rate going to the APi-TOF without chemical ionisation was increased to 6 lpm to reduce losses in the inlet.

All the instruments were connected to a Swagelock 4-way switching valve. The valve switched from one ASIT to background flushing air, the other ASIT and then ambient air and back to the first ASIT every 20 min. This way we could use all the instrumentation to measure both the ASITs, background air, and ambient air. 20 min was chosen as a compromise between instrument temporal resolutions and the need to measure both tanks as frequently as possible. When processing the data, we removed 3 min of data every time the valve position was changed to let the flows stabilise and take into account that for example for the PSM the final time resolution was 2 min.

The length of the 3/8" inlet from each tank to the 4-way valve was 214 cm. The distance the air travelled inside the valve was approximately 5 cm. After the valve we had 3/8" T from which we had in one direction Teflon tubing to the gas instruments. To another direction, we connected the APi-TOFs and the aerosol instrumentation. These instruments shared 15 cm of common 3/8" stainless steel inlet. After this we had 10 cm of 3/8" inlet to the CI-APi-TOF, 65 cm to the other APi-TOF and in the other direction we had 85 cm of 1/4" stainless steel and silicon inlet to the PSM, 108 cm to the total CPC, and 223 cm to the SMPS. The background flushing airline had a similar particle filter as the pumps used to flush the tanks and after the filter we had a T with another filter allowing air to exit when this air was not measured. From the T we had teflon tubing all the way to the 4-way valve. This air is later called pre-ASIT air.

For the ambient air, we first had a 6 m long 10 cm thick stainless steel tube going through the structure of the ship reaching approximately a meter away from the ship. The flow rate in this tube was kept at 140 lpm with the help of a blower to minimise the diffusion losses of small particles in the inlet. To the end of this inlet, we connected a 181 cm long 3/8" stainless steel inlet which was also connected to the 4-way valve.

Other air data handling included removing periods with potential anthropogenic contamination. This was done primarily based on SO₂ data. When the air was clean, the SO₂ values were below detection limit, but occasionally the air inlet got some of the ship's exhaust and the SO₂ peaked. If we detected a peak in SO₂ inside either of the ASITs or the flushing air, which were all coming from the same inlet, we removed 2 h 15 min of the data since in this time 90% of the air has changed. In addition to SO₂, we used masses 34, 57 and 93, corresponding to water clusters, butanol and toluene to filter out some pollution periods.

In addition to all the air instrumentation, the seawater was sampled frequently. Both tanks contained an exosonde below the water measuring temperature, salinity, pH, dissolved oxygen, chromophoric dissolved organic matter and chlorophyll. Daily water samples were taken through the tap at the side of the tank for chlorophyll-a, CDOM, nutrients, particulate carbon and nitrogen (POC/PON/PC/PN/13C/15N), dissolved DMS, DMSP, iodide, dissolved fatty acids, the composition of microbial community with flow cytometry, phytoplankton identification with FlowCam and phyto and zooplankton identification with microscopy. Additionally hydrolysable amino acids and total combined carbohydrates were sampled at the end of each experiment.

In addition to the bulk seawater composition, the surface microlayer (SML) water was

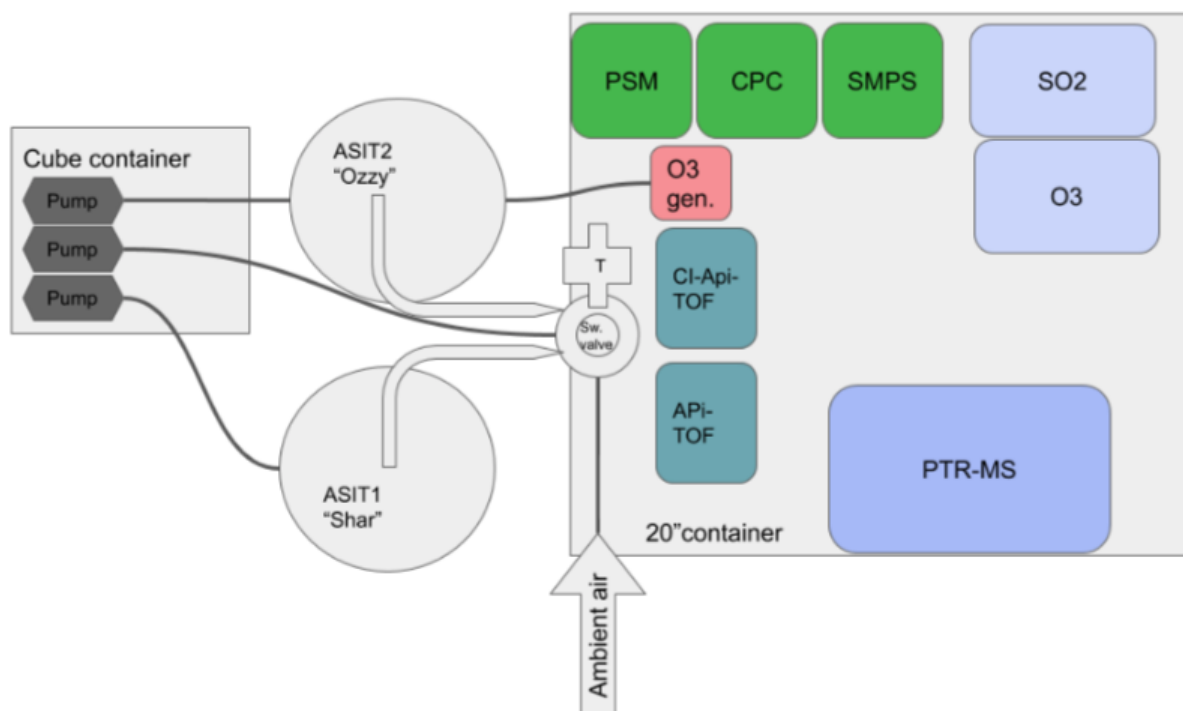


Figure 4.3: The tanks and instrument set up during the ship experiments, not in scale. Sw. valve stands for switching valve and the T illustrates distribution of air from the valve to different instruments.

sampled at the end of each experiment. This was done only at the end of the experiment since opening the tank to sample earlier would have contaminated the headspace. The SML samples included dissolved organic carbon and nitrogen. All the water sample analysis have not yet been analysed, so in the results we will only focus on a subset of the data

4.1.3 Additional experiments

In order to verify that there are no leaks and to determine the background particle concentrations and chemical composition, we performed blank experiments with teflon plates covering the bottom part of the tank. The idea of these experiments was to verify that the tanks are similar and that the tanks themselves do not emit compounds that could interfere with the experiments. We used the teflon plates because using water could have interfered with the background measurements. Without water the volume of the tanks would have been different and plastics at the bottom of the tank would have been exposed to the air.

The Teflon plates were cut into the shape of the cross section of the tank and attached with double-sided tape onto a plastic circle. The circle was then placed half way up in the tank with the teflon facing up and the plastic circle below the teflon supporting it. As the sides of the Teflon plate were not fully airtight, the space below the plate was filled with tap water to avoid air mixing from the plastic part at the bottom of the tank. This means that at the edges some contamination coming from tap water was possible, but this was the most feasible way.

After this, we did another repeatability experiment using the same water in both tanks but without using additional ozone to make sure that the differences observed between the tanks are caused by the addition of ozone and not by differences in the tanks. The water used in these experiments was collected from Evans Bay, meaning that it was coastal seawater and taken close to the city of Wellington. Same location was used for the ME3 experiments. In contrast with the experiments done at sea, during these experiments, we mixed the seawater by pulling water

from the bottom of the tank and returning it into the tank on the other side of the tank closer to the water surface. This was done to avoid all the plankton from settling at the bottom of the tank. We ensured that no bubbles were formed from the water mixing.

The blank experiments were conducted after the voyage in June-August 2020 at the NIWA Wellington site. As the tanks were outside and contamination of flushing air from anthropogenic sources was possible, for part of the experiments we used VICI Metronics T400-1 Sulphur traps to clean the in-going air from pollutants. The traps seemed to work well for cleaning the air, but they came with drawbacks. Firstly, they were designed for significantly lower flow rates and hence acted as big flow restrictions. Second, they also reduced the concentrations of oxidants, which likely had an influence on the chemical reactions in the headspace. Third, after some use, one of the traps started to emit high concentrations of particles. The reason for this remains unclear.

For these experiments after the voyage, less instrumentation was available. The setup was otherwise similar to the voyage, but now did not have the PTR-MS and SMPS and we only used one APi-TOF with nitrate chemical ionisation. We also used a different container than during the voyage and because of this we had to increase the length of the inlet between the valve and the CI-APi-TOF by 72 cm. During these experiments the seawater samples included chlorophyll-a, DMS, CDOM, flow cytometry, plankton microscopy and nutrients.

After the blank experiments we also did two other additional experiments to extend the data set. In the first of these experiments we did not use any additional seawater, but we filtered the seawater going into one of the tanks so that no living cells should have been in the tank. The water in this tank was continuously running through an UV-filter to make sure no cells survive alive. The water in the other tank was unaltered Evans Bay water. The idea of this experiment was to compare the difference between emissions from living cells and emissions from chemical reactions at the sea surface. In these experiments we did not use any additional ozone. The air measurements and water sampling was similar to the repeatability experiment.

One longer experiment was performed to study if dying plankton cells could emit chemical compounds as they decompose. We wanted to study this since previous research has shown that dying plankton cells can produce for example iodine species which could be important for particle formation (see for example Hepach et al., 2020). For this experiment we used unaltered Evans Bay water with an additional plankton monoculture. The monoculture consisted of *Cylindrotheca closterium* grown with nutrients in 5 l bottles. We added 4.9 l of the culture to each tank per tank and saved 200 ml for sampling to characterise the culture. The additional culture was used both to increase the biomass and because the ME3 results indicated that this plankton species could be important for particle formation.

At the beginning of the experiment, we fed the plankton with nutrients to increase the biomass and followed their growth by measuring the fluorescence of the seawater. Fluorescence was used because it is fast to measure and it is closely related to chlorophyll-a concentrations. The experiment was started on 24.7. and nutrients were added three times, on 29.7., 31.7., and 2.8. After this we let the population decline and the cells die. During the first two weeks of the experiment, we took two fluorescence samples from each tank daily and after this the sampling was reduced to every second day. Two samples per tank were taken to assure repeatability of the results. Other water samples were the same as for the other experiment in Wellington and they were taken only every third day. For this experiment additional ozone was used for Tank 2 as was done during the voyage.

4.2 Results and discussion

The objective of this study was to study new particle formation from seawater emissions and that is why the results focus on the aerosol measurements and their connection to chemical species observed in the air and the seawater chemical and biological properties. We start with

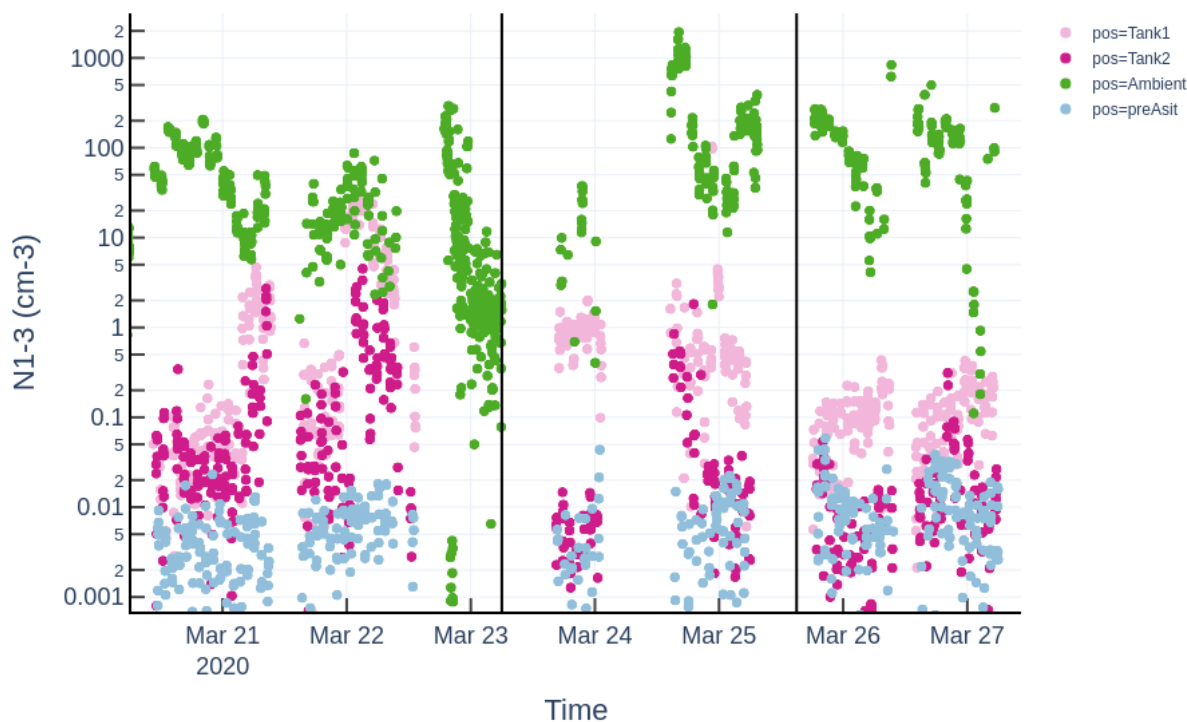


Figure 4.4: Time evolution of the number concentration of 1-3 nm particles during all the experiments on board Tangaroa in both tanks, in ambient air and pre-ASIT air. Different experiments (B-D) are separated by black vertical lines.

the experiments done during the Sea2Cloud voyage since for those experiments we had the best data availability and we were primarily interested in open ocean seawater.

4.2.1 Experiments on board RV Tangaroa

Aerosol data

Since we are specifically interested in new particle formation, let us start this section with PSM data. With the PSM, we can measure big molecular clusters and freshly formed particles. Figure 4.4 shows the time evolution of the particles in the smallest 1-3 nm size range during experiments B, C and D. The figure contains data from both ASITs as well as the background ('pre-ASIT') air which corresponds roughly to the air entering the ASITs as well as ambient air. Data from the first experiment was discarded due to leaks in the switching valve. During experiment B, we can see that N_{1-3} is higher than the pre-ASIT for both ASITs, but still below ambient air values. This shows that particles were formed in the ASIT headspaces. During experiments C and D, this is most of the time only true for Tank 1. On average the particle concentrations were higher in Tank 1 which did not have any additional ozone. This indicates that ozone likely suppressed particle formation, either by influencing emissions from the seawater, influencing the air chemistry, or both.

Because the pre-ASIT air came through a particle filter and after that only teflon and stainless steel tubing, we can assume that there were no particles in this air and the concentrations in the pre-ASIT air correspond to the background of the PSM. The values are generally below 0.01 cm^{-3} which is a low background for PSM. Previous work with PSM's has shown that backgrounds below 1 cm^{-3} can lead to underestimating the concentrations because at too low

saturation flow rates all particles do not get activated (Sulo et al., 2021). This means that it is likely that our PSM values are underestimations. Here, it should be also noted that since the inlets coming from the tanks to the valve to the 4-way valve were relatively long, the diffusion losses of sub-3 nm particles to the inlet walls were large. For example, out of 1 nm sized particles coming from one of the tanks only 1 % would pass all the way through the line to the PSM. For 3 nm particles this number would be 30 % and for 10 nm particles already 64 %. This is another factor that leads to an underestimation of particle concentration, especially for PSM data. If we consider both these effects, it is possible that N1-3 can be underestimated even by a factor of two if not more. Correcting for this underestimation is complicated since we cannot know how many particles were not activated in the PSM and the diffusion losses in the inlets vary by particle size and we only have two different size classes in the sub-10 nm size range. Additionally, especially in Tank 2 the values are often close to pre-ASIT data so it is hard to know whether particles were formed in the tank but they were never counted or whether no particles were formed during these time periods.

Figure 4.5 shows the time series for particles larger than 10 nm (N10) measured by the CPC. Here we can see that N10 in the tanks increases above the pre-ASIT level in both tanks during all the experiments, showing that part of the particles formed in the ASIT headspaces grew past 10 nm. Again, the concentrations in Tank 1 are higher than in Tank 2 and during the beginnings of Experiments C and D the concentrations in Tank 2 are in the same range with the background air. This confirms that particle formation was suppressed in Tank 2. As mentioned earlier, particles at 10 nm are several times more likely to survive through the inlet than sub-3 nm particles, so it is not surprising that N10 reaches higher concentrations than N1-3.

The SMPS data was not used since the instrument did not function properly with the pressure changes of the ASIT system. Unfortunately this means that we have no size resolved particle data above 10 nm and we cannot thus follow the particle growth in different size ranges above 10 nm nor calculate coagulation or condensation losses to pre-existing particle population.

4.2.2 Chemical species in the ASIT headspaces

To understand which chemical species are responsible for particle formation, we use the PTR-MS and CI-APi-TOF data. APi-TOF data was not used due to poor signal. Since the PTR-MS data is more quantified and easier to interpret because it contains less peaks and it was frequently calibrated during the campaign, we will start this analysis with the PTR-MS data. Figure 4.6 shows the time evolution of monoterpenes in both tanks and in ambient and pre-ASIT air. We can see that in both ambient and pre-ASIT air the concentrations are close to 0. In both of the ASITs the concentrations increase during all experiments with highest concentrations observed during the first experiment. During experiment B the concentrations are higher in Tank 1, but during experiments C and D the concentrations in the tanks are very similar to each other. If we compare the time evolution of monoterpenes to that of N1-3, we can see that they both reach their highest values towards the end of experiment B. This indicates that monoterpenes could have been one possible compound related to aerosol formation during this time. On the other hand, during experiments C and D, we saw clear differences in N1-3 in the two tanks, while for monoterpenes the tanks differed very little. This shows that other factors are needed to explain aerosol formation. Since ozone was added to Tank 2, one possible explanation is that ozone altered the oxidation mechanisms of the monoterpenes yielding to less particle forming oxidation products. Other possible explanations include

Monoterpenes are known to be one of the most important aerosol precursor species in boreal forest environments (Paasonen et al., 2018). In addition to monoterpene data, we will later use isoprene, its potential oxidation products methacrolein (MACR) and methyl vinyl ketone (MVK), methyl ethyl ketone (MEK), DMS, benzene, toluene, xylenes and iodomethane (CH₃I) from the PTR-MS data set. Isoprene can suppress particle formation from monoterpenes by producing compounds that are too volatile to participate in nucleation. MEK has been con-

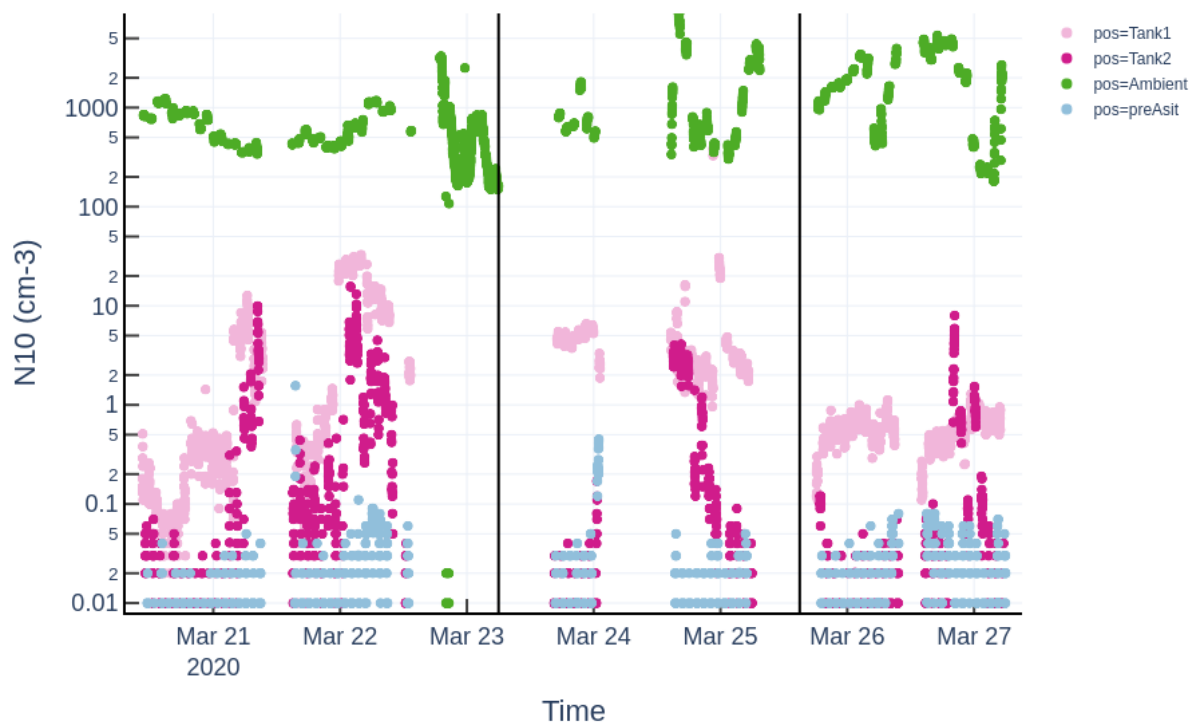


Figure 4.5: Time evolution of the number concentration of >10 nm particles during all the experiments on board Tangaroa in both tanks, in ambient air and pre-ASIT air. Different experiments (B-D) are separated by black vertical lines.

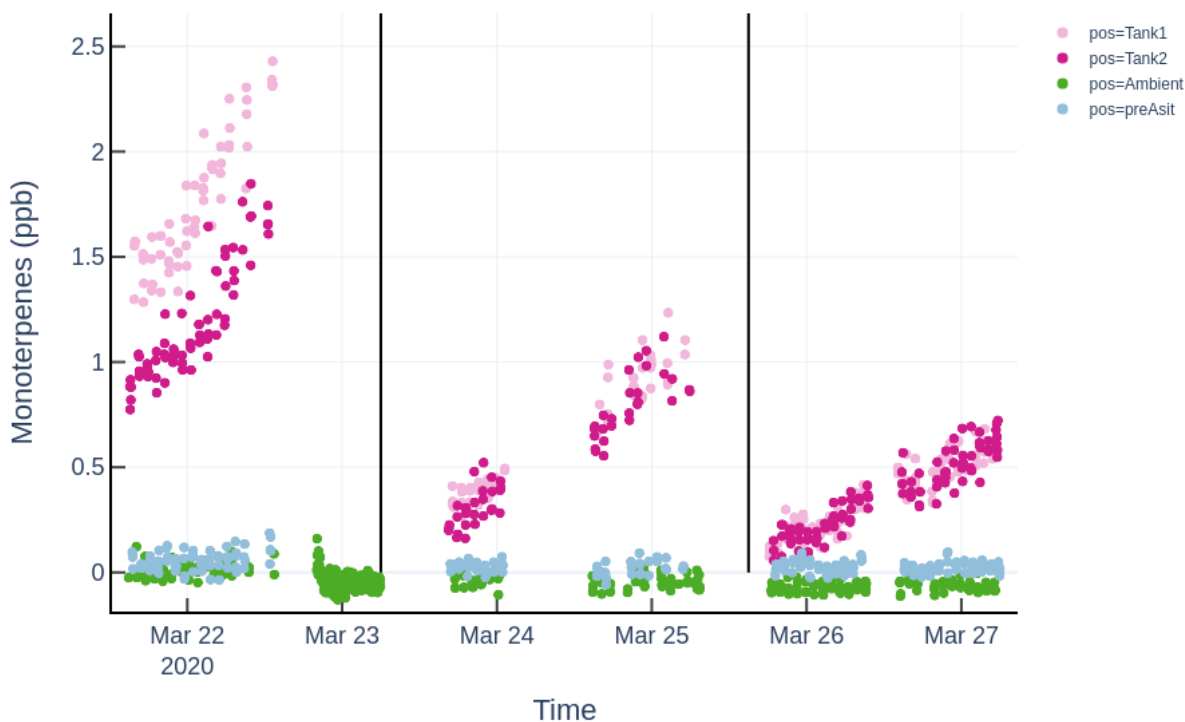


Figure 4.6: Time evolution of the monoterpene concentrations during the experiments in both tanks, in ambient air and pre-ASIT air. Different experiments (B-D) are separated by black vertical lines.

nected to plant stress and it can be important for atmospheric chemistry (Cappellin et al., 2019). Benzene, toluene and xylenes are traditionally known as anthropogenic compounds, but during the ASIT experiments we showed that they could potentially also come from natural sources (Rocco et al., 2021). These compounds can also be related to new particle formation (see e.g., M. Wang et al., 2020; Li et al., 2021a; Molteni et al., 2018). Iodomethane was chosen because it was the only iodine containing species measured with the PTR-MS and iodine oxides are important for particle formation (see e.g. He et al., 2021), but this data should be taken with caution since the instrument was not calibrated with iodomethane.

Since VOCs are as such too volatile to form new aerosol particles, in order to follow the steps between VOCs and particles, we need other data. With the APi-TOFs, we can measure the chemical composition of different molecular clusters. Handling the CI-APi-TOF data was complicated since the experimental setup is challenging for the instrument. This is because the inlets from the tanks to the instrument were very long, meaning high losses of low-volatility compounds on the inlet walls. Additionally, as we were in marine conditions and especially the air coming from the ASITs was humid, we observed plenty of water clustered with the nitrate ions and these peaks often dominated the mass spectrum. The tank setup was also challenging for the CI-inlet since its flow control is sensitive to pressure changes and when the container moved relative to the tanks this could push the inlet disturbing the sensitive air flows. The pressure changes led to variations in the signal when the switching valve changed positions. Container movements were especially a problem during the additional experiments in Wellington since the mobile container we used often moved in the wind while the ASITs did not.

Regardless of these issues, we have been analysing the CI-APi-TOF data in several different ways. First, we went through the different files to identify peaks in the data. Most of

the potentially interesting peaks such as sulfuric acid, iodine oxides or known organic species had low concentrations or were unobservable, so in this analysis we only include sulfate and methanesulfonate peaks from the high resolution analysis as example compounds.

Another way to approach APi-TOF data is to use unit mass resolution (UMR) data. This reduces the size of the data set and allows exploring the data without identifying all the peaks. Since monoterpenes were observed in the tanks, we used the unit resolution data to get an idea of their oxidation products. Monoterpenes contain 10 carbon atoms and their oxidation products typically fall in known mass ranges. These products are known as Highly Oxygenated organic Molecules (HOM). Here, we used the division also used by C. Yan et al. (2016) in which masses 201-290 correspond to light HOMs, masses 291-450 to HOM monomers (8-10 carbon atoms), and masses 451-650 to HOM dimers (16-20 carbon atoms). These are all clustered with NO₃-.

In Figure 4.7 we can see the time evolution of HOM monomers calculated with the UMR data. During experiment B, the HOM concentrations are the highest in both tanks close to the end of the experiment. This is similar to what was seen for the monoterpenes, showing that some monoterpenes likely had the time to get oxidised into HOMs. Contrary to what was seen with the monoterpenes, the HOM monomer group has more variable concentrations, the differences between the two tanks are smaller and the pre-ASIT and ambient air concentrations also fluctuate more. Specifically, during the first experiment, pre-ASIT and ambient concentrations rise after the concentrations in the tanks increase. This could mean that not all of the signal is produced in the tank.

Here, we have to remember that since we only use UMR data, part of the signal can be composed of compounds that do not belong to HOMs. In our data set in particular, the HOM mass ranges likely contain at least some nitrate-water clusters since these clusters were abundant in our data. Further work is needed to identify potential HOM peaks from the data to be sure if they are observed and how their concentrations evolved during the experiments.

Connecting particle formation to chemical precursors

To connect the different chemical species on particle formation, we studied the correlations between the selected chemical species and aerosol concentrations. We examined the correlations of different chemical species in air both separately for each tank and together for both tanks. For this analysis we used Spearman's correlation coefficients since unlike Pearson's correlation they take into account non-linearities in the data. Figure 4.8 shows an example of this analysis with the monoterpene data. We can see a clear positive correlation between monoterpenes and N1-3, confirming that monoterpenes could be one possible particle precursor species. As we explained earlier with the time series, we can see that particle concentrations are consistently higher for Tank 1, but the difference between the tanks is smaller for the monoterpenes.

Figure 4.9 summarises all the correlation coefficients when using data from both tanks. The table includes aerosol concentrations in different size ranges (1-3, 3-10, and over 10 nm), UV-A radiation, temperature, ozone, SO₂, potentially relevant compounds from the PTR-MS data set, sulfate and methanesulfonate ions from the high resolution APi-TOF data and the potential HOMs in different size ranges from the UMR APi-TOF data. We can see that N1-3 has its highest positive correlation with DMS. DMS is well known as an aerosol precursor species in marine atmosphere, but on the other hand its oxidation to sulfuric acid is also known to be slow. Potential oxidation products of DMS include sulfuric acid and methane sulfonic acid. DMS does have a positive correlation with the sulfate ion but not with methanesulfonate. This is understandable since methanesulfonate levels were very low. On the other hand many of the PTR-MS compounds correlate positively with each other and the sulfate ion correlates positively with most of the compounds from the PTR-MS data. The sulfate ions we observe were thus not necessarily formed from DMS in the tanks.

N1-3 has positive correlations also with isoprene, isoprene oxidation products methacrolein

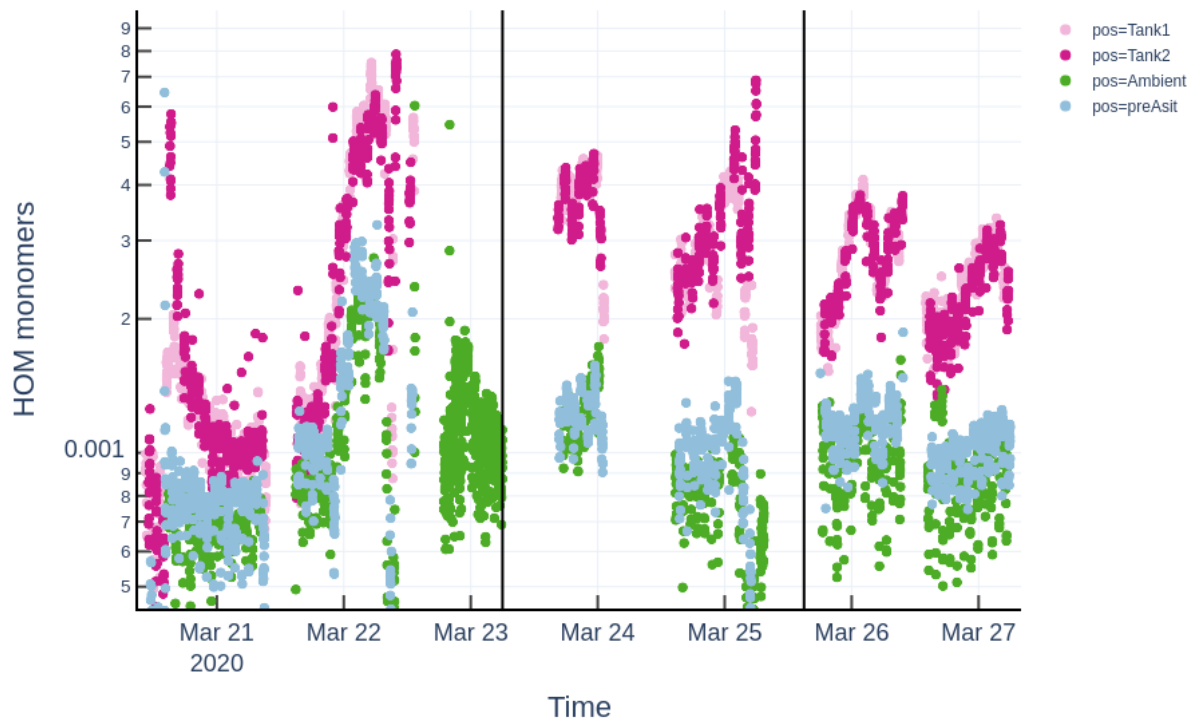


Figure 4.7: Time evolution of the potential HOM monomers in both tanks, in ambient air and pre-ASIT air. Different experiments (B-D) are separated by black vertical lines.

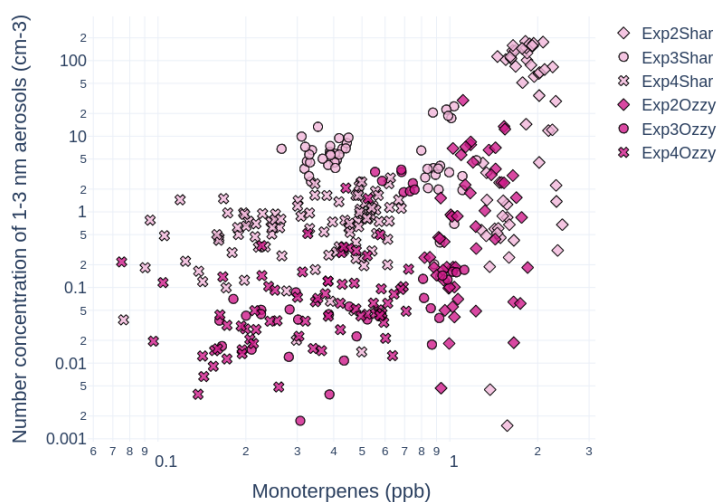


Figure 4.8: N1-3 as a function of monoterpenes. Exp 2 refers to Experiment B, Exp3 refers to experiment 3 and Exp 4 refers to experiment D. Shar refers to Tank 1 and Ozzy to Tank 2.

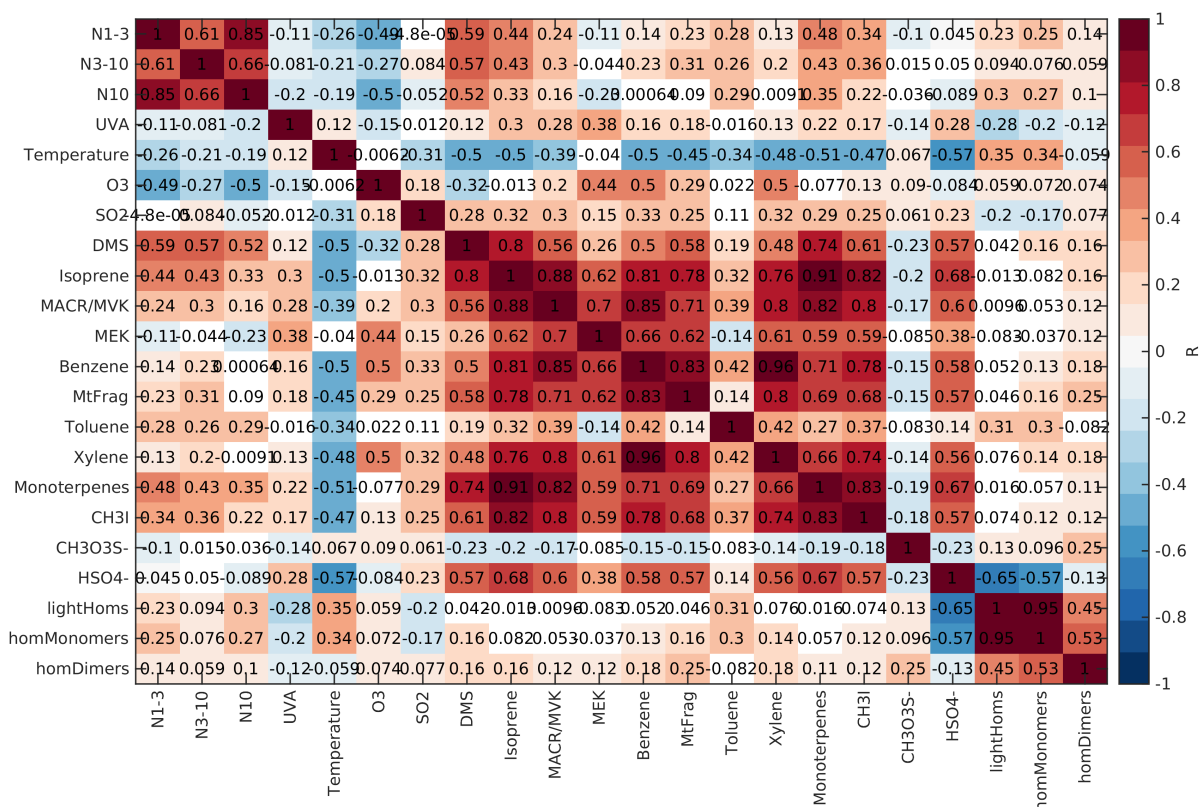


Figure 4.9: This table summarises all correlations using data from both ASITs. Each square represents the Spearman correlation between the variables on x- and y-axes. The value indicates the correlation coefficients and if the coefficient is statistically significant ($p < 0.05$), the square is coloured so that stronger correlation coefficients have darker colours.

(MACR) and methyl vinyl ketone (MVK), toluene, iodomethane, potential HOMs, and monoterpenes as shown earlier. It is not straightforward to show which of these species are actually involved in particle formation and which just happen to have positive correlations because they vary similarly to other compounds. Correlations with N3-10 are similar to N1-3 but in most cases weaker than for N1-3. This is reasonable since to grow past 3 nm, the particles need more time and the residence time of air in the tanks is limited. N10 also has positive correlations with similar compounds, showing that some particles were likely able to grow past 10 nm.

When it comes to the other variables, aerosol concentrations in all size ranges have negative correlations with UV-A radiation, temperature and ozone. The fact that the correlations with radiation are negative indicates that all the particle formation cannot be explained by photochemistry. The relationship with temperature is complicated to interpret. While lower temperatures would typically increase nucleation rates, temperature changes can also be related to changes in radiation levels and temperature can have an effect on the emission of different chemical species from the sea surface. The temperature does in fact have a weak positive correlation with UV-A radiation, meaning that part of the negative correlation could be explained by this connection. The negative correlation with ozone was expected since the earlier figures showed that aerosol concentrations were smaller in the tank with added ozone.

The correlations are similar if using data from only one tank, but now the positive correlations between the aerosol concentrations and different chemical species are in general higher. Figure 4.10 shows the correlation coefficients using only data from Tank 1. Some of the highest correlations are again observed with DMS, but now isoprene, benzene, monoterpene fragments, xylene, and monoterpenes also have correlation coefficients of 0.5 or higher. The correlations between N's and light HOMs and HOM monomers also have higher correlation coefficients than

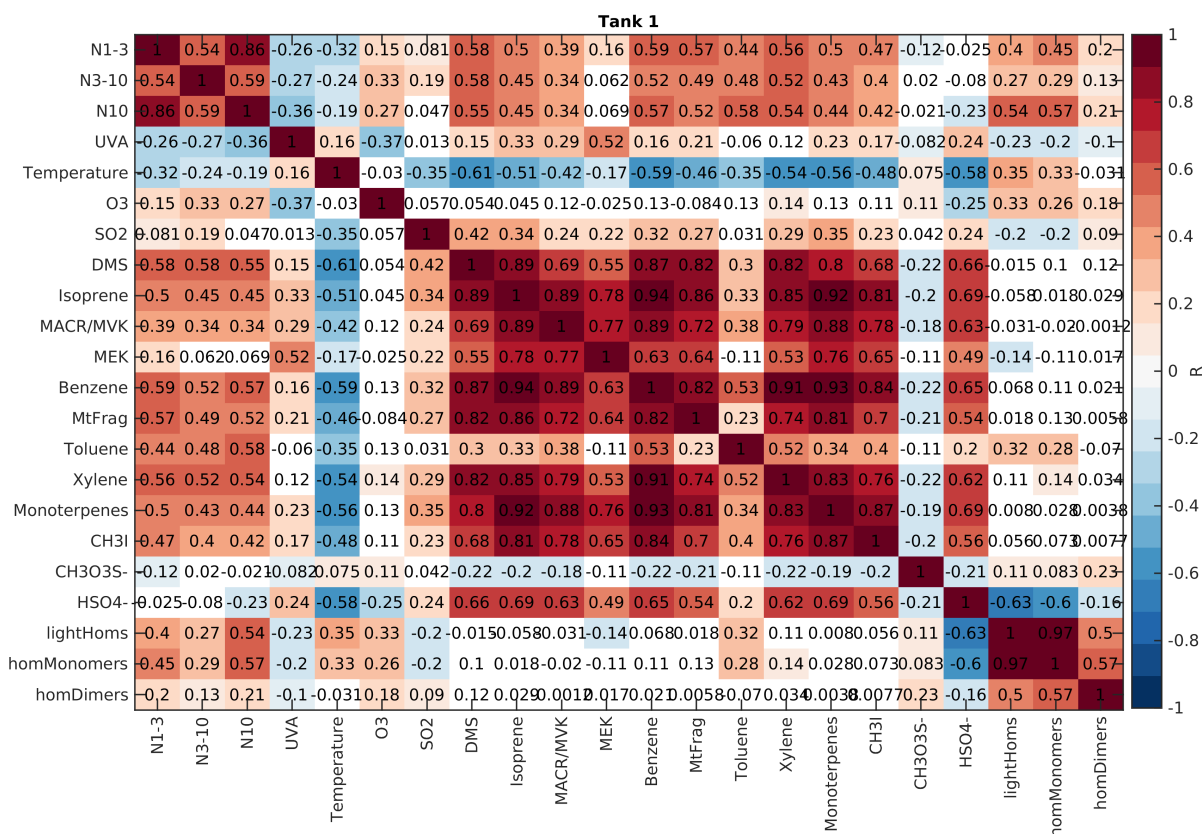


Figure 4.10: All correlations using only data from Tank 1. See Figure 4.9 for explanation.

when using data from both tanks. This shows that most of the correlations were not caused just by differences in the two tanks. This is not the case for ozone. When using only data from Tank 1 the correlations with ozone are positive, not negative like when using data from both tanks. It is possible that at lower ozone levels the ozone concentrations were not high enough to start the same processes that suppressed particle formation in Tank 2.

If we use data only from Tank 2, the correlation between the N's and different VOCs are similar to what was seen for Tank 1 (Fig. 4.11). Some differences can be seen for the correlation between aerosols and API-TOF data. While in Tank 1 light HOMs and HOM monomers had positive correlations with all the particle classes, for Tank 2 we can only see very weak correlations with N10. This could be related to the fact that the potential HOMs had very similar concentrations in the two tanks while particle concentrations were lower in Tank 2. One possible reason for this is that HOMs did not form particles alone and something more was needed. Another possible reason is that the UMR data that we use to represent HOMs does not fully correspond to true HOMs and has interference from other compounds. Since many of the chemical species are inter-correlated and the aerosol concentrations correlate positively with many different chemical species, even separating the data by tank does not solve the exact particle formation pathways. In the future we should look deeper into the CI-API-TOF data to see if we can find compounds that correspond to oxidation products of the compounds detected with the PTR-MS. We could also try to model the particle formation in the tanks by using the VOC data and known chemical mechanisms and try to match this with the aerosol data, but that would be a complicated task, since we observe so many different compounds and it is likely that not all the relevant chemical reactions are known.

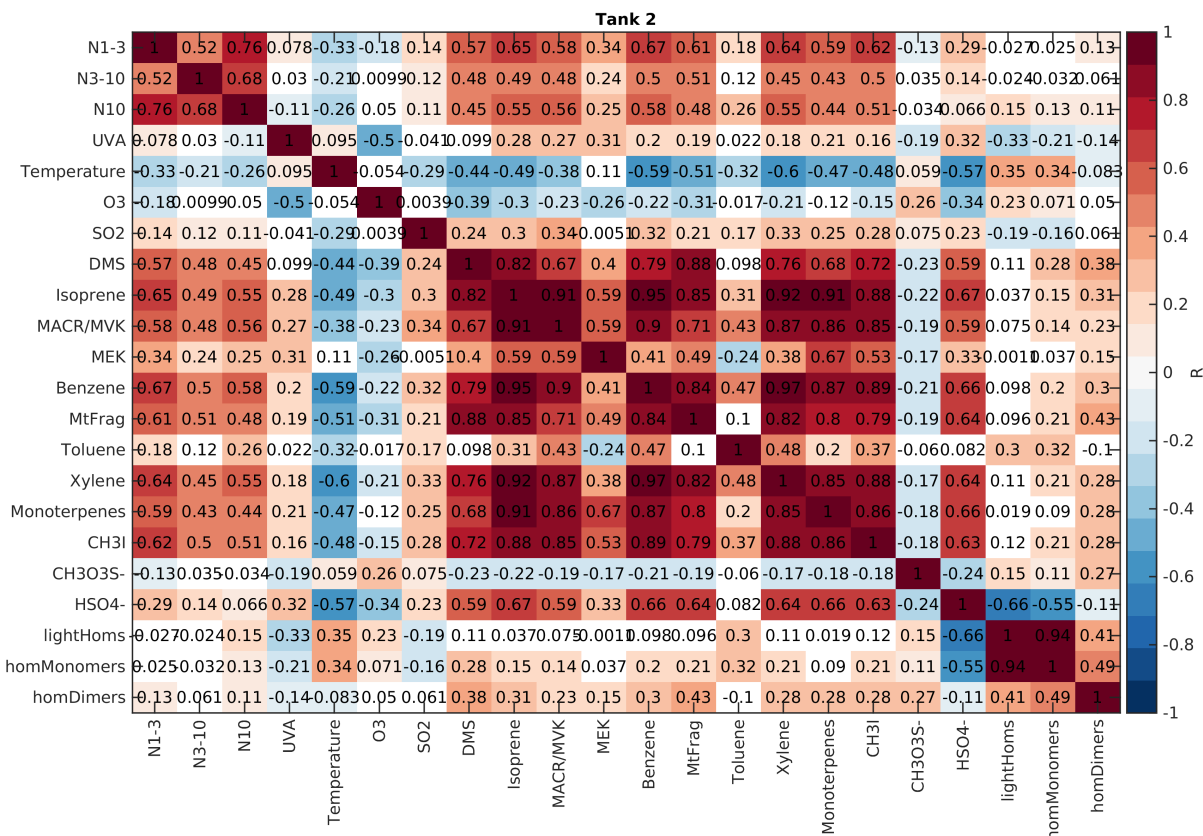


Figure 4.11: All correlations using only data from Tank 2. See Figure 4.9 for explanation.

4.2.3 Connecting particle formation to seawater properties

One of the main assets of the ASIT experiments is that we isolate the air above seawater and sample also the seawater properties. This way we can gain insights for example into which plankton species could be responsible for emitting particle precursor species. Next, we look into the seawater properties to see if we can better understand how different plankton groups and seawater chemical properties influence new particle formation.

One common way to track phytoplankton productivity is to measure chlorophyll-a concentrations. Figure 4.12 shows the time series for total chlorophyll-a in the ASITs. During experiment B Chl-a started high but declined during the experiment whereas during experiments C and D, Chl-a started lower and increased during the experiments. The values are similar and follow the same trends in both tanks. The fact that Chl-a decreased down from a relatively high value during experiment B is interesting since this is when we observed the highest monoterpene, HOM monomer and aerosol concentrations. One possible explanation is that dying plankton cells produced higher levels of monoterpenes. Cell lysis has been connected to higher VOC fluxes (Brüggemann et al., 2017), increased organic matter in sea spray aerosols (Miyazaki et al., 2020), and secondary organic aerosol formation (S. R. Schneider et al., 2019). Previous literature thus supports the hypothesis that cell lysis could lead to higher monoterpene emissions which could get oxidised and form aerosols.

Because Chl-a only tells about the primary production in general and it is not always directly connected to the chemical species emitted from the seawater, it is useful to also study different plankton groups separately. Figure 4.13 shows the time evolution of nanophytoplankton (phytoplankton sized 2-20 μm measured by flow cytometry). The nanophytoplankton concentrations have an increasing trend during Experiment B, remain relatively stable during Experiment C and increase again during experiment D. This is different from what was seen for the chl-a.

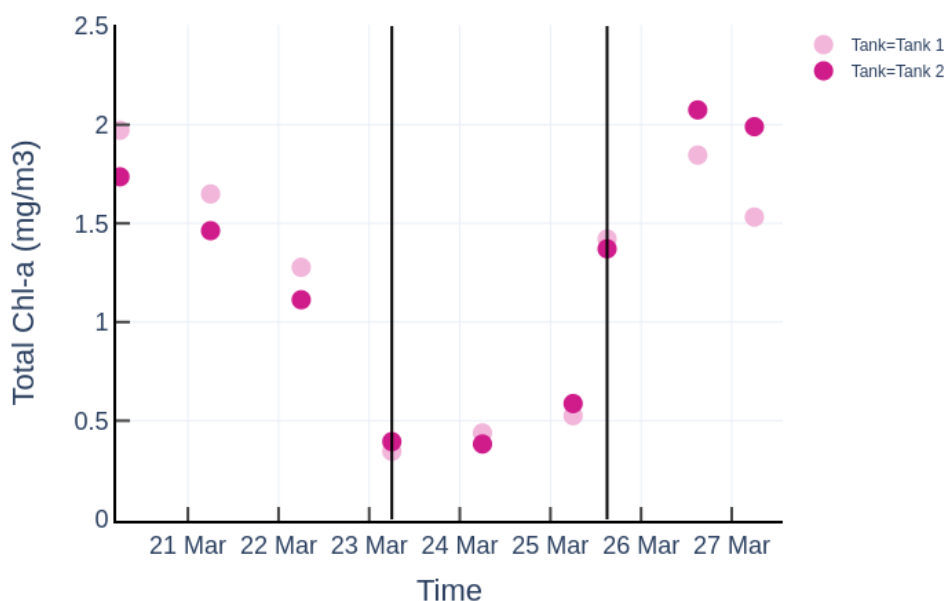


Figure 4.12: Time evolution of the chlorophyll-a (Chl-a) during the ASIT experiments in the tanks during the voyage. Different experiments (B-D) are separated by black vertical lines.

Now, nanophytoplankton concentration is at its highest when monoterpene concentrations were highest. This presents an alternative hypothesis that nanophytoplankton could act as an active emitter of monoterpene.

If we compare the plankton data to aerosol data, we notice that out of the flow cytometry data only nanophytoplankton has a positive correlation with N1-3 ($R = 0.37$, Fig. 4.14). Here we use a 7 hour average of the particle concentrations starting from one hour before the water sampling time. This was done because the water samples were only taken once a day and we wanted the measurement time of the air data to be close to the seawater sample time. For prokaryotic picoplankton, we find a negative correlation of -0.51 and for picophytoplankton a negative correlation of -0.18. These results are in line with the results from the ME3 experiment in the previous chapter which also indicated that nanophytoplankton is a possible source of aerosol precursor species. With total chlorophyll-a the correlation with N1-3 is only -0.05. This shows that chlorophyll-a data alone is not a good predictor of aerosol formation. All of the seawater data has not been processed yet and the connection of the rest of the seawater data to particle formation will be studied later. In the future, it would be good to perform experiments with different plankton monocultures and also let these monocultures go through cell lysis to unravel the exact connections between different plankton species and new particle formation.

4.2.4 Additional experiments

As the measurements on the ship were interrupted early, we continued experiments with the ASITs in Wellington later. Figure 4.15 shows the time series of N10 during the first three additional experiments in Wellington. During the first experiment, the bottoms of the tanks were covered by Teflon plates, meaning that no new particle formation should be observed. During the first couple of days this held well, but on July 3rd, which was the first sunny day during this experiment, we can see particle concentrations increase in Tank 1. We assume that the primary reason for the formation of these particles would be the fact that these experiments were conducted on a parking lot in a semi-urban area. Since the air going into the tanks was

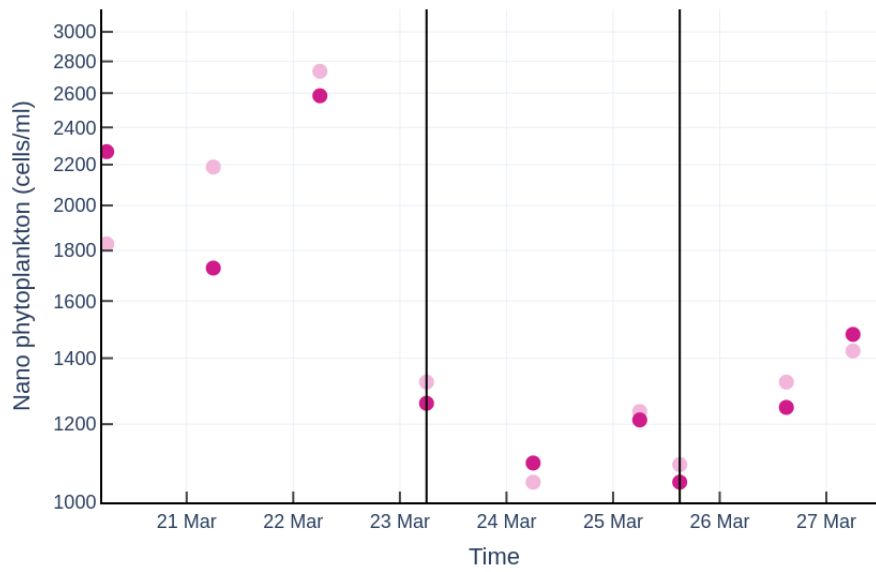


Figure 4.13: Time evolution of the nano phytoplankton cell abundance in the two tanks during the experiments during the voyage. Different experiments (B-D) are separated by black vertical lines.

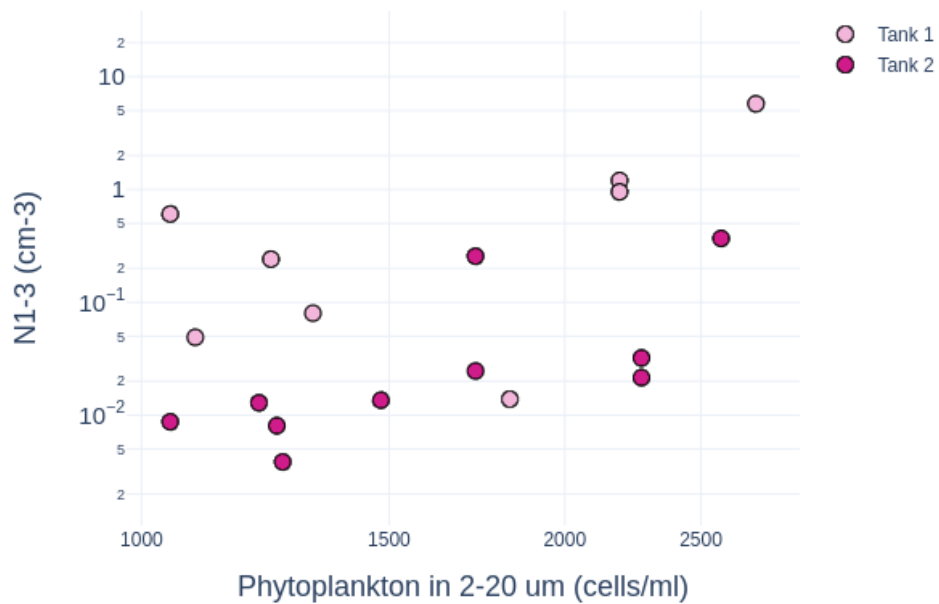


Figure 4.14: Particle number concentration in 1-3 nm (N1-3) concentrations as a function of nano phytoplankton cell abundance in the two tanks.

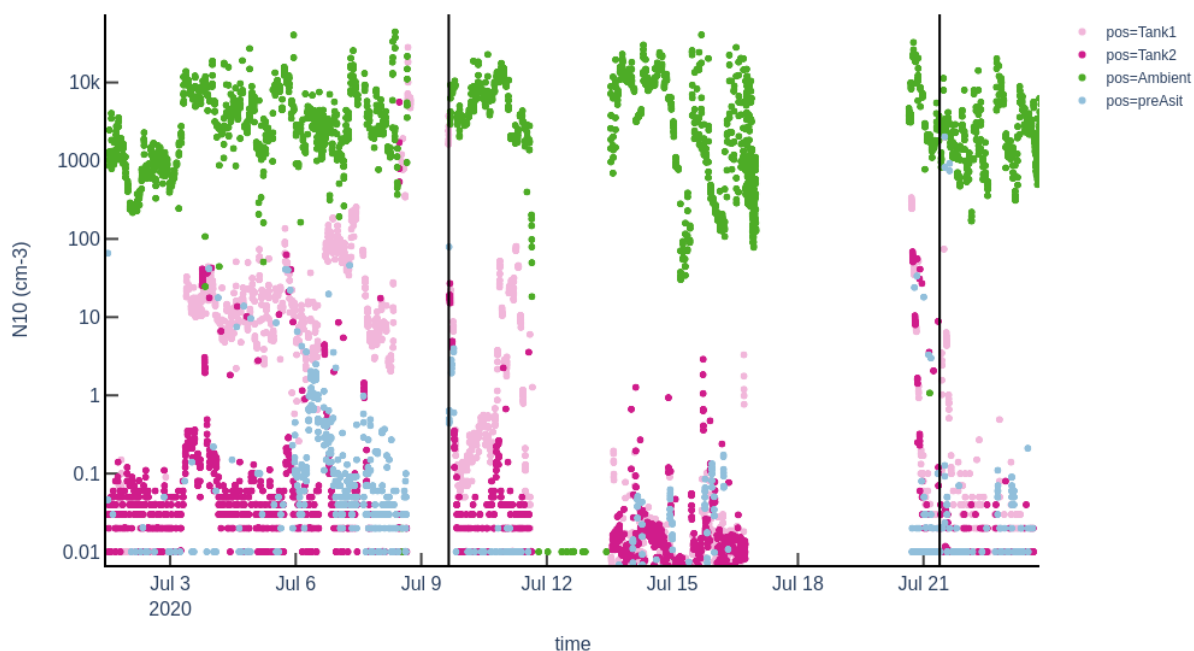


Figure 4.15: Time evolution of concentration of particles larger than 10 nm (N_{10}) during the first three additional experiments in the tanks, in ambient air and pre-ASIT air. The black vertical lines mark the start times of the second and third experiments.

only filtered for particles it is possible that anthropogenic gases entered the headspaces of the tanks with the flushing air and then got oxidised and formed particles in the ASIT headspaces when the sun came out. This is why we later, after July 6th, started experimenting with the use of sulfur traps in the flushing lines. The sulfur traps should get rid of not only sulfur, but also VOCs. The traps, however, came with two issues. First, they were designed for lower flow rates (0.5 lpm) whereas our flow rate aim was 25 lpm. This meant that the traps were a big flow restriction, which strained the pumps we used for the flushing air. This led to some changes in flow rates later on. Second, the traps also reduced the amounts of oxidants entering the tanks which limits the chemical reactions that can occur in the tanks. This could reduce for example the ozone concentration even by up to 20 ppb. The setup was thus not optimal and caution needs to be taken when interpreting these results.

In the second experiment both tanks contained the same water and no ozone was added. It was started without the sulfur traps to mimic the conditions on the ship traps and the traps were added on the second day. At the beginning of the experiment, starting from July 9th, we can see some more particles in Tank 1 compared to Tank 2 and pre-ASIT line, but later the concentrations are similar and there is very little particle formation. Note that the CPC was not functioning properly around July 13th.

During the 3rd experiment where we compared unaltered and filtered and UV-sterilised Evans Bay water the particle concentration remained low in both tanks (last days after the second vertical black line in Figure 4.15). Since no particle formation was observed, we could not study comparing emissions from dead and living cells. It would have been interesting to have PTR-MS data from this experiment, because with PTR-MS data it could have been possible to see if there were any differences in the emissions of VOCs even if no particles were formed. It should be noted that all the additional experiments were conducted during the winter, which meant less biological activity in the seawater and less available radiation. If we would have conducted the experiments towards the summer, the results could have been different. This is

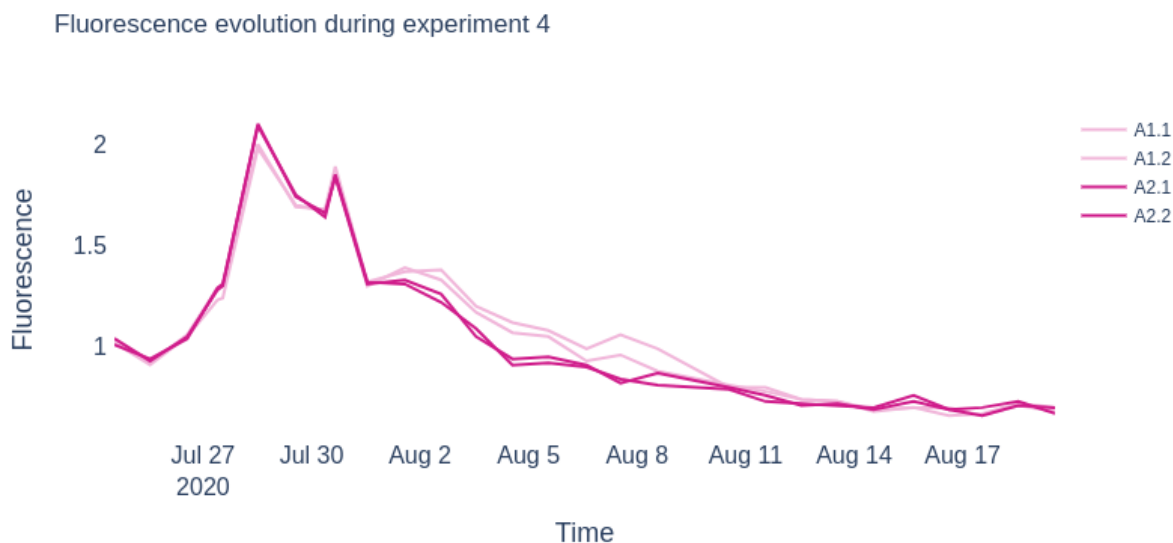


Figure 4.16: The time evolution of fluorescence during the last additional ASIT experiment. A1.1 and A1.2 were sampled from Tank 1 and A2.1 and A2.2 were sampled from Tank 2.

why it could be interesting to try this experiment again later.

Figure 4.16 shows the time evolution of fluorescence during the last experiment, which used an additional plankton monoculture and studied the effect of cell lysis over time. We can see a small decline in both tanks in the beginning when the plankton population adapts to the new conditions and after this the fluorescence increases thanks to the nutrition additions. After the nutrition additions were ended, fluorescence and presumably the phytoplankton populations declined. The replicates of the fluorescence samples agree well with each other, showing that the data is reliable. During the first week of the experiment the fluorescence was very similar in both tanks, but the decline was slightly slower in Tank 1. This could be explained for example by differences in light conditions. The ozone added to Tank 2 could also make a difference by for example acting as a stress factor for the plankton. The evolution of fluorescence indicates that the plankton population followed the pattern we wanted it to follow.

The particle data measured during this experiment is shown in Figure 4.17. In the beginning of the experiment the particle concentrations in the tanks remained low and close to the pre-ASIT values. After August 2nd, we can see a clear increase in particle concentrations in Tank 2, but after a while we found out that the source of the particles was the sulfur trap that we used to clean the air entering the tank. This data is thus not usable. We can also see that the pre-ASIT N10 increased to levels above Tank 1, indicating that there were problems with this airline too. To conclude, at the beginning of the experiment we did not observe particle formation and after the first day technical issues made the data unusable. As for the previous experiment, it could be interesting to reproduce this experiment in more favourable conditions.

4.3 Conclusions

The experiments with Air-Sea-Interaction Tanks showed that this is a promising way to study new particle formation directly from marine emissions. During our experiments on RV Tangaroa, we observed particle formation within the tanks' headspaces and explored possible chemical pathways of particle formation. One potential formation pathway was the formation of HOMs from monoterpenes. A preliminary look into the plankton data showed that nanophytoplankton could produce chemical species that can form aerosols. This was in line with the results from

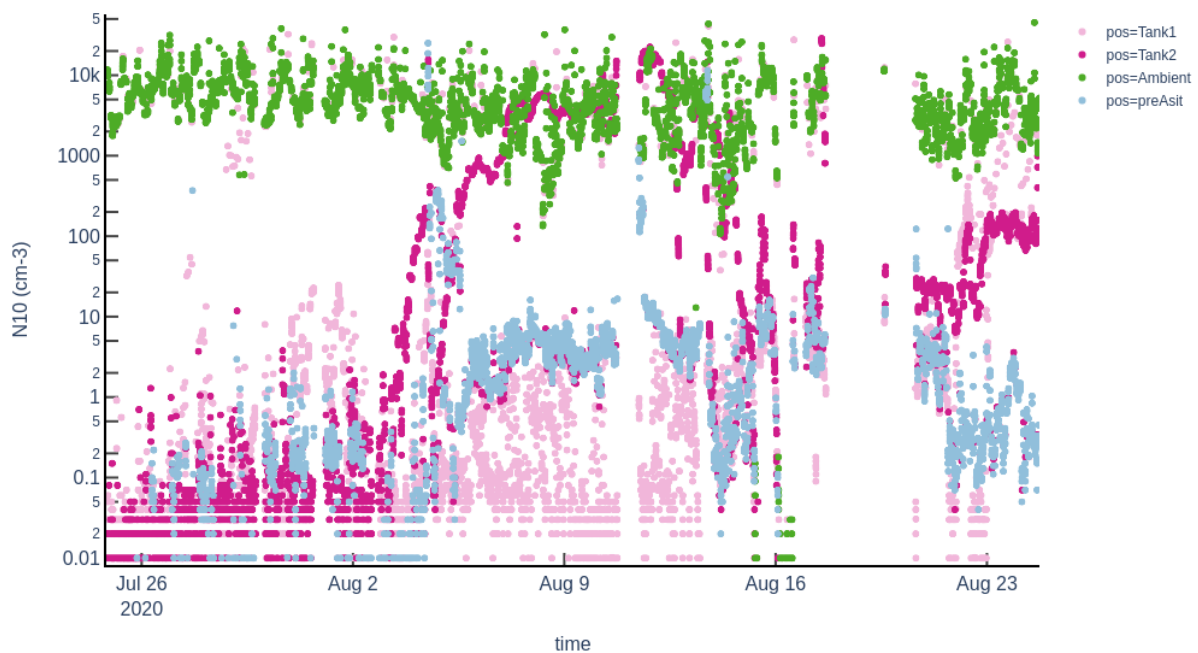


Figure 4.17: Time evolution of concentration of particles larger than 10 nm (N_{10}) in the tanks, in ambient air and in pre-ASIT air during the last additional experiment.

the ME3 campaign in the previous chapter.

One of the drawbacks of these experiments was that our time on the ship was cut short due to the pandemic. This limited the amount of available data, which is problematic especially when it comes to connecting the atmospheric data to seawater data since seawater samples were taken only once a day. In the original plans we would have also used seawater collected from further away from Chatham Rise area which would have made the seawater sets more diverse.

If we would have had the chance, we should have conducted blank experiments at sea with full instrumentation instead of doing them with less instrumentation in a different environment. Especially during the additional experiments we had many technical difficulties with the flushing pumps, cleaning the flushing air and some of the instrumentation. Overall, the additional experiments were interesting, but due to several technical issues and the likely low biological activity and radiation levels, we did not get all the results we expected. Having more spare parts and better designing the measurement environment would be useful for future campaigns. More experiments could be done for example with different plankton monocultures to characterise the emissions from single phytoplankton species. Conducting more longer lasting experiments where the plankton cells have time to degrade would also be interesting.

Chapter 5

New particle formation and aerosols in ambient air

To understand how important aerosol formation is in the real atmosphere in marine conditions, we conducted ambient aerosol measurements at Baring Head station in coastal New Zealand. This chapter explains the done measurements and studies aerosol properties and new particle formation at the station in both clean marine and land-influenced air masses. The results of this chapter are currently in review in Atmospheric Chemistry and Physics.

5.1 Measurement setup

This section describes the measurement setup that we used for long term measurements at Baring Head. The measurements described here are used both for this and the next chapter. Baring Head (41.4083 °S, 174.8710°E) has been used for background CO₂ measurements since 1972 due to its capability to capture clean marine air that has not been influenced by land in several days (Stephens et al., 2013). This is the same reason we chose the station to study aerosol formation in pristine marine air.

New Zealand sits in a maritime mid-latitude westerly air-flow. The Southern Alps present a barrier to these westerlies but this is broken by the Cook Strait between the North and South Islands. For a range of prevailing synoptic situations which bring westerlies from north-west, through to south-west, air is funnelled through the Strait as a north-westerly or northerly wind at Baring Head located on the north-eastern side of the Strait. These directions result in air masses that have been impacted by the land to the north of the station. There are two main types of situation that cause wind direction to switch and arrive from the south at Baring Head. Firstly, cyclonic situations where low centres pass to the north or across the North Island, drive southerlies or south-easterlies into the Strait. Secondly, there are anticyclonic flows when an anticyclone passes to the south of the South Island or builds in the Tasman Sea to the west of New Zealand. As pressure builds and the ridge moves east, air is deflected around the South Island and arrives at Baring Head as an anticyclonic southerly. These air masses have typically spent several days over the sea and are considered clean marine air. According to Stephens et al. (2013) south and southeast air mass trajectories are observed on average 27 % of the time, being more frequent during the winter than summer. Out of this 27 %, part is still contaminated by land-influences and after filtering, less than 10 % of the data is used for baseline CO₂ calculations (Brailsford et al., 2012; Stephens et al., 2013).

The site is described by Stephens et al. (2013). Our aerosol and chemical measurements were conducted in a separate hut 20 m east and uphill from the main buildings. Our main inlets were 7 meters from the cliff edge at 110 cm height off the ground. Figure 5.1 shows the arrangement of the main instrumentation used in this study.

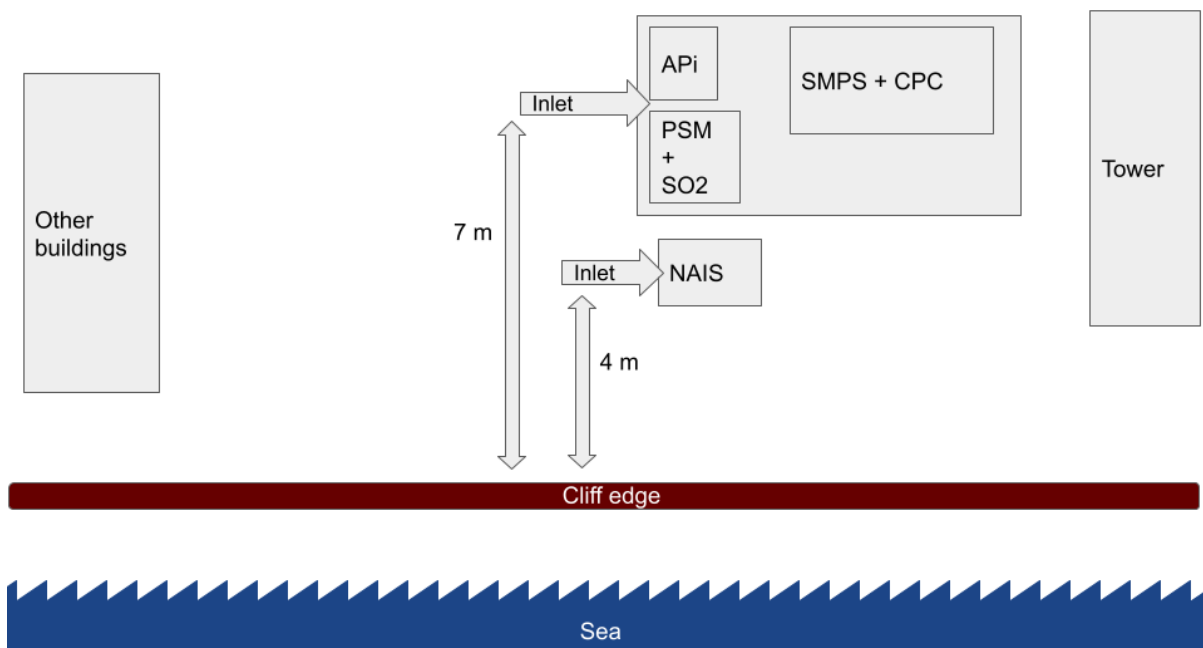


Figure 5.1: Measurement setup at Baring Head, not in scale.

5.1.1 Aerosol measurements

To characterise the aerosol properties at Baring Head, we measured aerosol and air ion number concentrations in different size ranges using several different instruments. A Scanning Mobility Particle Sizer (SMPS) was used to measure the aerosol number size distribution in 10–450 nm during 20.4.2018–13.6.2018 and in 10–500 nm during 12.6.2020–1.3.2021 with a time resolution of 13 min. The fact that the upper limit of the SMPS was lower during the earlier measurement period should not make significant difference for total particle concentrations as particle number concentrations are typically dominated by smaller particles. In fact, during the later measurement period, particles larger than 450 nm contributed only 2% of the number concentration of particles above 100 nm and 0.3 % of total particles. The total length of the SMPS’s 1/4” inlet was 312 cm, containing a 73 cm silica gel dryer. To accompany the SMPS, we used one Condensational Particle Counter (CPC) to measure the total concentration of aerosols above 10 nm. From 22.7.2010 to 24.12.2020 the used model was TSI 3010 and from 24.12.2020 to 17.2.2021 it was model TSI 3760A. The inlet to the CPC was in total 268 cm long and 1/4” thick with the first 103 cm stainless steel and the rest silicon tubing.

To obtain aerosol concentrations in smaller size ranges, we used Particle Size Magnifier (PSM, Vanhanen et al., 2011). During 12.6.2020–17.9.2020, we used a model A09 with supersaturation fixed at 1 lpm. Then, during 17.9.2020–17.2.2021, we used an A11 PSM in then stepping mode with saturation flow rate switching between 0.1 and 1 lpm every 60 s. To assure that changing the instrument did not affect our results, we compared the two PSM’s in laboratory over three days. During the intercomparison, the median relationship of model A09 and A11 number concentrations at 1 lpm supersaturation was $\frac{N_{1,A09}}{N_{1,A11}} = 0.93$ (25th and 75th percentiles 0.75 and 1.24) meaning that the concentrations were on average close to each other, but the relationship varied to both directions. The inlet to the PSM was a 122 cm long 1/4” stainless steel tube. The first 103 cm of this inlet was shared with the CPC to increase the flow rate through the inlet, because increasing the total flow rate from 2.5 to 3.5 lpm decreases the particle losses due to diffusion in an inlet with this diameter.

In addition to SMPS and PSM, we used Neutral cluster and Air Ion Spectrometer (NAIS, S. Mirme and A. Mirme, 2013) from 7.8.2020 to 28.2.2021. The NAIS measures the size distribution

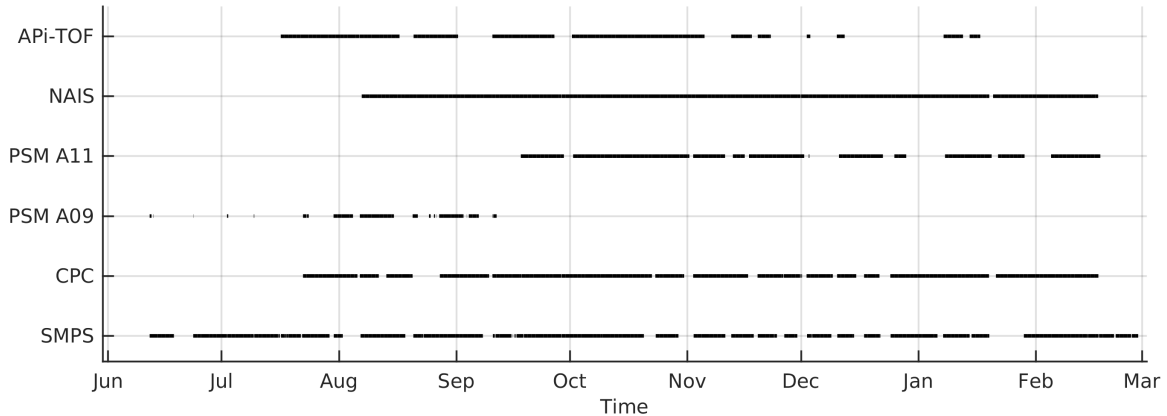


Figure 5.2: Black lines indicate when data is available for each instrument.

Table 5.1: Percentage of data available for each instrument each month calculated based on 30 minute averaged data.

Month	PSM A09	PSM A11	CPC3010	CPC3760A	SMPS	NAIS
April 2018	0	0	0	0	33	0
May 2018	0	0	0	0	96	0
June 2018	0	0	0	0	38	0
June 2020	2	0	0	0	46	0
July 2020	11	0	31	0	94	0
August 2020	63	0	68	0	78	81
September 2020	19	38	97	0	88	100
October 2020	0	97	95	0	82	100
November 2020	0	86	86	0	76	100
December 2020	0	51	53	24	73	100
January 2021	0	62	0	94	64	97
February 2021	0	46	0	59	94	59

of particles in 2–42 nm and ions in the electric mobility range from 3.2 to 0.0013 $\text{cm}^2\text{V}^{-1}\text{s}^{-1}$. The inlet of the NAIS was 3 meters closer to the cliff edge than the other instruments and at 70 cm height. The data availability from all particle instruments during the 2020–2021 period can be seen in Figure 5.2 and SI Table 5.1. For 2018, we only had SMPS data and it was available for the whole measurement period of 20.4.2018–13.6.2018.

The data availability from all particle instruments during the 2020–2021 period is illustrated in Figure 5.2 and summarised for each month in Table 5.1. The Figure includes also API-TOF data which is explained in the next chapter.

5.1.2 Ancillary data

In addition to aerosol measurements, we used the station’s permanent ozone, radon, and meteorological measurements for temperature, global radiation, relative humidity and wind. The meteorological data can be downloaded from <https://cliflo.niwa.co.nz/> (last accessed May 2021). Ozone data are from long-term measurements of the station conducted with Thermo Scientific Model 49i Ozone Analyzer. Radon data were used to assess land-influence. The measurements were done with ANSTO designed high-sensitivity site background radon detector (Ansto, Australia www.ansto.gov.au, Chambers et al., 2014).

As the station is coastal, tides heights can also have an effect on the atmospheric composition. This is why we also used wave height data from Greater Wellington Regional Council (

<http://graphs.gw.govt.nz/>, last accessed May 2021, data available only for 2020-2021) and estimated tide heights for Wellington from Land Information New Zealand <https://www.linz.govt.nz/sea/tides/tide-predictions> (last accessed May 2021). The tide height data were interpolated with Piecewise Cubic Hermite Interpolating Polynomial to obtain data with higher time resolution.

Air mass back trajectories were calculated with HYSPLIT (Stein et al., 2015; Rolph et al., 2017) for 72 hours with one hour time resolution. The input meteorological data are from the Global Data Assimilation System (GDAS) model with a one-degree resolution. To separate between land-influenced and marine air masses, we used landmask code (<https://se.mathworks.com/matlabcentral/fileexchange/48661-landmask>, last accessed 13 May 2021)

They were used to separate between marine and land-influenced air masses and to study the origins of new particle formation. In this study, we consider only moments when the air mass arriving to the station has spent 100% of the time over sea as marine air masses and everything else is considered as land-influenced. As noted in earlier studies (e.g. Stephens et al., 2013), the resolution of the back trajectories can sometimes mask small land masses, meaning that if the air has spent only a short time over a small piece of land, it might not be detected as a land-influenced data. At Baring Head this is quite common when the winds are Northerly.

5.2 Data analysis

CPC data were used to check the quality of SMPS data. We compared total SMPS concentrations to total CPC concentrations. All in all, the instruments agreed well, but the SMPS seems to slightly underestimate concentrations with the median of $N_{\text{tot, CPC}}/N_{\text{tot, SMPS}}$ being 1.51. The differences could be due to higher losses in the SMPS inlet and dryer or lower detection efficiency of SMPS's CPC. This is why we decided to correct the SMPS data by multiplying the concentrations with this value. Part of the difference could also be due to the fact that the CPC measured all particles above 10 nm while SMPS measured only particles in the 10-500 nm size range, but typically particle number concentrations are dominated by smaller particles, so we consider this negligible. It should be also noted that particle diffusion losses in the inlet and dryer are larger for the smaller particles. This can lead to a bias in the size distribution, and in the case of low nucleation mode particle concentrations, a total loss of particles in the smallest sizes. In addition to the correction made to SMPS data, we removed negative values from N1-10, as has been done previously for PSM data (e.g., Sulo et al., 2021). Negative particle concentrations are non-physical and can be both due to differences in instrument efficiencies and measurement times.

The SMPS data were also used for event classification and condensation sink, growth rate, and formation rate calculations with methods explained in Chapter 2. NAIS data were also used for event classification.

5.3 Results

To give an overview of new particle formation at Baring Head, we begin this section by classifying all days to event and non-event days with traditional methods and characterise these events. Then we look at aerosol concentrations in more detail and study aerosol formation and growth. Finally, we focus on the special characteristics of new particle formation in marine air masses.

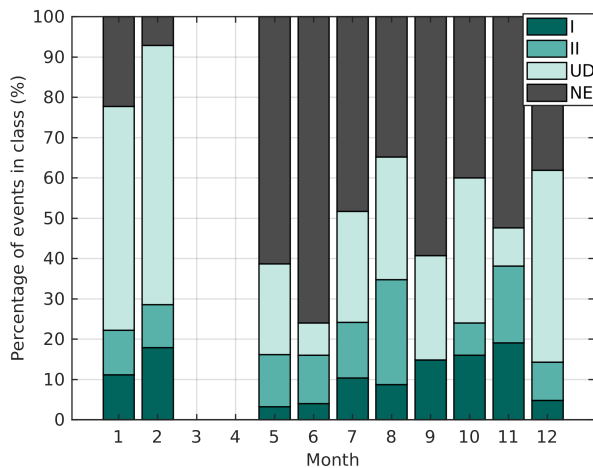


Figure 5.3: Bar plots show the fraction of each event class during each month.

5.3.1 New particle formation events

Event occurrence and characteristics

To get a general overview of how common new particle formation is at Baring Head, all days with SMPS data were classified with the criteria by Dal Maso et al. (2005) as explained in Section 2.2.2. Over all, 10.9% of the days were clear NPF events that classified as Class I events. Additionally, 12.1% of the data were classified as Class II events, meaning clear events with a fluctuating particle mode, making the total average event frequency 23.0%. 32.3% of the days were classified as undefined, leaving 44.8% as non-events. Even though most previous studies of NPF frequencies have been made for continental Northern Hemisphere sites, our numbers are comparable to other remote sites (Nieminen et al., 2018). NPF events in New Zealand have been previously observed in Auckland at a site that was 20 km from the sea (Coulson et al., 2016). They hypothesised that particle formation was favoured by low pre-existing aerosol concentrations and particle forming vapours could have been a combination of biogenic emissions from both the ocean and a forested area and urban precursors, but no data confirming this hypothesis were available. Similar factors likely played a role at Baring Head.

The seasonal cycle of the fraction of event classes (Fig. 5.3), shows that the highest event frequency is observed during late spring in November (38.1 %). The lowest event frequency (14.3 %) is observed in December, but this month contains many undefined days, making the fraction of non-events no higher than most months. Both the lowest numbers of Class I events and highest numbers of non-event days were observed in May-June, indicating that particle formation was less frequent during the winter. The data from April were not included in the seasonal cycle as we only had 10 days of data from April. The only two coastal sites at similar distances from the equator in the study of Nieminen et al. (2018) were Mace Head in Ireland and Finokalia in Crete. The lowest event frequencies at both of those stations were observed during the winter, with 6.5% for Mace Head and 16.3% for Finokalia. Highest values were observed during the spring with 29.3% for Mace Head and 36.6% for Finokalia. Our results are similar to these stations, especially to Finokalia which has a more similar distance to the equator.

Previous studies at Baring Head and its surroundings have observed more DMS (M. Harvey et al., 1993) and more non sea salt sulfate (Law et al., 2017; Li et al., 2018) during the late spring and summer. This could be one of the factors increasing NPF frequency during this time. As photochemistry is important for particle formation, another possible factor is more favourable meteorological conditions during the summer. In addition to longer days, the summer at Baring Head is characterised by less southerly winds than during the winter season (Stephens et al.,

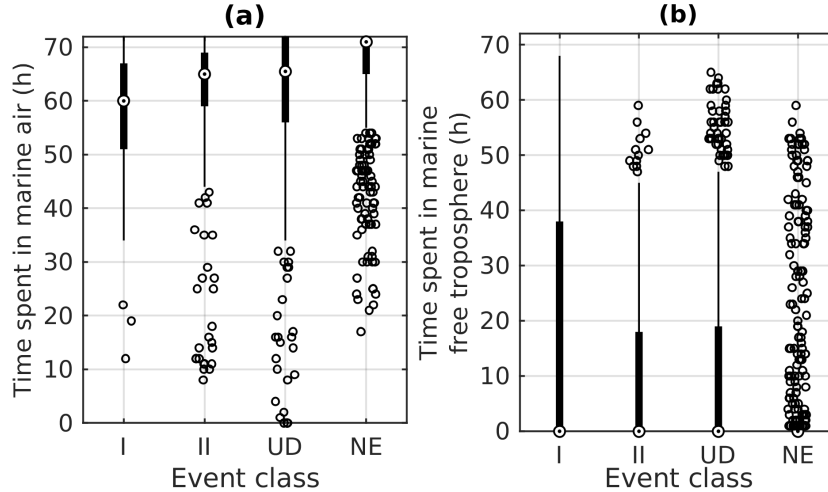


Figure 5.4: Time that the air mass has spent in (a) marine air and (b) marine free troposphere between 8-15 h on during days classified to Class I (I), Class II (II), undefined (UD) and non-event (NE) days. The circles are the median concentrations for each month, black boxes mark the 25th and 75th percentiles, the whiskers mark 1.5 times the interquartile range and rest of the points are outside this range.

2013) and southerly winds are often related to cloudy, windy, and rainy weather which would inhibit NPF.

Figure 5.4 illustrates the time that the air mass had spent in marine air and marine free troposphere during each of the event classes. It should be noted that this analysis contains all the data between 8–15 h and while that corresponds to typical event times, the event times vary day to day (see Fig. 5.6). This analysis shows that most of the Class I events are likely influenced by some time spent over land, with the median time that the air masses had spent over land during those days being 13 h. Many of the Class II and undefined days had also land influence, with the median time spent over land being 7 h. Non-event days, on the other hand, were more common when the air mass had spent all of its time in marine air. This shows that NPF events classified with the Dal Maso et al. procedure are relatively rarely found in pure marine air. Observing particle formation in air masses that come from the sea and then cross over land is not surprising since marine air is typically characterised by low particle concentrations and the sources of particle precursor vapours over land are typically higher than over the oceans. If we look at the time spent in the marine free troposphere (Fig. 5.4b), we see that during events, the air masses were more likely to have spent time in the free troposphere than they were during non-event days. This could be explained both by lower pre-existing particle concentrations in the air that came from the troposphere or the transport of particle precursor vapours or particles themselves from higher altitudes. Here, it should be noted that the division to free tropospheric air was only done based on a fixed threshold for the altitude of the air mass back trajectories even though the start height of the free troposphere can be variable.

In order to obtain more information about the NPF events, we used a second classification method developed by Dada et al. (2018) which characterises the events with more detail. This classification is based on NAIS data, meaning that data were not available for most of the winter months (see methods). With this method, we observed regional events that start from ions of 2-4 nm and continue to grow past 7 nm on 26.2% of the days. 15.4% of the days were classified as transported events where the first steps in ions are not seen, but a nucleation mode is observed. Only 6.7% of the days were ion burst days during which ions in 2-4 nm appear but do not grow to larger sizes. The rest (51.8%) were non-events.

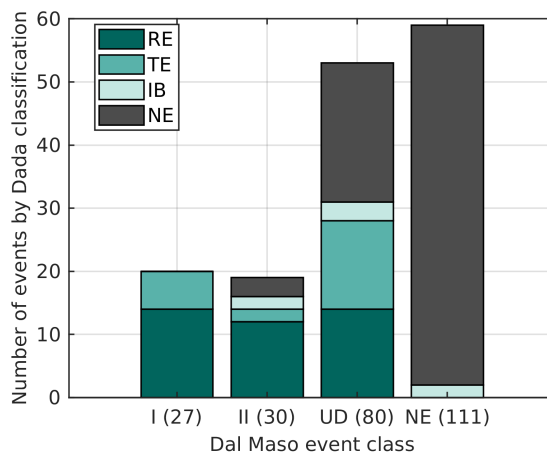


Figure 5.5: Comparison of the results of two event classification methods.

Comparing these results to the classification by Dal Maso et al. (2005) (Fig. 5.5) showed that all the Class I events and most of the Class II events were regional or transported events, which is in line with the fact that this class requires clear growth in nucleation mode. Two of the Dal Maso et al. non-events were classified as ion bursts, which is reasonable as ion bursts appear in a size range smaller than that used for the Dal Maso et al. classification. This shows that Dal Maso et al. classification might miss the initial steps of NPF if no further growth occurs. Many of the undefined days are classified as non-events by the Dada et al. (2018) method, but this is explained by the fact that the undefined class includes days where growth in pre-existing Aitken mode was detected.

We used the method by Dada et al. (2018) also to define event start and end times (Fig. 5.6). This definition is based on the time evolution of the concentration of ions in the 2-4 nm size range and thus tells about the first steps of NPF. The average event duration with this method was only 3 hours. Typical start times were around 8-10 h in the morning and typical end times around 13-15 h in the afternoon. It should be noted that particles might continue to grow in larger size ranges even after small ions are no longer detected, meaning that this method might underestimate the total event duration. One weakness of this method is also the fact that, as it is using the night time concentrations as background concentrations, nighttime events could not be detected with this method. Based on visual inspection of the data, no clear NPF events occurred during the nighttime, but few potential night time ion burst events did happen and as shown later in Section 5.3.5, we saw nighttime increases in sub-3 and sub-10 nm particle concentrations.

To see more quantitatively how many of the events occur in marine air, we checked the percentage of time that the back trajectories were marine during the events (Fig. 5.7). This was calculated for regional and ion burst events, as start and end times are only defined for these event classes. Air masses during all events had spent over 50% of time over sea. For 12 events, the air masses had only spent time in marine air according to the back trajectory calculation. This is 18.75% of the total RE and IB events and 6.15% of all days for which NAIS data were available. Half of these fully marine events were classified as regional events and half as ion bursts. However, out of these 12 events, only one met the other criteria for clean marine air and had radon below 100 mBq m^{-3} and this event was surrounded by land-influenced periods. This means that during most of the events, the air had recently passed the southern tip of North Island and these events could have some land-influence. Based on this, events classified with the Dada et al. criteria in completely clean marine air seem rare, but on the other hand, only 7.3 % of our measurement time was classified as clean marine air and there were only 26 days that had more than 30 % of data in clean marine air, so longer time series would be required to get more

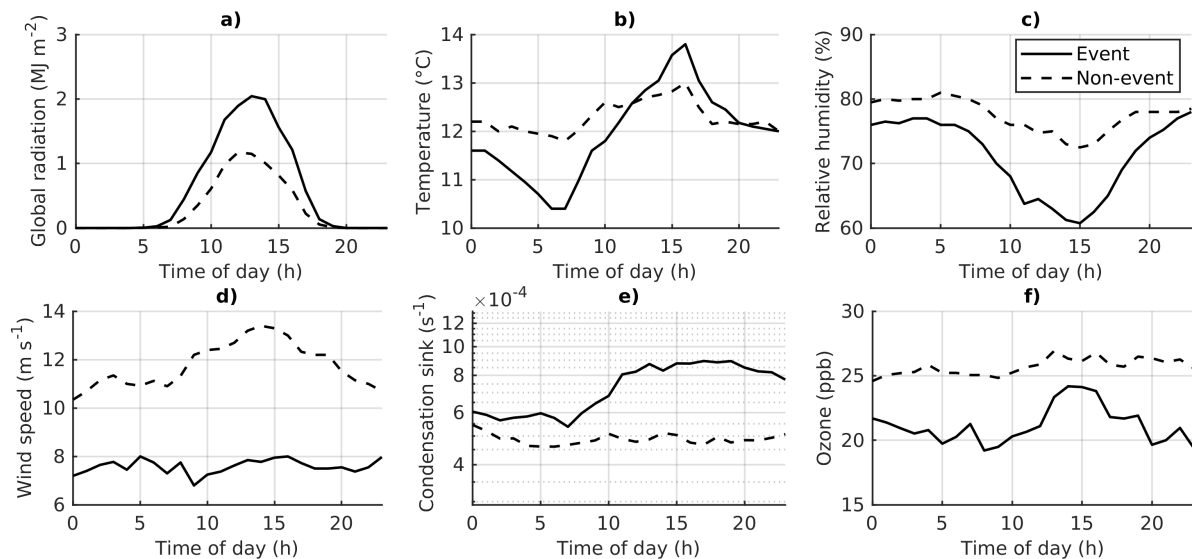


Figure 5.8: The diurnal cycles of different meteorological variables, condensation sink and ozone during event and non-event days.

the start of new particle could be favoured by cold conditions. The daytime increase can be explained by sunny conditions warming the air during the day. This trend is similar to what Jokinen et al. (2021) observed in Northern Finland.

With relative humidity, lowest values are observed during events and highest during non-events (Fig. 5.8c). This could be expected based on the results with radiation, since high relative humidity typically correlates with low level clouds which block radiation (Hamed et al., 2011). Previous work at a remote coastal site in Australia has also shown that new particle formation occurred when radiation levels were high and RH was low (Modini et al., 2009).

Figure 5.8d shows that events are favoured by low wind speeds. Wind speed can be related to both the amount of sea spray aerosol in the air and the time that the air has spent over land. At high wind speeds, waves are typically higher and produce more sea spray aerosols which can act as a sink for aerosol forming condensable species. On the other hand, at Baring Head, the wind speeds are typically lower when the air mass has spent more time over land and we saw earlier, events are more likely to occur when the air mass has spent some time over land.

With condensation sink (CS), we can see that on non-event days the CS is low while on event days CS is slightly higher and increases clearly during the day. This shows that new particle formation can likely increase the CS. Having higher CS on event days is opposite to what has been seen for example in Southern Finland (Dada et al., 2018) and the common assumption that higher condensation sink would prohibit NPF by acting as a sink to particle precursor vapours. Our results are nevertheless reasonable since at Baring Head the events occurred primarily over land whereas non-event days had primarily marine air. Over land, the sources of aerosol precursor species seem to be more intense than over the ocean. This can set off particle formation if the CS has not yet increased too much and meteorological conditions are favourable. Similar results have been seen at mountain sites (Boulon et al., 2010; Rose et al., 2015b).

Finally, for ozone (Fig. 5.8f), the levels are lower during event days compared to non-event days. The data should be studied further to understand whether this is a question of ozone chemistry influencing NPF or just a difference between land-influenced and marine air masses.

5.3.2 Aerosol concentrations

Since these are to our knowledge the first measurements of aerosol particle number concentrations starting from 1 nm in New Zealand and the longest data set of aerosol number concentrations at Baring Head, we explore the seasonal and diurnal cycles of particle number concentrations. The cycles can also give us information about the factors controlling aerosol concentrations at Baring Head. The size ranges we use here are 1-10 nm (N1-10), 10–100 nm (N10-100), and above 100 nm (N100). N1-10 typically consists of new particles formed in the atmosphere, N10-100 can contain both secondary particles that have grown from sizes below 10 nm and primary particles and for N100 primary particles are likely more important than for the smaller particles.

All the data were divided into marine and land-influenced data points based on air mass back trajectories, radon, and wind direction. Aerosol number concentrations in all used size ranges were lower in marine air masses than in land-influenced air masses, with median (25th-75th percentile) N1-10, N10-100, and N100 nm being 270 (100–730), 580 (360–890) and 110 (80–180) cm^{-3} in marine air and 710 (300–1630), 1020 (540–2010) and 170 (100–280) cm^{-3} in land-influenced air. This is reasonable as marine air masses are typically cleaner than continental air masses.

A previous voyage conducted east of Baring Head observed particle concentrations of $534 \pm 338 \text{ cm}^{-3}$ in clean marine air and $1122 \pm 1482 \text{ cm}^{-3}$ during land influence (Law et al., 2017). Our results are within the same range. Voyages west of New Zealand have observed N10 of 681 (388–839) cm^{-3} at latitudes similar to Baring Head (Humphries et al., 2021), which is also in line with our results. Out of other coastal sites, previous work at Mace Head by Dall’Osto et al. (2011) saw N10 of 327 cm^{-3} in open ocean air and 1469 cm^{-3} during open ocean nucleation. During coastal nucleation and anthropogenic influence, the numbers were higher (nucleation 2548 cm^{-3} , anthropogenic 1580 cm^{-3}). Our numbers are between their two open ocean classes, which is logical since coastal sources do not seem to be important at Baring Head (see Section 5.3.5).

Seasonal cycles can be observed for the particle concentrations in all the size ranges (Fig. 5.9). For the smallest size range of 1-10 nm particles, we only have enough data from 7 months (in June and July 2020 data available only 2% and 11% of the time), but we can still see that the concentrations are the lowest in both land-influenced (Fig. 5.9a) and marine (Fig. 5.9d) air masses during late winter and early spring (August-September) and higher later during the spring and summer. The differences between months are more significant in the marine air masses than in land-influenced air, but this could be partly explained by the fact there are less marine data. The median monthly particle concentration in marine air is only 64 cm^{-3} in August and increases significantly during the spring, reaching the highest median of 637 cm^{-3} in October. During the spring (September-November), N1-10 comprises 29 % of the total particle number in marine air, indicating that nucleation likely occurs in these air masses with a large enough frequency and intensity to influence the total aerosol particle concentration. This also implies that classification of NPF events with the classical criteria (Dal Maso et al., 2005; Dada et al., 2018) originally designed for a continental site might not be suitable for the detection of nucleation in a remote marine environments. The seasonal cycle can be related to both biological sources of particle precursors and meteorological conditions favouring nucleation during the spring and summer.

In the second size bin of 10-100 nm (Figs. 5.9b and e), the lowest concentrations are observed during June and July in both air mass classes. Similar seasonal cycle for Aitken mode particles in marine air has been observed before at Cape Grim (Bigg et al., 1984). Again, during the winter we are less likely to see new particle formation. Another reason that could decrease particle concentrations in this size range more in winter compared to the summer is losses due to more wet deposition by rain. For particles larger than 100 nm, the seasonal cycles are less clear, but the smallest medians are again observed during the winter and the highest during

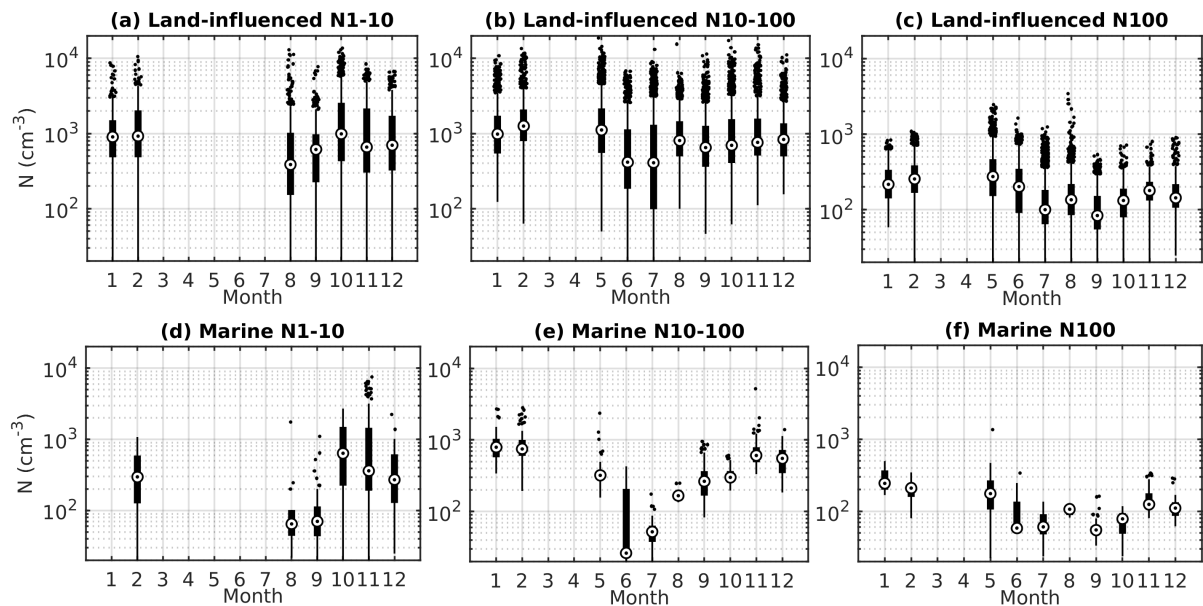


Figure 5.9: Seasonal cycles of particle number concentrations in 1-10 nm, 10-100 nm and above 100 nm during land-influenced (a-c) and marine (d-f) land masses. The circles are the median concentrations for each month, black boxes mark 25th and 75th percentiles, the whiskers mark 1.5 times the interquartile range and rest of the points are outside this range.

summer and late autumn. The fact that the cycle is less clear than in Aitken mode likely indicates that primary emissions, such as sea salt in the marine air and anthropogenic emissions in the land-influenced air, are more important relative to secondary particle formation in this size range compared to smaller sizes. The higher summer values can again be explained both by meteorological conditions and more active biological source during the summer. As mentioned earlier, previous work at Baring Head has shown that non-sea-salt sulfate concentrations in fine aerosols are higher during the late spring and summer (e.g., Li et al., 2018; Allen et al., 1997) and this secondary sulfate could increase particle concentrations in climate relevant sizes as well.

Looking at the diurnal cycles of particle concentrations can give us more information about the processes controlling particle concentrations. The clearest diurnal cycles can be seen for land-influenced N1-10 and N10-100 which both increase during the day (Fig. 5.10a-b). Median N10-100 is below 700 cm^{-3} in the morning and increases to above 1000 cm^{-3} in the afternoon. This is likely explained by particle formation during the day. N100 has a similar but weaker cycle, with median concentrations increasing during the day by less than 35 % compared to early morning hours. The fact that the concentrations in all size ranges increase steadily through the day, rather than for example having peaks during rush hours indicates that particles could grow past 100 nm with photochemistry during the day.

In marine air, the cycles are less clear and the concentrations vary less, especially in sizes past 10 nm. This is partly due to the fact that we have a lot less data from clean marine air masses, but it could also indicate that photochemistry and secondary aerosols play a smaller role in marine air than in land-influenced air.

Finally, we look deeper into the effect of land influence on particle concentrations. Figure 5.11 illustrates the effect of time spent over land on particle number concentrations. While time spent over land does not explain all of the variations in particle concentrations, the connection is clear. For sub-100 nm particles, the concentrations increase clearly during the first day spent over land, but after this the concentrations are more variable. This is logical, since when the air mass arrives from the sea to land, particle concentrations and the condensation sink are

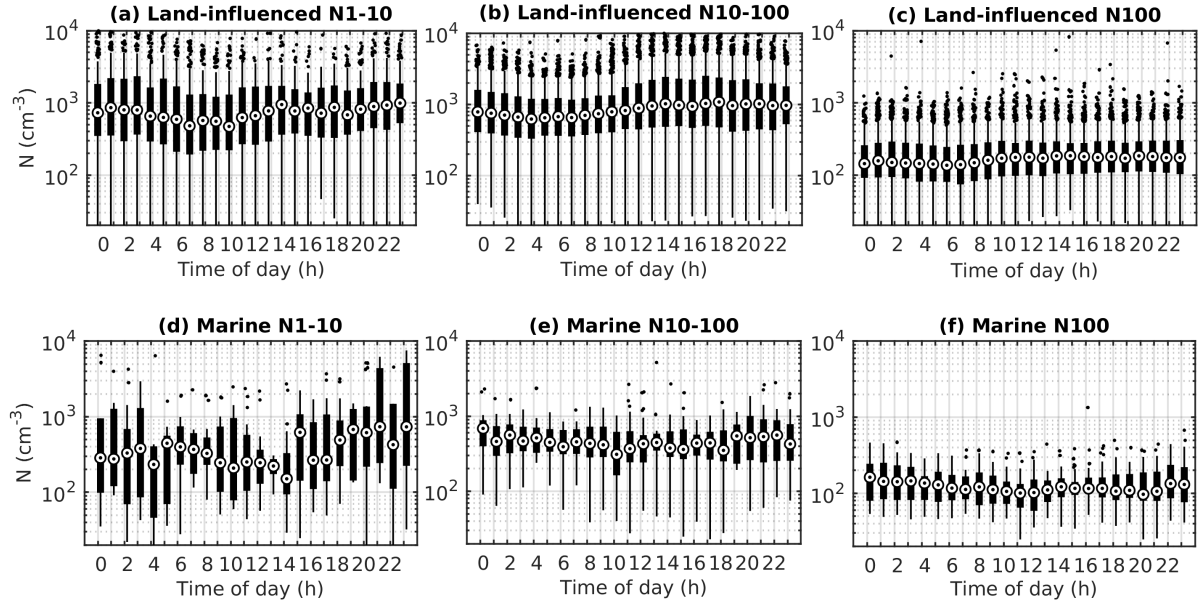


Figure 5.10: Diurnal cycles of particle number concentrations (N) in different size ranges separated by air mass origin. The circles are the median concentrations, black boxes mark 25th and 75th percentiles, the whiskers mark 1.5 times the interquartile range and rest of the points are outside this range.

low which favours new particle formation. This increases the sub-100 particle concentrations, but after a while the concentrations get saturated because the condensation sink increases and starts to limit NPF.

For N100, the increase is slower and continues a longer time. This is partly due to a larger fraction of the accumulation mode particles being primary particles. Primary particle emissions would not be suppressed by increasing condensation sink the same way secondary are. This trend is also influenced by the fact that it takes time for particles formed from NPF to grow past N100 and N100 is less sensitive to coagulation losses than smaller particles. While the number increase in accumulation mode is slower than for the smaller modes, the concentration is lower to begin with and it doubles in approximately one day. The concentration of accumulation mode particles is very important for cloud formation, because in this size range aerosols are likely to activate to CCN. Previous work has shown that doubling cloud droplet number concentration can nearly double the cooling effect of low-level marine clouds (Rosenfeld et al., 2019). Aerosol production over New Zealand is thus likely to play an important role in regional cloud formation over New Zealand and its surroundings.

5.3.3 Growth rates

To understand secondary aerosol formation at Baring Head better, this section shows the behaviour of aerosol diameter growth rates. Particle growth is important also because larger particles can in general activate as CCN at lower supersaturation levels (e.g., Kerminen et al., 2012). In total, the automated method calculated 652 growth rates out of which 197 started in nucleation mode, 356 in Aitken mode and 99 in accumulation mode. The average growth duration was 3 h 17 min.

The median growth rates were 1.6 (25th-75th percentiles 0.6–2.6), 1.6 (0.7–2.9) and 3.6 (1.6–6.2) nm/h for nucleation, Aitken and accumulation modes, respectively. A global study looking into nucleation mode growth rates saw slightly higher values at coastal sites with annual median growth rates of approximately 2.5 and 4 nm/h for Mace Head and Finokalia (Nieminen

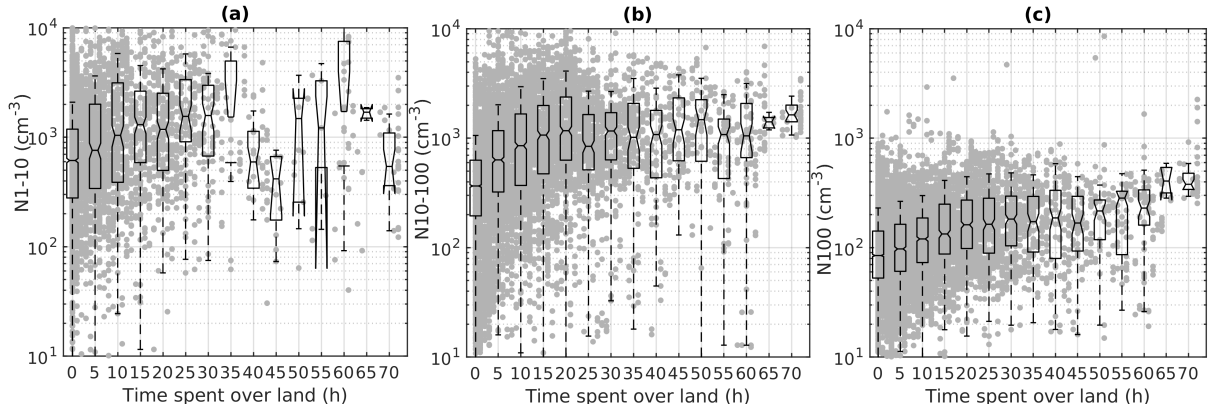


Figure 5.11: Number concentrations of particles in 1-10 nm (a), 10-100 nm (b) and above 100 nm (c) as a function of time spent over land in grey with the 5 hourly statistics displayed with the black boxplots. The horizontal lines of the boxplots mark the medians, the notches their uncertainty, the lower and upper limits of the boxes the 25th and 75th percentiles and the whiskers 1.5 times the interquartile range.

et al., 2018), respectively, which is reasonable since our site is more remote. Growth rates being higher for larger sizes has been previously observed for a boreal forest and around the Atlantic Ocean (Paasonen et al., 2018; Burkart et al., 2017). In those studies the increase of growth rates at larger sizes was explained by the role of semivolatile species, which are involved at a later stage of the growth.

If we divide the growth rate data set to fully marine and land-influenced growth rates, only 70 of the growth rates fit our criteria of clean marine air with fully marine back trajectories, average radon during growth below 100, and wind direction between 120–220°. Out of these 17 were in nucleation mode, 39 in Aitken mode, and 12 in accumulation mode. This means that we observed growth starting from nucleation mode 16.2 % of the time in clean marine air. For Aitken mode, this percentage was 26.4 %, and for accumulation mode 7.1 %. For marine air only, the median growth rates were 0.7 (0.4–2.0), 0.6 (0.1–2.3) and 2.5 (1.2–3.7) nm/h, for nucleation, Aitken and accumulation modes, respectively. The growth rates are lower in marine air than in land-influenced air which can be explained by lower concentrations of particle growing precursor species. A previous study looking into nucleation and Aitken mode growth in open ocean air at Mace Head saw typical growth rates of 0.8 nm/h (C. O’Dowd et al., 2010), which is similar to our results. These results show that even if we did not observe classical NPF events in clean marine air, particle growth starting from the nucleation mode is still frequent, meaning that new particle formation may have occurred but may have not been classified as a NPF event in the conventional classification designed for continental data. Moreover, we also observe the growth of larger particles frequently, meaning that secondary aerosol formation can be important for the marine CCN budget.

The diurnal cycles of growth rates in different modes (Fig. 5.12) were made based on a half an hourly time series made out of the growth rate data. It shows slightly higher nucleation mode growth rates during the day compared to before 9 h. This is logical since photochemistry can produce vapours that participate in particle growth. For Aitken mode particles, growth rates show morning (5–6 h) and early evening (16–18 h) minimums with median growth rates being highest during the day and late evening. In accumulation mode, the median values increase over the morning with maximums around midday and late evening. One possible factor explaining the higher growth rates towards the end of the day could be that the particles have grown to larger sizes by then and as mentioned before, larger particles can grow faster. Although both nucleation and Aitken modes have relatively high values during the summer (January), no well-defined seasonal cycles were seen for the GRs of any of the modes (Fig. 5.13). There are

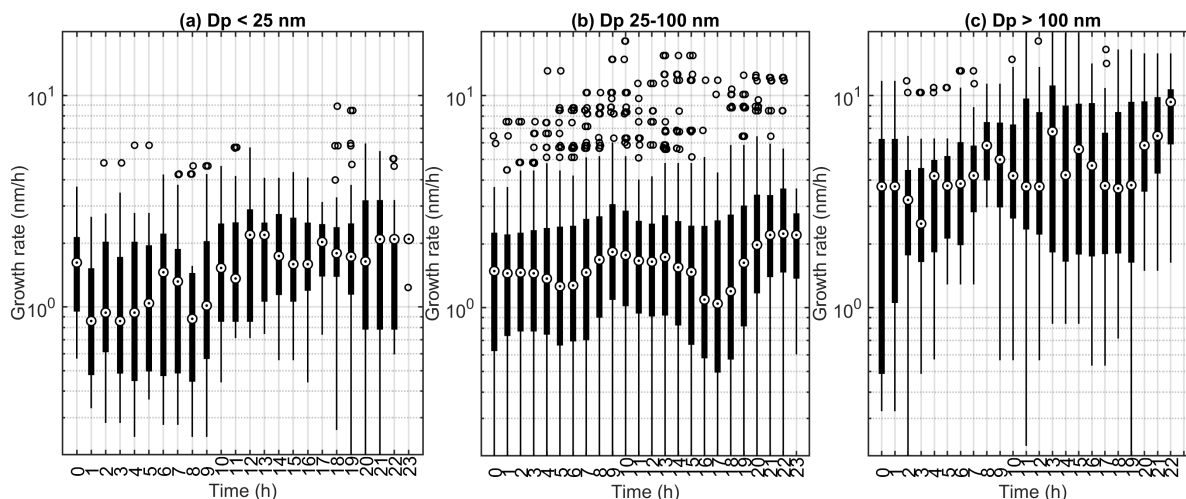


Figure 5.12: Diurnal cycles of growth rates divided by the diameter (D_p) of growing particles. The circles are the median concentrations, black boxes mark 25th and 75th percentiles, the whiskers mark 1.5 times the interquartile range and rest of the points are outside this range.

so few growth rate values for marine air that the diurnal and seasonal cycles are not reported separately for marine and land-influenced air.

5.3.4 Formation rates

Formation rates describe the intensity of particle formation and are proportional to the concentrations of particle forming chemical species. We found in total 28 Class I event days for which calculation of growth rates with the traditional mode fitting method was possible. The median formation rate of all these events was 0.18 (0.07 – 0.40) $\text{cm}^{-3}\text{s}^{-1}$. Our values fall in the same range as the values reported by Nieminen et al. (2018) for rural sites. In their study, the only coastal sites were Finokalia and Mace Head and their annual medians were around 0.35 – 0.4 $\text{cm}^{-3}\text{s}^{-1}$, which is approximately the double of ours. Again, this is presumably due to the remoteness of the Baring Head site. None of the events for which formation rates were calculated met our criteria for clean marine air. For four events, the air had spent over 95 % of the time above oceans and for these events formation rates were below 0.12 $\text{cm}^{-3}\text{s}^{-1}$, which is below the total median, again supporting the interpretation that the amount of particle forming and growing precursor vapours is lower in the marine atmosphere compared to land-influenced air. However, no correlation was found between formation rates and time spent above land or radon concentration.

5.3.5 Marine new particle formation

The unique location of the Baring Head station enabled studying clean marine air masses that had spent several days over open ocean before arriving at the station. This is why we were especially keen on studying secondary aerosol formation in these marine air masses. Even though most of the classical new particle formation events were observed in land-influenced air masses, the previous sections showed that sub-10 nm particles and particle growth from nucleation mode were frequent in the marine air masses. This section studies the potential sources of marine aerosols in more detail and shows examples of new particle formation in clean marine air.

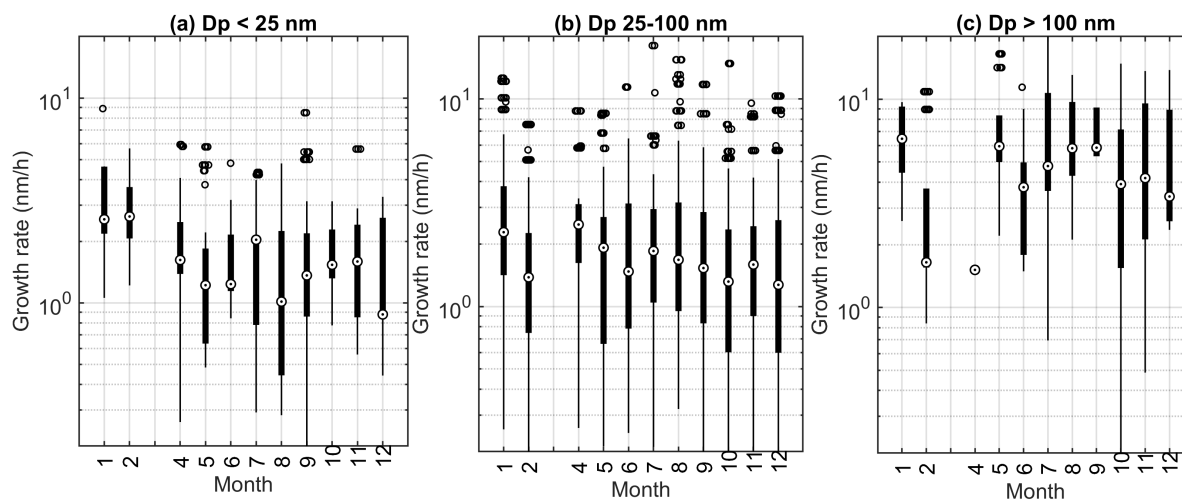


Figure 5.13: Seasonal cycles of growth rates in different modes. The circles are the median concentrations, black boxes mark 25th and 75th percentiles, the whiskers mark 1.5 times the interquartile range and rest of the points are outside this range.

Coastal effects

At some coastal sites, such as Mace Head, coastal sources can play a large role in NPF (e.g., Dall’Osto et al., 2011), because when coastal macroalgae are exposed to air, they can emit particle producing iodine species. To see if that is the case at Baring Head, we studied the relationship of negative 2-4 nm ions and tide height (Fig. 5.14). We decided to use this ion concentration, since it marks the first steps of particle formation. We used only data between sunrise and sunset since photochemistry would likely be important. We coloured the data in Fig. 5.14 with wind direction to see if more particles are produced from some direction, for example, if there is more macroalgae that produces particle precursors on one side of the station. No correlation was observed between ion concentration and tide height ($R = 0.0092$, $p = 0.5082$), which indicates that coastal sources are likely not important for particle formation at Baring Head. The wind direction colouring also shows no effect on ion concentrations. The vertical ‘lines’ in the tide height data in the plot are due to the 0.1 m resolution of the tide height data. The lack of connection to tides can be partly explained by the fact that at Baring Head, the tide height varied by less than 1.5 m, whereas in Galway Bay, where Mace Head is located, the water level can vary by up to 4 m (Ren et al., 2015). Iodine emissions are also very different for different algal species (Carpenter et al., 2000) and we do not know which species are present close to Baring Head.

Regions favouring particle formation

To obtain more information about geographical locations that could favour particle formation, we used the air mass back trajectories to see if back trajectories coming from some areas would be more likely to form particles than others. This could be the case for example if some areas of the ocean were more biologically active and produced more particle emitting precursor species. A similar method has been earlier used by Rose et al. (2015a). Figure 5.15a shows all the back trajectories weighted by 2-4 nm ion concentrations. This parameter was chosen because it often indicated the start of NPF. The highest ion concentrations are observed when the air masses come from Tasmania and the sea east of Tasmania. This could be explained both by the transport of particle precursors from Tasmania and the fact that when the air mass comes from this direction, it typically has to cross over the Wellington region before arriving at the station.

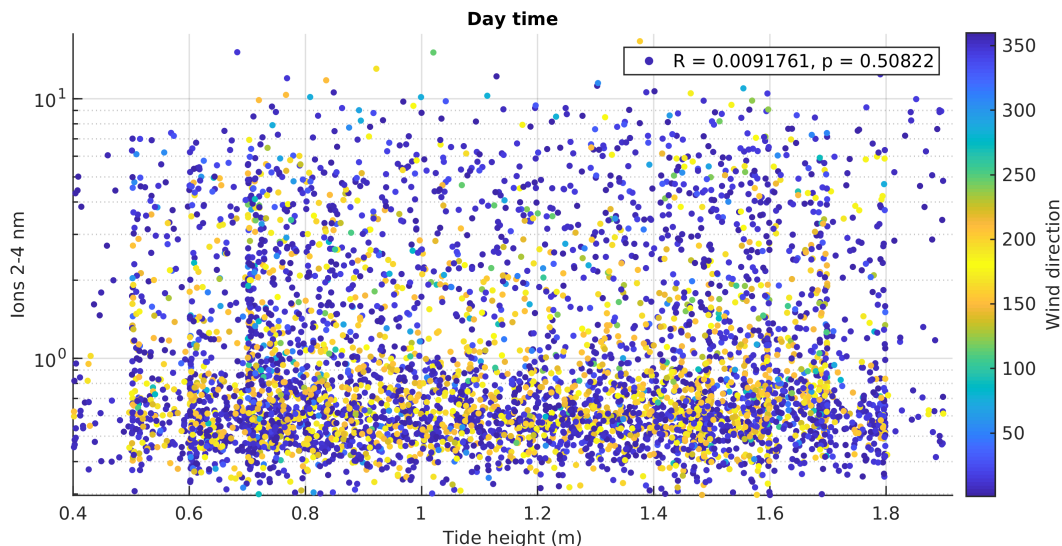


Figure 5.14: The number concentration of ions as a function of tide height coloured with wind direction. Only data after sunrise and before sunset are included.

Apart from the high concentrations coming from Tasmania, some higher concentrations can be seen just north of New Zealand and in some patches over the Southern Ocean. The area north of New Zealand could be related to air masses passing through the North Island. Patches with higher concentrations in the south could be related to air transport from more biologically active areas.

Figure 5.15b follows the same concept as Figure 5.15a, but uses only back trajectories that were classified as fully marine and come from the southerly wind sector ($120\text{--}220^\circ$). We did not use the radon criteria for this figure since there were too little data. Now the highest ion concentrations appear for the most northwestern back trajectories. This could be explained by these air masses crossing the coast of the South Island. Apart from that area, the trends are not too clear, meaning that the geographical area from which the air masses come from over the ocean is likely not important for particle formation when looking at data integrated over several seasons.

Example of marine new particle formation

Since both sub-10 nm particles and particle growth starting from nucleation mode were frequent in clean marine air masses, but these did not classify as traditional NPF events, marine new particle formation should be studied with different criteria than classical NPF. Here, we look deeper into some of these new particle formation and growth events in clean marine air and the conditions prevailing during the events. This way, we can better understand the processes driving new particle formation and growth in clean marine air.

Figure 5.16 shows an example of several growth periods, occurring in clean marine air during the 9th and 10th of November 2020. Part of these growth periods start from the nucleation mode and part from larger sizes. During this time, the aerosol size distribution is largely dominated by two modes, one centred around 20-30 nm and another around 90-140 nm. The whole period is characterised by high wind speeds ($> 18 \text{ ms}^{-1}$) and temperatures below 11°C (Fig. 5.17). Significant wave heights vary between 1.7–5 m and clouds are likely present for most of the period. On the 9th, the fact that global radiation levels are elevated but do not follow a clear parabolic shape likely indicates the presence of scattered clouds. On the 10th, on the other hand, global radiation levels remain below 0.5 MJm^{-2} during the whole day, indicating that the day was very cloudy. This is supported by the relative humidity being above 80 % from

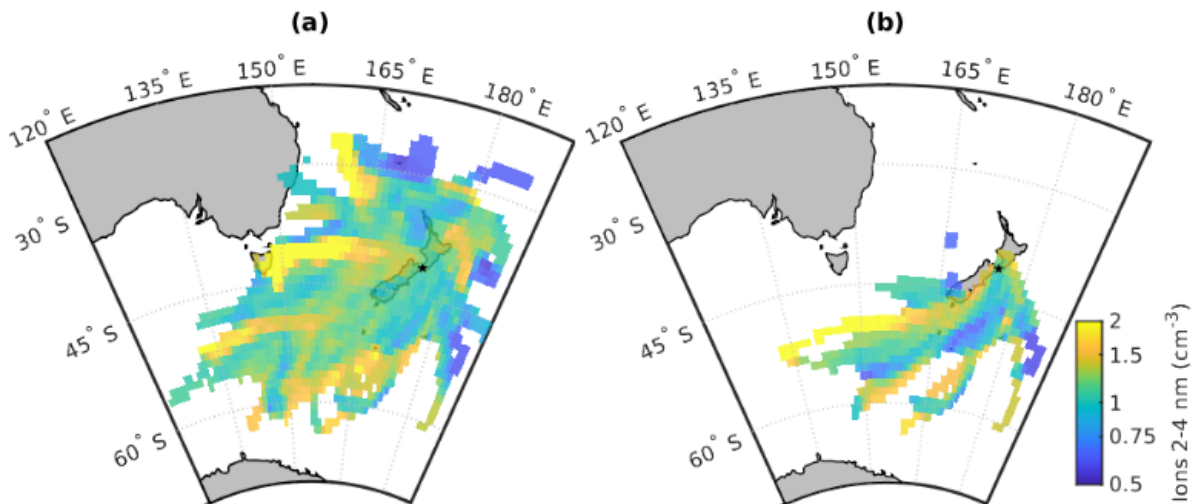


Figure 5.15: Source regions of 2-4 nm ions for all data (a) and only marine data (b).

midnight to late afternoon. All air mass back trajectories during this period originated from the ocean south west of New Zealand (SI Fig. 5.19). The heights of all the back trajectories remained below 400 m, indicating that the air masses had likely spent the past three days within the marine boundary layer.

The 9th of November day was not classified as an NPF event by the Dada et al. (2018) method and it was only an undefined day with the Dal Maso et al. (2005) criteria, because nucleation mode particle concentrations were already high at the beginning of the day. However, there are several growth periods, most of which occur between midday and midnight of the 9th. During this time, wind speed and wave height are lower than before and after this period, which likely decreases the sink of condensing vapours. Compared to the second day, this day is also less cloudy, which enhances the photochemical processes. On the second day (November 10th), we see only a very weak growth in Aitken mode in the afternoon, which is not surprising since the day is very cloudy and there are high waves and wind speeds.

While the lowest size bin of SMPS data remains low for most of the time, in the early hours of November 9th, the concentrations of sub-10 nm and even sub-3 nm particles peak clearly (Fig. 5.16b). The fact that the sub-10 nm particles reach concentrations as high as 1600 cm^{-3} during this clean marine air period indicates that nucleation can occur within the marine boundary layer and at nighttime. When the concentration in the sub-10 nm size classes decreases, we can see some particles in the lowest size bin of SMPS data, indicating that these particles grew past 10 nm. After 6 h, however, this mode seems to weaken. This coincides with the sunrise, so one possible explanation is that when the sun rose, boundary layer height increased and the particles concentrations were diluted. The N1-10 remains relatively high until 12–13 h, when we see the appearance of a clearer growing nucleation mode. It is thus possible that the particles that were formed after midnight survived and only started growing in nucleation mode in the afternoon when there was more radiation. It should be noted that the particle concentrations in the lowest size bins of the SMPS data are likely underestimated because of diffusion losses in the inlet, the dryer and the instrument itself. This is to some extent true also for the sub-10 nm and especially sub-3 nm particle concentrations although the inlets to the PSM and CPC were shorter than the SMPS inlet and did not contain a dryer. This example illustrates that event though this day is not classified as a typical 'banana' type event, new particles likely formed and grew within the marine boundary layer.

Simultaneous growth of the smaller and larger modes during the 9th shows again that growth is faster for larger particles. The highest growth rate of 8.5 nm/h observed between 12 and 18

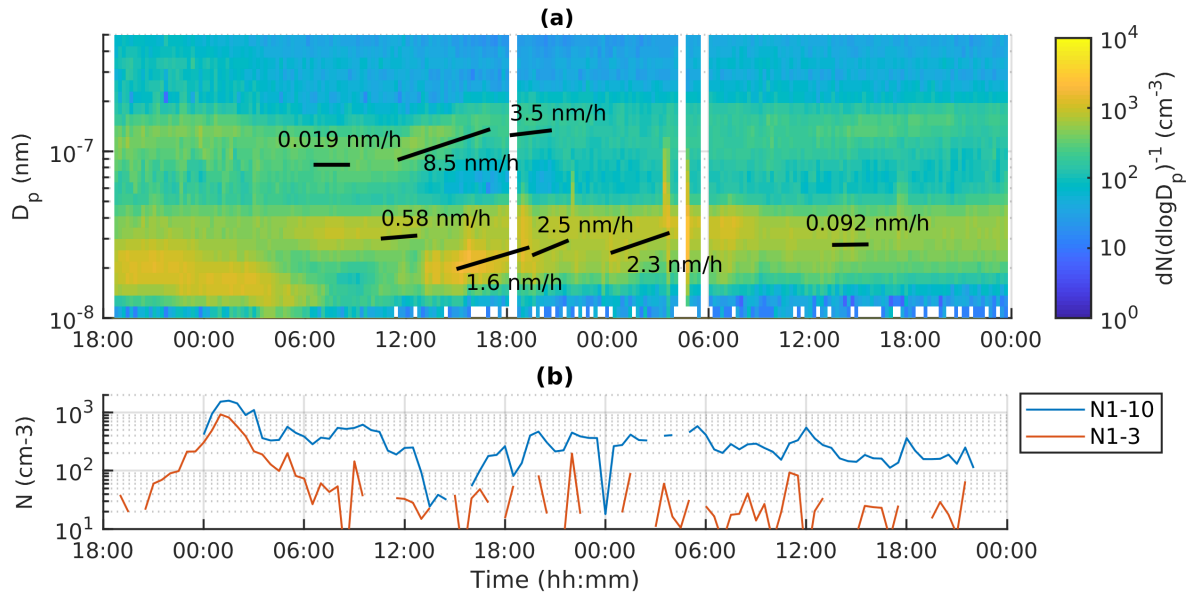


Figure 5.16: An example of particle size distribution and observed growth rates (a) with the number concentrations observed with PSM (b) from November 8th at 18:00 to end of November 10th 2020. The vertical white stripes in the size distribution correspond to land-influenced periods that were not included here.

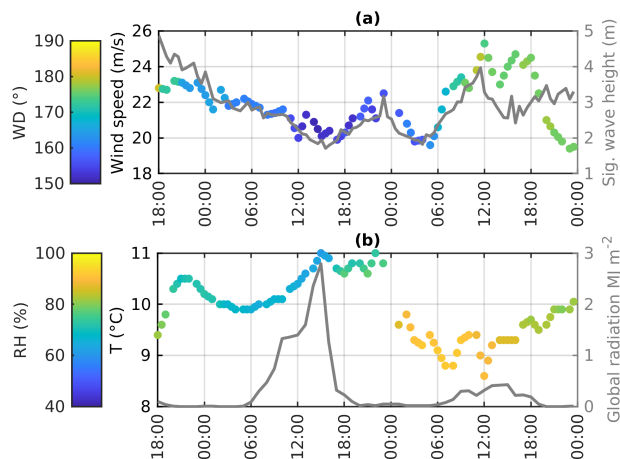


Figure 5.17: Summary of meteorological conditions (wind direction (WD), wind speed, relative humidity (RH), air temperature (T) and global radiation) and wave height from November 8th at 18:00 to end of November 10th 2020.

h on the 9th could be related to cloud processing and aqueous phase processes increasing the particle size. This is supported by a decrease in the concentration of 60-90 nm particles below the growing mode. Particles in this size range correspond to sizes in which the particles could have been activated into cloud droplets and grown due to cloud processing leading to a so called Hoppel minimum (see e.g. Noble and Hudson, 2019).

While it is possible that some of the nucleation mode particles that we see growing in the clean marine air come from sea spray (A. N. Schwieter et al., 2015; Forestieri et al., 2018), observing particles below 10 and even below 3 nm strongly indicates that nucleation can also occur in the marine boundary layer and the freshly nucleated particles can grow to larger sizes. Previous studies at Mace Head, in Ireland, have observed growth events similar to ours in open ocean air masses but whether these particles originated in the marine boundary layer or free troposphere was not certain (C. O'Dowd et al., 2010; Dall'Osto et al., 2011). Since our observations also contain measurements of aerosol particles in the size range of freshly nucleated particles, our work shows evidence that nucleation could be occurring within the marine boundary layer. One key message from our work is that marine secondary aerosol formation should not be studied with the same criteria as continental new particle formation.

Factors favouring new particle formation in marine air

As shown in this chapter, particle formation in marine air masses does not follow the traditional event criteria. This is why, in addition to the analysis in Section 5.3.1, we compared meteorological conditions in marine air with high and low concentrations of sub-10 nm particles to understand the factors driving marine particle formation. Here, we separate the data in marine air masses to times when N1-10 is less than 500 or over 500 cm^{-3} . This somewhat arbitrary limit was chosen because in the example figure (Fig. 5.16), the clearest peak in N1-10 exceeded this limit. Most of the conclusions of this analysis remained the same even if the limit was increased to 1000 cm^{-3} or decreased to 100 cm^{-3} . Out of all the data in clean marine air, 12.7 % had N1-10 over 500 cm^{-3} . This is close to the fraction of time during which we observed growth starting from nucleation mode. With this data partition, we can see that global radiation levels are similar independent of N1-10 levels (Fig. 5.18a). This is not surprising, since our previous results showed that N1-10 could be high even during the night. Marine cluster formation cannot thus be explained by photochemistry alone.

With temperature, we can see at that times when N1-10 is higher, temperatures are on average lower (Fig. 5.18b). This is logical, because low temperatures can favour NPF by increasing nucleation rates (see e.g., Burkholder et al., 2004; Simon et al., 2020). For relative humidity (Fig. 5.18c), we see lower values when N1-10 is high. This is reasonable since high relative humidity can be related to weather with fog or low rainy clouds which would increase particle losses.

With wind speed, we can see higher N1-10, when wind speeds are lower (Fig. 5.18d). This makes sense because at high wind speeds waves and sea spray aerosol production would typically be higher and sea spray aerosol can act as a sink for the smallest particles and their chemical precursor species. This can be also seen with the condensation sink, which is on average lower when N1-10 is high (Fig. 5.18e). Previous work at Baring Head has estimated that the CS at the station would be too high for NPF to occur (J. Cainey and M. Harvey, 2002). Their work focused only on particle formation from SO_2 from marine sources, but since then, many other particle precursors have been identified, meaning that even if nucleation from SO_2 was unlikely, nucleation from other precursors can still occur.

With ozone, we see slightly higher values when N1-10 is high (Fig. 5.18f), but the differences are small. Ozone could play some role in the chemical processes that influence particle formation in marine air, but the exact mechanisms cannot be studied with this data.

This analysis shows that initial particle formation in marine air is favoured by low temperatures, low relative humidity, and low wind speeds. While this is in line with what we saw with

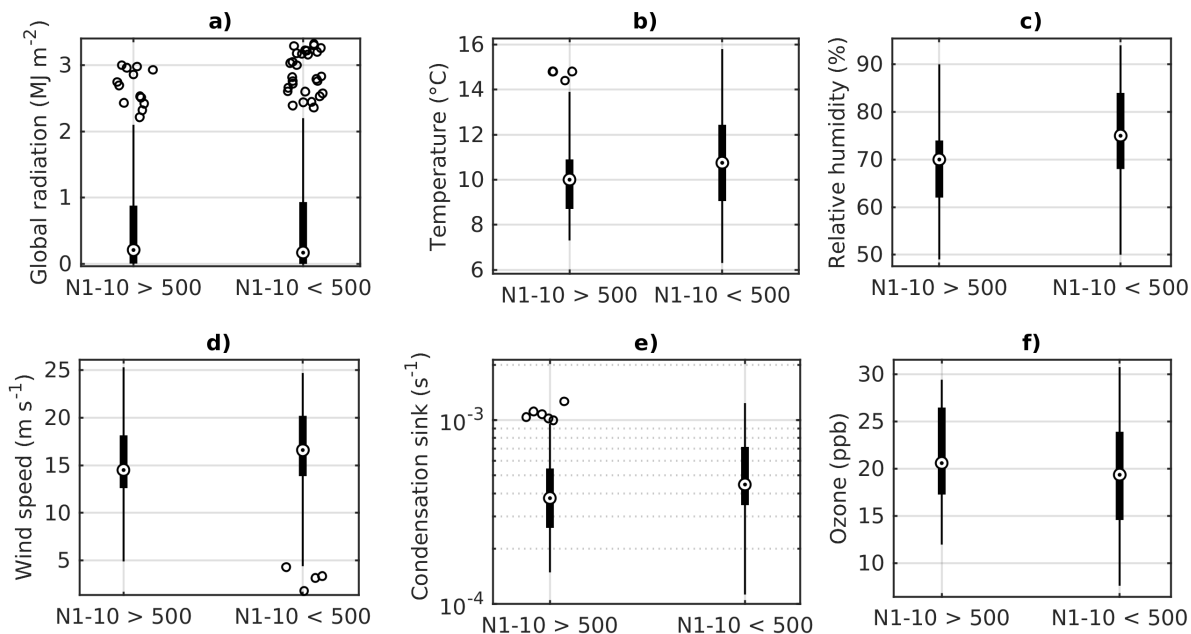


Figure 5.18: Box plots for different meteorological variables, condensation sink and ozone in marine air when N1-10 is a) over 500 b) and under 500 cm^{-3} .

the traditional event analysis, the traditional events were also favoured by high global radiation levels and likely driven by photochemistry, which is not true for particle formation in marine air. the next chapter will study the different chemical species observed at Baring Head and look deeper into the factors controlling NPF at the site.

5.4 Conclusions

We studied new particle formation and typical aerosol number concentrations at Baring Head, New Zealand. The site is remote and enables studying clean marine air masses. During our 10 month measurement period, the average event frequency was 23 %, with the least events observed during the winter. These events detected with a traditional method designed for continental sites occurred primarily in land-influenced air and were favoured by high global radiation levels, low relative humidity, and low wind speeds. Aerosol number concentrations in all size ranges were significantly higher in land-influence air compared to clean marine air. The concentrations increased when the air mass spent more time over land, with accumulation mode particle concentrations doubling in a day, showing that aerosol production over New Zealand could have an effect on the regional cloud formation and properties.

In clean marine air, clear new particle formation events, when detected according to the NPF classification methods made for a continental site, were rare. However, we observed both sub-3 nm particles and particle growth starting from the nucleation mode in air masses that had only spent time within the marine boundary layer, showing that nucleation can happen within the marine boundary layer. Whilst these events do occur, they are weaker than terrestrially influenced NPF events. Unlike at some other coastal sites, coastal sources did not seem to play a significant role in aerosol formation at Baring Head. Formation of sub-10 nm particles was favoured by low temperatures, relative humidity and wind speeds. Our results highlight the need to study marine NPF with different criteria than continental NPF.

During our measurements, only 7.3 % of the data could be classified as clean marine air. In the future, it would be good to continue the measurements over longer periods to obtain more

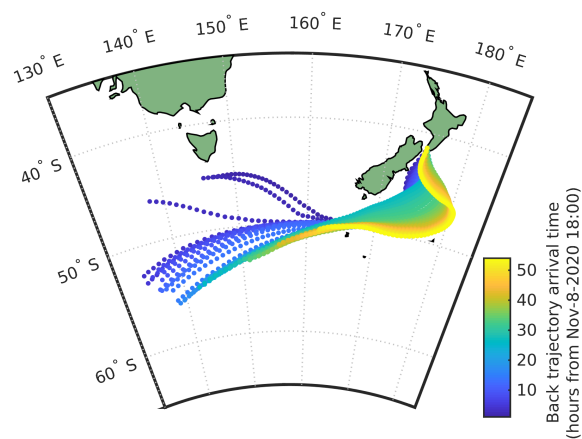


Figure 5.19: Back trajectories for time from November 8th at 18:00 to end of November 10th 2020.

information on the importance of new particle formation in open ocean air. The next chapter will focus on identifying the chemical precursors of new particle formation and growth at the site to provide a more complete picture of factors driving the particle concentrations both at the site in general and specifically in open ocean air.

Chapter 6

Chemical composition of ambient ions and their connection to new particle formation

This section describes the chemical composition of negative ambient ions measured at Baring Head over a 7 month period with the APi-TOF mass spectrometer. We show which chemical species are most commonly observed and explain their typical behaviour in clean marine and land-influenced air masses. Then we use these data to study how different chemical species influence new particle formation and growth.

6.1 Measurement setup

The measurements used in this chapter are otherwise the same as those used in the previous chapter, but here we use also APi-TOF data to determine the chemical composition of ambient ions. The APi-TOF was located in the same space with the aerosol instrumentation and the location of its inlet was also the same as for the main aerosol instruments. The inlet was made of stainless steel, its diameter was 3/8" and its length was 91 cm. The APi-TOF was originally installed at the station in June 2020. In the beginning of the measurements the flow rate to the instrument was approximately 6 lpm, but on July 16th 2020 the flow rate was increased to 11 lpm to decrease diffusion losses. The flow rate is important because it influences the diffusion losses of the ions to the inlet walls. It has been shown that losses of ions due to coagulation are twice as high as for neutral clusters (Mahfouz and Donahue, 2020) and we could see that changing the used flow rate clearly affected the results, showing that inlet losses were important. The data after July 16 has more observable peaks than the earlier data and the peaks that were observable earlier have higher signals. To keep the data at different times comparable, we use only data after July 16. The measurements continued until January 2021 and the data availability for this period was illustrated in the previous chapter.

6.2 Detected species

Figure 6.1 shows an example mass spectrum of APi-TOF data summed over 24 h. The largest peaks consist of nitrate ion, its water cluster, bisulfate and its cluster with sulfuric acid. This is similar to what has been observed previously with an APi-TOF in a boreal forest (Junninen et al., 2010). Pure sulfuric acid clusters were detected up to the trimer, which is what has been observed earlier with similar measurements in a boreal forest (C. Yan et al., 2018), but contrary to their work, we saw no sulfuric acid clustered with ammonia.

In addition to the highest peaks, we can observe clear peaks for chloride, iodate and different organic compounds. Around m/Z 300–400 we can see peaks that correspond to highly oxygenated organic molecules (HOM) and are likely monoterpene ($C_{10}H_{16}$) oxidation products (see for example C. Yan et al., 2016). The highest peaks in this mass range corresponded to $C_{10}H_{14}O_7NO_3^-$, $C_{10}H_{14}O_9NO_3^-$, $C_{10}H_{16}O_9NO_3^-$, and $C_{10}H_{14}O_{11}NO_3^-$, which have earlier been observed to be the highest peaks in a boreal forest and in α -pinene oxidation chamber experiments as well (see, Ehn et al., 2012). The majority of the observed peaks were below m/Z 400 with barely any peaks observed above m/Z 500. The lack of peaks at higher masses can be explained by a combination of clean air, losses in the inlet and potential non-optimal tuning of the instrument. Baccharini et al. (2021) had similar issues of not detecting expected peaks at higher masses in the Southern Ocean close to Antarctica despite using chemical ionisation. Future studies in clean air should aim to further lower the detection limits of the instrument or to optimise instrument settings so that compounds with larger masses could be observed and identified as well.

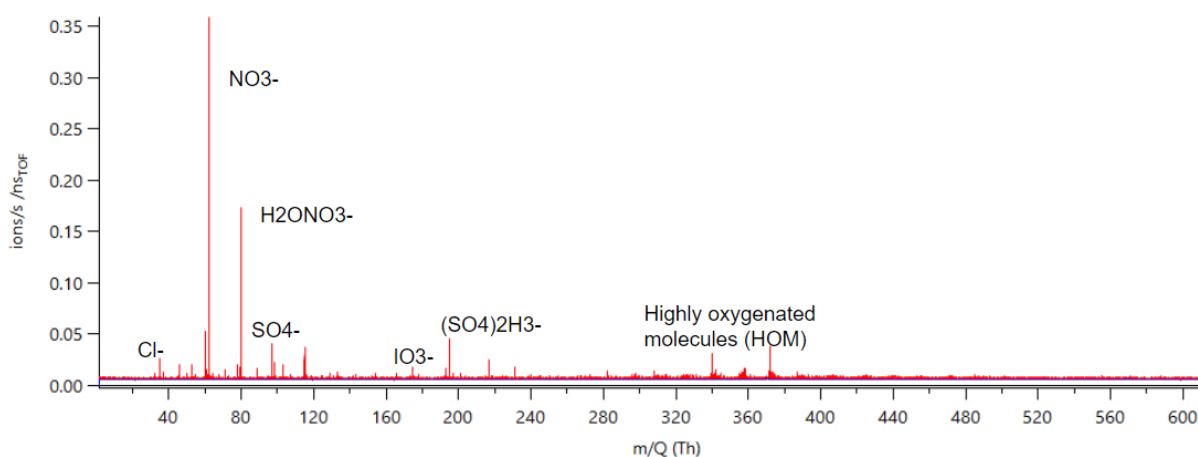


Figure 6.1: Example of APi-TOF spectrum summed over 24 h with some of the major peaks identified.

6.2.1 Identifying relevant compounds

In addition to identifying major peaks in the mass spectrum, we fitted all the peaks that could be found in the APi-TOF data and grouped potentially interesting species based on their correlations with each other and the aerosol data. For this we used so called 'schemaball' plots (<https://se.mathworks.com/matlabcentral/fileexchange/42279-okomarov-schemaball>, last accessed June 2021). In the schemaball plots, each line corresponds to a correlation between two different variables and the colour of the line is relative to the strength of the correlation. Only correlation coefficients with p-values smaller than 0.05 are drawn. The idea of these plots is to visualise the interactions between all the selected peaks and to create useful compound groups for further analysis. In addition to using all the peaks that we were able to fit to the data, we included particle number concentrations and growth rates in different size ranges to see if some compounds correlate with these variables. This was done because later we want to connect the chemical species to aerosol formation.

We drew these plots for both marine and land-influenced air and for different times of the day in these air mass classes (0-5 and 8-15 h, not shown here). Figure 6.2 shows the schemaball for land-influenced air using all times of day. Observed negative correlations can be explained by the diurnal variations of the compounds, which will be further discussed in the next section. For example NO_3^- has negative correlations with sulfate and its clusters, because daytime spectra are dominated by sulfate while NO_3^- is typically the most abundant nighttime ion. Positive

correlations can be seen with similar compounds, for example IO_3^- and H_2IO_4^- , compounds with sulfuric acid, and different HOMs correlate positively with each other. In marine air (Fig. 6.3), the observed negative correlations are primarily similar to land-influenced air. For positive correlations, the most striking difference to land-influenced data is the lack of strong correlations between different HOMs.

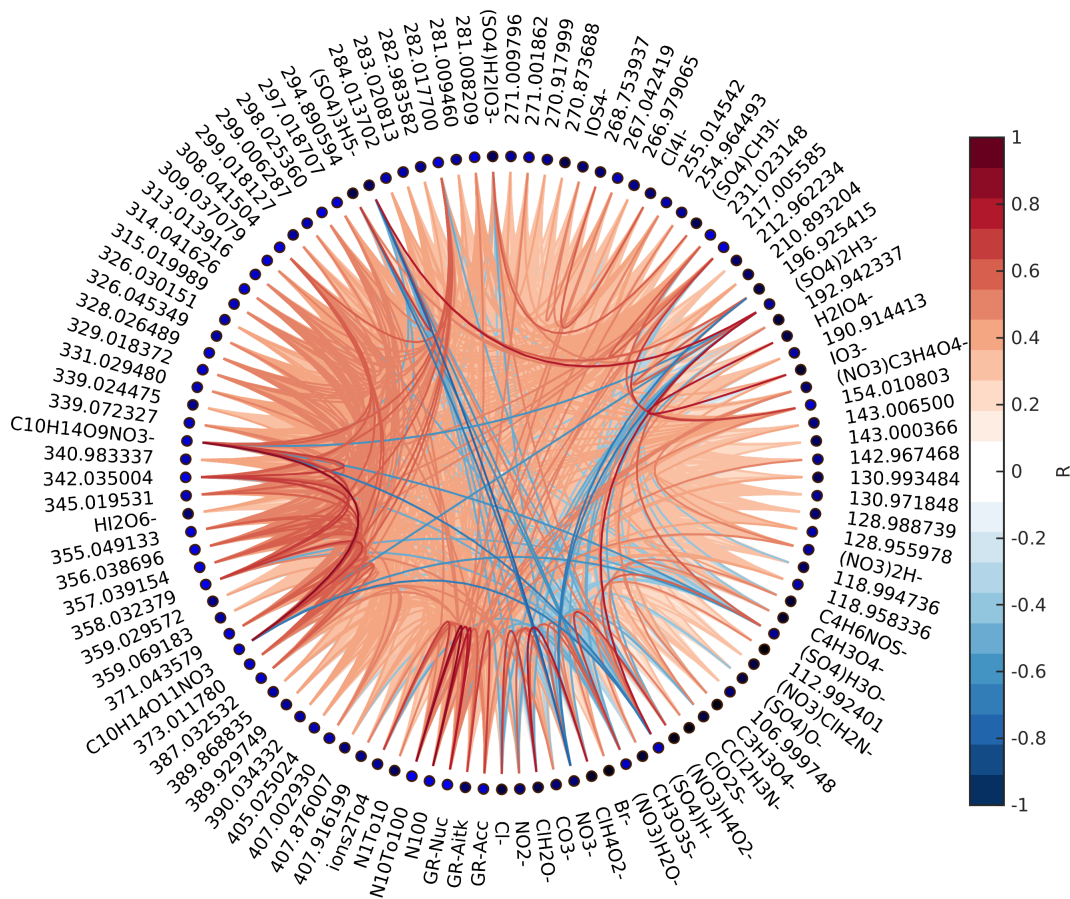


Figure 6.2: Correlations between different APi-TOF peaks, particle number concentrations and growth rates in land-influenced air. Each line corresponds to one correlation coefficient and the strength of the correlation defines the colour of the line (see colour bar). Lines are drawn only for correlation coefficients with p-values below 0.05.

Based on these figures and similar figures limited to night- (0-5 h) and daytime (8-15 h) data, we chose 11 compound groups and 4 groups of unidentified ions for further analysis. The groups with identified compounds are ΣNO_3 (NO_3 , $\text{NO}_3\text{H}_2\text{O}$ and $(\text{NO}_3)_2\text{H}$), ΣSA (HSO_4^- , $(\text{SO}_4)_2\text{H}_3^-$ and $(\text{SO}_4)_3\text{H}_5^-$), MSA ($\text{CH}_3\text{O}_3\text{S}^-$), ΣCl (Cl^- , ClH_2O^- and ClH_4O_2^-), bromide, ΣI (IO_3^- and H_2IO_4^-), HI_2O_4 , $\Sigma \text{S+I}$ ($(\text{SO}_4)\text{CH}_3\text{I}^-$ and $(\text{SO}_4)\text{H}_2\text{IO}_3^-$), ΣHOMs ($\text{C}_{10}\text{H}_{14}\text{O}_7\text{NO}_3^-$, $\text{C}_{10}\text{H}_{14}\text{O}_9\text{NO}_3^-$, $\text{C}_{10}\text{H}_{16}\text{O}_9\text{NO}_3^-$ and $\text{C}_{10}\text{H}_{14}\text{O}_{11}\text{NO}_3^-$), and $\Sigma \text{Malonate}$ ($\text{C}_3\text{H}_3\text{O}_4^-$ and $(\text{NO}_3)\text{C}_3\text{H}_4\text{O}_4^-$) and $\text{C}_4\text{H}_3\text{O}_4^-$, which is either maleate(1-) or fumarate(1-), but here we will call it simply maleate.

As mentioned in the previous section, nitrates and sulfuric acid compounds have typically the highest concentrations of all ions. Additionally, sulfuric acid is known to be important for aerosol nucleation and growth. Methane sulfonic acid (MSA) is a dimethyl sulfide oxidation product and can also be important for marine aerosol formation. Halogens chloride, bromide and iodine can all have important roles in atmospheric chemistry and especially iodine oxides are known to be potential aerosol precursors (see e.g., Nicovich et al., 2006; Muller et al., 2019; He et

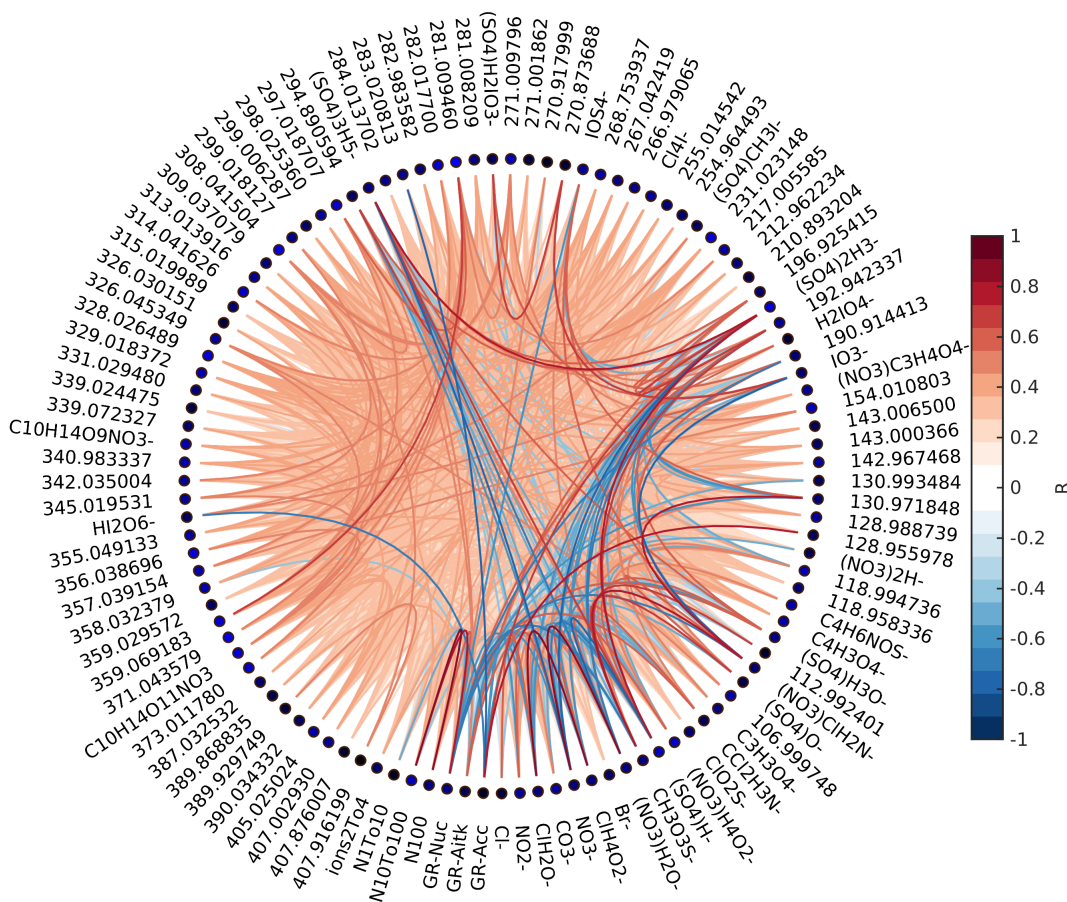


Figure 6.3: Correlations between different API-tof peaks, particle number concentrations and growth rates in marine air. See Figure 6.2 for explanation.

al., 2021). We divided the identified iodine oxides into two groups, one with IO_3^- and H_2IO_4^- , since these two species had a positive correlation with each other and HI_2O_4^- separately since it was not observed as often as the two other iodine species and it was the only iodine oxide with a larger mass that was identified. Additionally, we have a group that contains compounds with both iodine and sulfur. This group is specifically interesting since recent modelling work has indicated that having both MSA and iodine oxides present could increase particle formation rates compared to particle formation from iodine oxides alone (Ning et al., 2021). For organic species we have the most abundant HOMs in one group and two different groups for organic acids (malonate and maleate). HOMs are able to form new aerosol particles (e.g. Bianchi et al., 2019). Malonic acid is a saturated dicarboxylic acid and it has been found to be the second most abundant dicarboxylic acid in the Southern and Pacific Oceans after oxalic acid (H. Wang et al., 2006). Maleic and fumaric acids are unsaturated dicarboxylic acids and a previous campaign in the Southern Ocean found maleic and fumaric acids to have an order of magnitude lower concentrations than malonic acid (H. Wang et al., 2006). Dicarboxylic acids can be derived from isoprene emissions and unsaturated fatty acids at the sea surface (Bikkina et al., 2014), which can both be related to new particle formation (see, Alpert et al., 2017; Meskhidze and Nenes, 2006). This is why all of these compounds are of interest and relevant for studying new particle formation.

Additionally we have four groups containing unidentified compounds. These groups were

chosen so that we would not miss potentially important compounds. Group "Other1" contains peaks at masses 281.0094 and 359.0691, since they showed strong correlations in marine air. "Other2" contains peaks at 143.006, 271.009, 326.04 and 299.006 since these compounds had relatively stronger correlation in marine air during the night. "Other3" contains peaks at masses 154, 217, and 231 because they showed correlations in land-influenced air. "Other4" contains peaks at 331.02, 339.02, 345.01, 373.01 as they seemed important in land-influenced air during the day. At least some of these peaks are likely organics, since some of them correlated with other organic species and the peaks did not match for example any iodine oxide or sulfuric acid peaks that we would be aware of. One of the reasons why we use several different groups for unidentified species was to ensure that important species were not missed by grouping species from different sources to the same group.

In the following sections we study the behaviour of these groups and use them to study the sources of different chemical species and possible new particle precursors.

6.2.2 General comparison of marine and land-influenced air masses

To gain some understanding on where different compounds come from, Figure 6.4 illustrates how the average concentrations of selected ions differ in marine and land-influenced air masses by showing the ratio of average marine to land-influenced ion groups' concentrations. Most of the ions are more abundant in marine air, which shows the importance of ion losses to aerosol population in land-influenced air. The most significant difference can be observed for MSA, which has around 14 times as high concentrations in marine air as in land-influenced air. This is not a surprise since MSA comes from marine sources and when the air has spent time over land, MSA from the ocean has likely had some time to condense on the aerosol surface. Chloride and bromide are also relatively high in marine air which is expected since they have marine sources as well.

The only species that seem to be higher in land-influenced air are organics and unknown compounds, which are also likely organics. The difference is clearest for the HOMs which were likely monoterpene oxidation products and their likeliest source is the forests. The only organic group in this analysis that has higher concentrations in marine air is maleate. It can be produced by photochemistry and it can be derived from compounds produced in biologically active marine areas, which would explain why it is more abundant in marine air.

6.3 Diurnal cycles

To understand the processes controlling the concentrations of key ion species, we plotted the diurnal cycles of the ion groups separately for clean marine and land-influenced air (Fig. 6.5). The separation of the two air mass classes is the same as used in the previous chapter. The important thing to remember when looking at ion concentrations is that they are driven not only by changes of concentrations of neutral species, but also by charge availability and losses.

The first ion group is the sum of nitrates (Fig. 6.5a). Nitrate is one of the most common ions in the atmosphere (Eisele, 1989). The nitrate ions have a clear diurnal cycle with lower daytime concentrations and increase during the night. This is because during the day, NO_3 is destroyed by photolysis (e.g. Wayne et al., 1991). Another possible daytime loss term of nitrate ions is the loss of charge to sulfuric acid. This has been seen before at other measurement sites (Eisele and Tanner, 1990; C. Yan et al., 2018). The diurnal cycles of nitrates are similar in marine and land-influenced air. During the day, around 11-13 LT, marine air has slightly higher concentrations than land-influenced air. A possible explanation for this is that total ion losses in marine air are lower than in land-influenced air, because the total aerosol surface area (condensation sink) is lower (see previous chapter).

The second ion group is the sum of bisulfate ions and bisulfate ions clustered with sulfuric

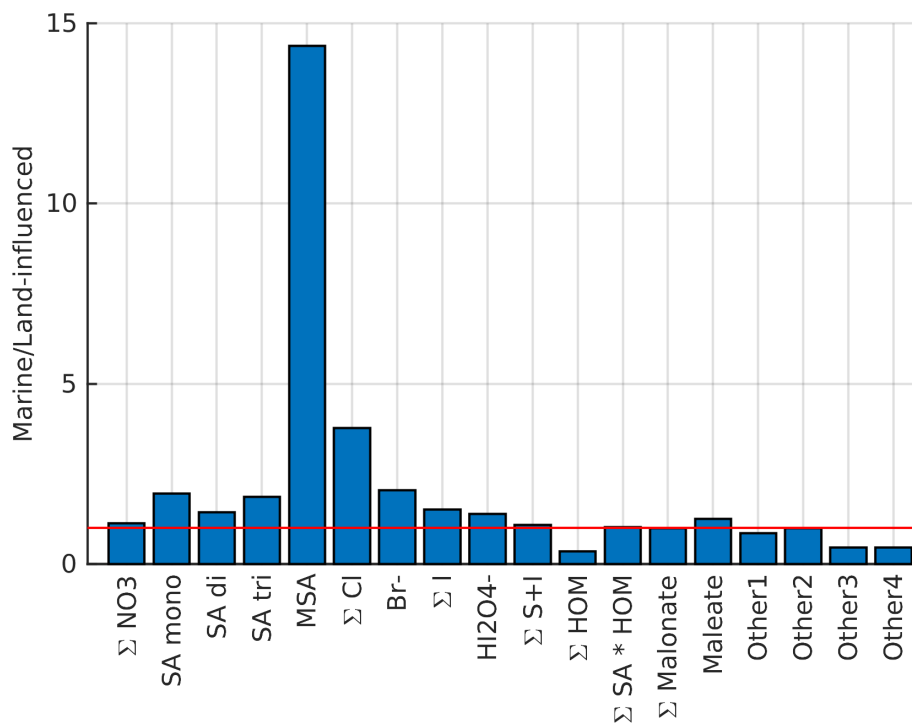


Figure 6.4: Comparison of ion signals in marine and land influenced air masses.

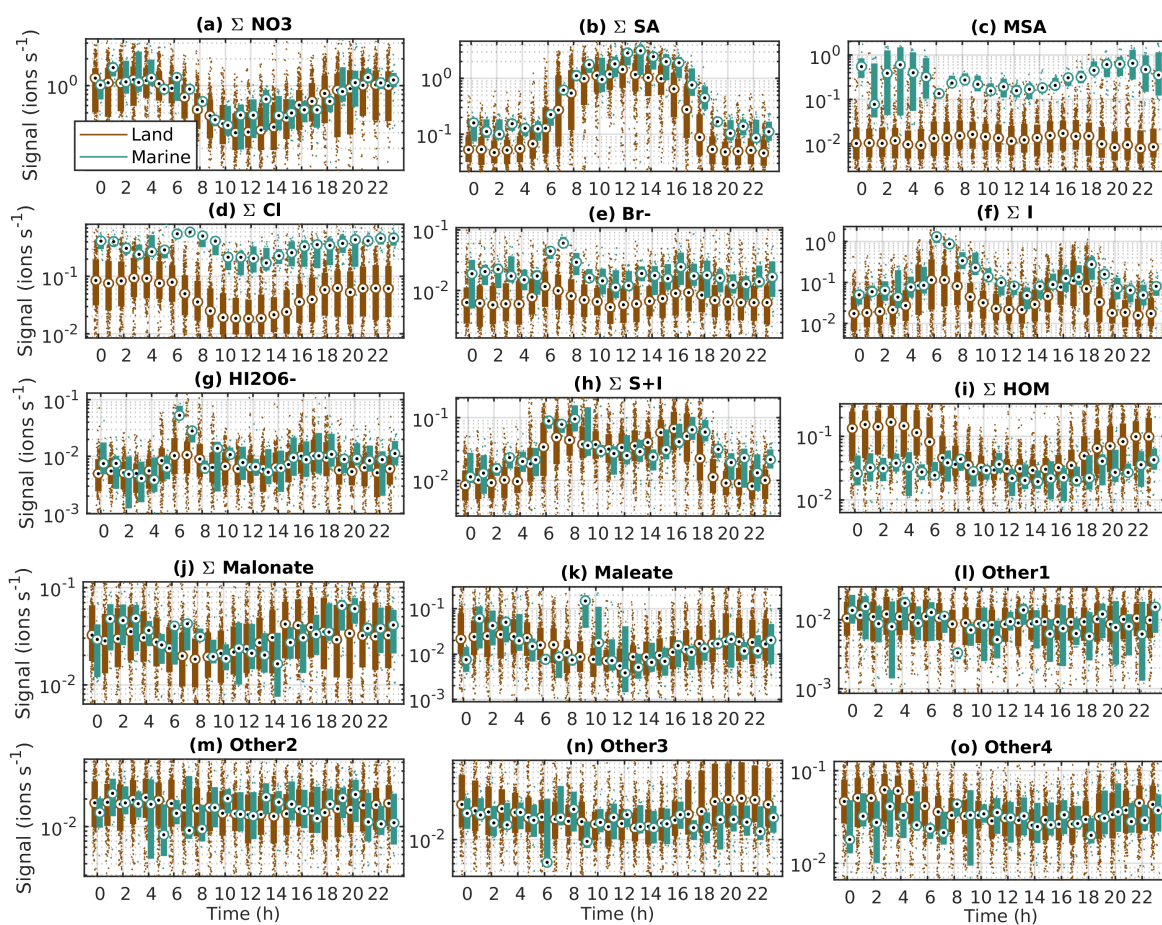


Figure 6.5: Diurnal cycles of example compounds at Baring Head in clean marine and land-influenced air.

acid clusters (SA, Fig. 6.5b). Bisulfate ions are also one of the most abundant ambient ions observed. For SA, we observe a clear diurnal cycle in both land-influenced and clean marine air masses. The concentrations increase in the morning after 5 am, reach a maximum around midday, and decrease in the evening. This is a very typical cycle for sulfuric acid because its production in unpolluted environments is driven by the oxidation of SO_2 and other sulfur species by OH radicals in the presence of sunlight, and its losses are driven by condensation to aerosol particles and other surfaces (see e.g., Tanner and Eisele, 1991; Dada et al., 2020).

Sulfuric acid has very low proton affinity and this is why changes in its concentration are important for the concentrations of ions of other chemical species (see e.g. Ehn et al., 2010). If sulfuric acid is present in the atmosphere it is more likely to be negatively charged, compared to other typical atmospheric chemical species with higher proton affinities.

If we compare the diurnal cycles in marine and land-influenced air masses closely, we can see that SA increases in both air masses around the same time, but in marine air, the median SA concentrations reach higher values in the afternoon and decline slower in the evening than in land-influenced air. This can be explained by smaller aerosol losses and thus longer SA lifetimes in clean marine air. This is in line with results observed earlier when comparing observations at Mauna Loa, in Hawaii and Cheeka Peak Research Station, in western coastal USA. Tanner and Eisele (1991) showed that while diurnal cycles of SA, NO_3 and MSA were clear at the coastal station, at Mauna Loa the diurnal cycles were weaker and this was attributed to the lower aerosol concentrations at Mauna Loa.

Another major compound containing sulfur is methane sulfonic acid (MSA, Fig. 6.5b). MSA is clearly higher in the clean marine air and displays only a weak diurnal cycle in both air masses. MSA is known to come from marine sources and when the air has passed over land, MSA has had time to condense on aerosols. In marine air, MSA levels are also more variable and reach higher values during the night whereas during the day the concentrations vary and are in general lower. Again, the daytime minimum is likely explained by charge loss to SA. According to Tanner and Eisele (1991), both MSA and SA are produced during the day, but the lifetime of MSA is much longer and its proton affinity is higher. Because of the higher proton affinity, MSA ion peak is masked by the charge loss to SA during the day, but after SA concentrations decrease, MSA ion signal peaks. The decay of the MSA peak takes longer because it is more volatile than SA and is not lost by condensation as fast as SA. Later results from neutral MSA and SA measurements supported this hypothesis (Eisele and Tanner, 1993).

On the other hand, more recent research has also shown different explanations. One possible explanation for the weaker MSA diurnal cycle was given recently by Baccarini et al. (2021). They studied MSA concentrations in the Southern Ocean close to Antarctica and observed no diurnal cycle. They suggested that a large fraction of MSA is produced in aqueous phase from which it later evaporates to gas phase. Similar results have been seen previously at Mace Head when measuring total concentrations of MSA and SA rather than only ions (Berresheim et al., 2002). According to their results, MSA peaks were caused by advection of air enriched with MSA or evaporation of MSA from aerosols in relatively warmer and drier air masses. Interpreting the sources of MSA from our ion data is thus not straightforward.

The next ions are halogen species. For the chloride group we can see that the concentrations are clearly higher in marine air and in both air mass classes the concentrations are lower during the day (Fig. 6.5d). The source of chloride is likely the surface of the ocean or sea spray. In land-influenced air, the concentrations are smaller since the sources of chloride are smaller and the losses to the pre-existing particle population are likely higher. The daytime decrease can be explained by either nighttime production of chloride ions or daytime losses by charge loss to sulfuric acid or photochemical reactions.

For bromide, the marine concentrations are again higher than land-influenced air concentrations (Fig. 6.5e). In both air masses we can see morning and evening peaks, with the marine morning peak being the most distinguishable. The morning increase indicates that more bro-

mide is formed when photochemistry takes place. The midday decrease could be related to charge loss to sulfuric acid. Similar results have been seen before at Jungfraujoch, a high altitude station in Europe (Frege et al., 2017).

For the most abundant iodine oxides (IO_3^- and H_2IO_4^- , Fig. 6.5f) we can observe two peaks in both marine and land-influenced air masses as seen for bromide. The iodine oxide concentrations are in general higher than bromide concentrations and the diurnal cycle is even clearer. The first peak occurs around 7 LT and the second around 17 LT. This is somewhat similar to patterns observed with a similar instrument at Jungfraujoch (Frege et al., 2017). In marine air masses the peaks are typically higher than in the land-influenced air, especially for the morning peak. This is reasonable since the sources of iodine oxides are likely marine and the sink is higher over land. As for sulfuric acid, we can see that the decrease of iodine oxide peaks is slower in marine air, which is likely explained by the longer lifetimes due to smaller particle sink.

The fact that we observe peaks in the morning and evening is likely explained by photochemistry producing these iodine oxides during the day. One possible explanation for the daytime decrease is photolysis or reactions with other chemical species such as halogen atoms or OH-radicals (Frege et al., 2017). One possible explanation is again the charge stealing by sulfuric acid. The proton affinity of iodic acid is higher than that for sulfuric acid (see, e.g. Sipilä et al., 2016), meaning that SA is more likely to obtain the charge. While SA formation requires UV light (Eisele and Tanner, 1990; Eisele and Tanner, 1993) and its formation can be disturbed even by passing clouds, iodine oxides can form even in cloudy conditions (He et al., 2021). This could explain why iodine oxides start forming earlier than SA.

Baccarini et al. (2021) observed similar morning and evening peaks for iodide with nitrate chemical ionisation in the Southern Ocean. They hypothesised that this would be due to less iodate produced when the radiation levels are higher. The nitrate ionisation is, however, also affected by the limited affinity of nitric acid and thus the nitrate chemical ionisation technique might be non-optimal for the detection of iodate (M. Wang et al., 2021), so it is possible that their results are also related to charge loss to sulfuric acid during the day. On the other hand Sellegri et al. (2016) observed bi-diurnal iodine peaks in aerosol chemical composition data from mesocosm experiments, which would support the need for other mechanisms of iodine formation to vary over the day.

For the only identified iodine oxide with higher molecular weight, HI_2O_4^- , the concentrations are lower than for the lighter iodine oxides and the diurnal cycle is less clear (Fig. 6.5g). We can, however, still see the highest concentrations of this species in marine air around the same time as for the smaller iodine oxides. This shows that if the conditions are favourable, larger iodine oxide molecules can be present at detectable quantities as well.

For compounds containing both sulfur and iodine species, we can see that the concentrations are lowest during the night and relatively high during the day with highest peaks occurring at the same time with iodine oxide peaks (Fig. 6.5e). The fact that the decrease during the day is smaller for species containing both iodine and sulfur than for species containing only iodine oxides shows that when sulfur is involved, the molecule is more likely to be charged even during the day when sulfuric acid concentrations are high. Again, the evening decline in concentrations is slower in marine air, showing that the lifetimes of these compounds are higher in clean air.

Out of the organic compounds examined, the clearest diurnal cycle can be observed for the HOM group (Fig. 6.5i) in land-influenced air. The concentrations of these HOMs are highest during the night. This is reasonable since all the compounds in this group were charged by nitrate. HOMs could also be charged by sulfate ions during the day (see e.g., Bianchi et al., 2017), but we did not find any peaks corresponding to organosulfates. Another factor contributing to higher nighttime concentrations can be the height of the planetary boundary layer. During the night, the boundary layer is typically lower than during the day, meaning that the emissions from ground level are mixed to a smaller volume of air. The peaks in this group

have been observed to be the largest HOM peaks also at a boreal forest site and in α -pinene oxidation in a chamber experiment (Ehn et al., 2012). This and the fact that we observe the highest concentrations of these compounds in land-influenced air means that the forests in New Zealand are likely to emit α -pinene. This is supported also by previous work in New Zealand that studied the composition of monoterpenes measured from radiata pine wood samples and found β - and α -pinenes to be the most abundant monoterpenes (McDonald et al., 1999).

The other identified organic compounds were dicarboxylic acids, malonate and maleate (Figs. 6.5j and k). They both have low concentrations and the levels are similar in marine and land-influenced air masses. In land-influenced air, the concentrations have a morning minimum and then increase over the day. Previous work has shown that malonic acid can be produced by photochemical oxidation (Kawamura and Sakaguchi, 1999), so the increase during the day seems reasonable. In marine air, we can also observe peaks during the morning around 7-8 h and evening around 19-20 h for malonate and one peak around 9-10 h for maleate, but otherwise the cycle is similar to land-influenced air. The times of the peaks of maleate are similar to the iodine oxide peaks in marine air. The morning and evening peaks could be related to proton affinity as in the case of iodine oxides. The proton affinity of malonic acid is lower than that of nitric acid (Ehn et al., 2010), but higher than some of the other important compounds, meaning that malonate is more likely to be charged than nitric acid, but less likely than for example SA or MSA. This supports the idea that the daytime malonate concentrations we observe are limited by charge loss. The reason why the morning peak is higher for maleate and observed later is not clear but it could be related to maleate having different sources than malonate and the limited length of our data set.

The fact that highest hourly median values of malonate and maleate are observed in clean marine air is not surprising since malonic acid has been connected to marine sources previously (Kerminen et al., 2000; Röhrl and Lammel, 2001). Dicarboxylic acids have also been related to biologically active marine areas and they are expected to be derived from isoprene emissions and unsaturated fatty acids at the sea surface (Bikkina et al., 2014).

Out of the 'Other' compound groups (Figs. 6.5 l-o), the first two do not show clear diurnal variations or clear differences between land-influenced and marine air masses. Other3 increases in the evening in land-influenced air after SA concentrations have decreased and then decays overnight. This means that the compounds in this group have likely formed during the day, but not been charged due to the abundance of SA. During the night their concentrations then decay due to lack of photochemical production. The decay seems slower than for example the decay of iodic acid in land-influenced air, potentially meaning that these compounds are more volatile or less reactive. The Other4 group also shows some higher nighttime concentrations in land-influenced air, but this increase is observed later, with highest concentrations observed only after midnight. This is more similar to what was seen for the HOM group and the masses in this group are also in similar range with the HOM group, meaning that these compounds are likely unidentified HOMs. It should be noted that all the masses in this group are non-even whereas the compounds in the HOM group are at even masses. Based on the nitrogen rule, these unidentified compounds should thus contain an even number of nitrogen if they have been charged by proton transfer (Junninen et al., 2010).

6.4 Seasonal cycles

In this section, we study the seasonal cycles of different chemical compounds to expand our understanding of the sources of different chemical species. We use only 8 groups as opposed to the 15 groups in the previous section as similar groups are likely to have similar seasonal cycles. Even though we lack data for part of the year and especially for the summer months when the data are sparse, seasonal cycles can be observed for some of the compounds (Fig. 6.6). To verify that the seasonal cycles observed for the other compounds are not driven by changes in

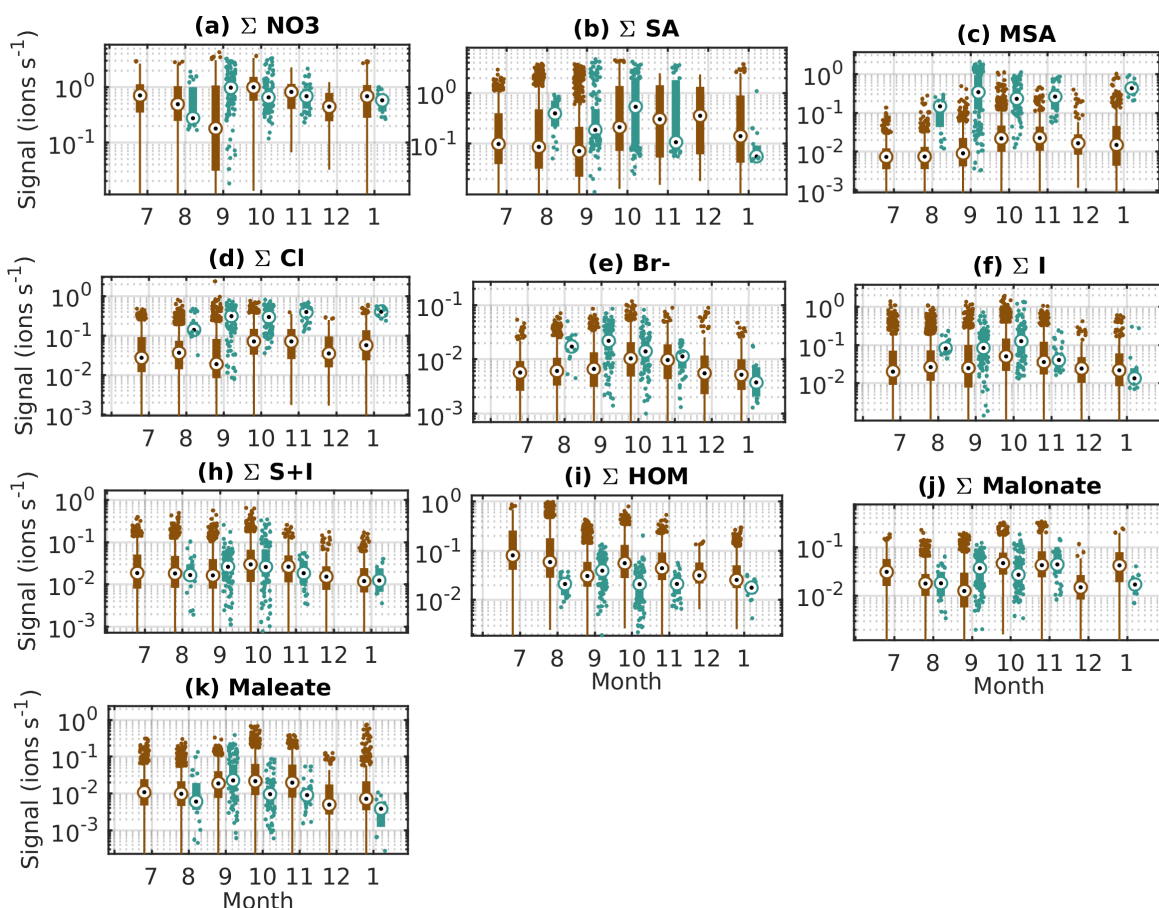


Figure 6.6: Seasonal cycles of example compounds at Baring Head in clean marine and land-influenced air.

sulfuric acid concentrations and charge availability, in Figure 6.7 we plot the seasonal cycles for the same species but divided by the sum of all ions.

In both seasonal cycle plots, chloride seems to increase towards the summer in both marine and land-influenced air masses. The reason for this trend is not clear, but it could be related to photochemical release of chlorine from the sea surface or sea spray aerosol surfaces. For nitrate ions, we can observe some month-to-month variation, but no clear seasonal trends in neither total ion signal nor ion fractions. This is not surprising since nitrate is always abundant in the atmosphere.

Sulfuric acid concentrations are higher during the summer in land-influenced air and this trend is even clearer if we look at its ion fraction. January is an outlier, but this could be explained by the small quantity of usable data for this month. The increase towards summer can be explained by the increase in radiation levels and more biological activity. On the other hand, in marine air, we cannot see a similar trend. One reason for this could be the fact that we have a lot less data from the clean marine periods. Another possibility is that when SA production is higher, more aerosols are formed and the loss term is higher as well. In marine air masses, the changes in the losses can be more significant than in land-influenced air, where the losses are practically always higher than in marine air.

MSA increases towards the summer and has highest median values during the spring in both air masses. This can be explained by marine biogenic sources and availability of radiation. As the sources of MSA are marine, we can assume that the MSA in land-influenced air is from marine sources too. This is in line with previous work at Baring Head and in the Chatham Rise area, which has shown increased sulfate production during the late spring and summer (Li

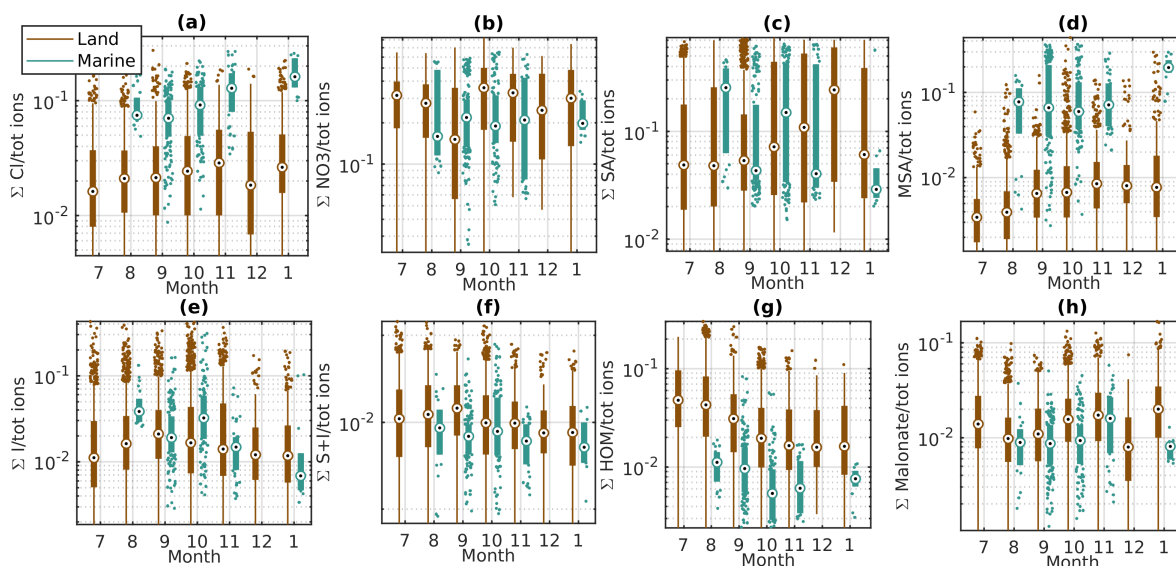


Figure 6.7: Seasonal cycles of the ion fraction of the example compound groups at Baring Head in clean marine and land-influenced air.

et al., 2018; Allen et al., 1997; Law et al., 2017).

When looking at the total ions, iodine oxide levels seem highest in August-October. The trends are similar but weaker for compounds containing both sulfur and iodine. The fact that iodine concentrations are highest during the spring indicates that they are connected to oceanic biological activity. One factor decreasing iodine peak levels during the summer could be increased losses to existing particle population and charge losses to sulfate.

The HOMs are highest during the winter in land-influenced air. This is interesting considering that monoterpene emissions are typically higher at higher temperatures (Guenther et al., 1993). On the other hand, to our knowledge the seasonal cycle of monoterpene emissions has not been measured in New Zealand. One reason for the higher wintertime concentrations could be lower boundary layer heights during the winter. In addition, the HOM concentrations should depend also on the availability of oxidisers and their sink, not only on monoterpene levels. The highest malonate concentrations in marine air are observed around November, which again points to a marine biological source. In land-influenced air, malonate concentrations are more variable and the reason for the trends is not clear.

6.5 Geographical source regions

To find out if different geographical regions were responsible for emitting more particle producing vapours, we drew source maps for the most relevant ions with the same method that we used in the previous chapter for studying nucleation. Here we use all air masses, because limiting the air masses to only clean marine air would leave us with too little data.

The first map is for sulfuric acid dimer (Fig. 6.8a). We chose to display the monomer rather than the sum of all peaks or the monomer, since the monomer is typically the highest peak and always abundant, meaning that little differences can be seen with it. The dimer can also be a good indicator of NPF probability. The highest SA signals are observed northwest of New Zealand. One possible reason for this is the transport of SO_2 from Australia. Some of the patches with higher SA signals could also be related to shipping, which has previously been identified as the second most important source of non-sea-salt sulfate aerosol at Baring Head with DMS oxidation being the most important source (Li et al., 2018). One likely significant source of shipping emissions is the Wellington harbour, which is approximately 15 km northwest

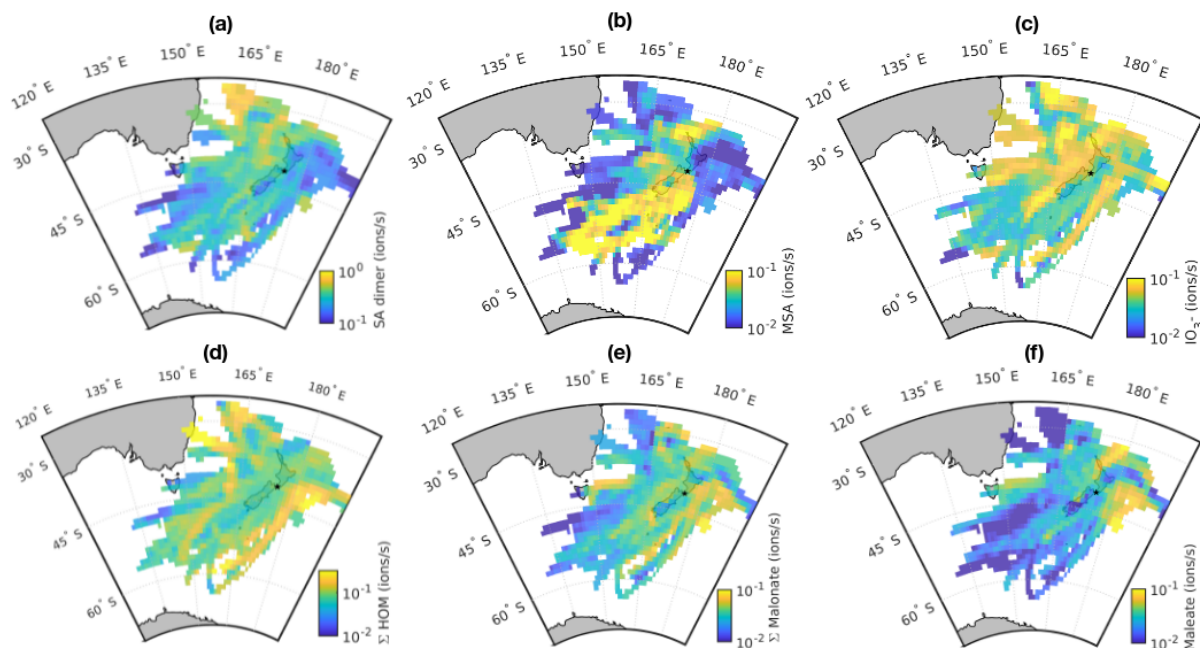


Figure 6.8: Source areas for a) sulfuric acid dimer, b) methanesulfonate (MSA), c) IO_3^- , d) Σ HOM, e) malonate and f) maleate. The station is marked with a small black star. See text for description.

from the station.

MSA is also a DMS oxidation product, but unlike SA, it does not have anthropogenic sources. With MSA, we can see clear regional differences (Fig. 6.8b). Highest MSA concentrations are observed when air masses come from the direction of the Southern Ocean. One possible explanation for this is transport of DMS and or MSA from the Southern Ocean and Antarctic coast. For example, Baccarini et al. (2021) observed higher concentrations of MSA at latitudes greater than 60° and link this to higher production of DMS close to Antarctica and lower temperatures increasing yield of MSA over sulfuric acid. Another possible reason for higher MSA concentrations when the air masses come from south is that on their way to the station they pass the biologically active Chatham Rise area which can produce DMS (see e.g., Law et al., 2017). One more possible explanation is also higher losses of MSA when the air comes from other directions. The air masses coming from the south have typically not been in contact with land and if the air mass passes over land, the particle concentrations and thus MSA sink increase.

For iodate, the patterns are less straightforward to explain. Figure 6.8c shows that there are stripes of higher iodate signal in several different directions. One possible explanation could be coastal sources of iodine and thus increased iodate concentrations when the air masses pass through certain regions. While iodine emissions can be high in some coastal environments such as Mace Head (e.g. Dall'Osto et al., 2011), iodine emissions depend on both algae types (e.g. Carpenter et al., 2000) and how much the macroalgae are exposed to air when tides change. For example, previous work at Cape Grim has shown that there iodine emissions from the local macroalgae are significantly smaller than at Mace Head and that the emissions only have a rather local effect on air chemistry (Grose et al., 2007; J. M. Cainey et al., 2007). In our data, the correlation between tide height and iodate concentrations during the day seems very small if not negligible ($R = -0.037$ $p = 0.038$), meaning that the main source of iodine is likely open ocean rather than coastal sources.

Figure 6.8d shows the source area plot for HOMs. One of the areas with highest concentrations is coming from the direction of Australia, meaning that either monoterpenes get transported all the way from Australia or that the air masses coming from this direction pass

a monoterpene source for example at the southern tip of North Island. Two other areas with higher HOM concentrations appear east and west of New Zealand. The area to the east is partly similar to the higher iodate signal area. The reason for this is not clear, but part of these trajectories could correspond to air masses that come from the ocean but pass over the North Island during the last day before reaching the station as is shown later in the case study for land-influenced NPF.

Figure 6.8e shows the source map for malonate. The signals of malonate are similar in all directions but seem highest when the air masses come from the east side of New Zealand or pass close to the west coast of New Zealand. As discussed earlier, dicarboxylic acids can be produced by photochemistry and biologically productive marine areas are one of their possible sources, which is an option here too. With maleate, we see higher signals east of the station and north of North Island (Fig. 6.8f). This could be related to biologically active marine areas or air masses crossing over the North Island.

6.6 New particle formation precursor species

6.6.1 Correlations between chemical species and aerosol data

Now that we have developed a basic understanding of the behaviour of different ions at Baring Head, we want to use these data to see which chemical species could be responsible for new particle formation and growth observed at the station as described in the previous chapter. One way to look into the significance of different species for particle formation is to compare correlations between different species and particle concentrations and growth rates in different size ranges. We did this separately for land-influenced and marine data and for daytime and nighttime data. Because the concentrations of both different chemical species and aerosol concentrations have clear diurnal cycles and this could affect the interpretation of the results, we look at the correlations separately for nighttime (0-5 h) and daytime (10-15 h) data. Here we use the same groups that we used for the diurnal cycles before, but separate the sum of sulfates to bisulfate ion (SA mono) and bisulfate ion clustered with one sulfuric acid (SA di), because the dimer is a better indicator for new particle formation (see e.g., Cai et al., 2021). The trimer is not showed since its correlations were similar to the dimer.

In the land-influenced air during the day (Fig. 6.9) we can see nucleation mode growth rates having a positive correlation with the Other4 group and negative correlations with MSA and HI_2O_4 . Other4 is likely to contain HOMs, showing that organics could play a role in growing the particles in land-influenced air during the day. MSA and HI_2O_4 are again likely to have marine sources, so air with high concentrations of these ions has probably not spent too long over land. For Aitken mode growth rates, we only see some weak negative correlations, but for accumulation mode, we also see positive correlation with SA monomer and chloride ions. It is interesting to see that while the SA monomer has a positive correlation with accumulation mode GR, the dimer has a negative correlation. One possible explanation could be that when there is a growing accumulation mode, SA condenses on it easily and does not have the time to form as many dimers. The reason for the positive correlation with chloride ions remains uncertain but it could be related to sea spray forming both accumulation mode particles and chloride ions. The accumulation mode growth rate has also a positive correlation with ozone, indicating that ozone could play a role in growing larger particles.

For 2-4 nm ions we only see a weak positive correlation with SA dimer, once again confirming the likely role of SA in land-influenced particle formation. Most of the correlations seen between the particle concentrations and different chemical species during the day are negative, which is related to the losses of ions to the particle population.

At night (Fig. 6.10) no clear NPF was observed in land-influenced air, but looking into the correlations can still shed a light on for example the growth processes. Growth rates in all

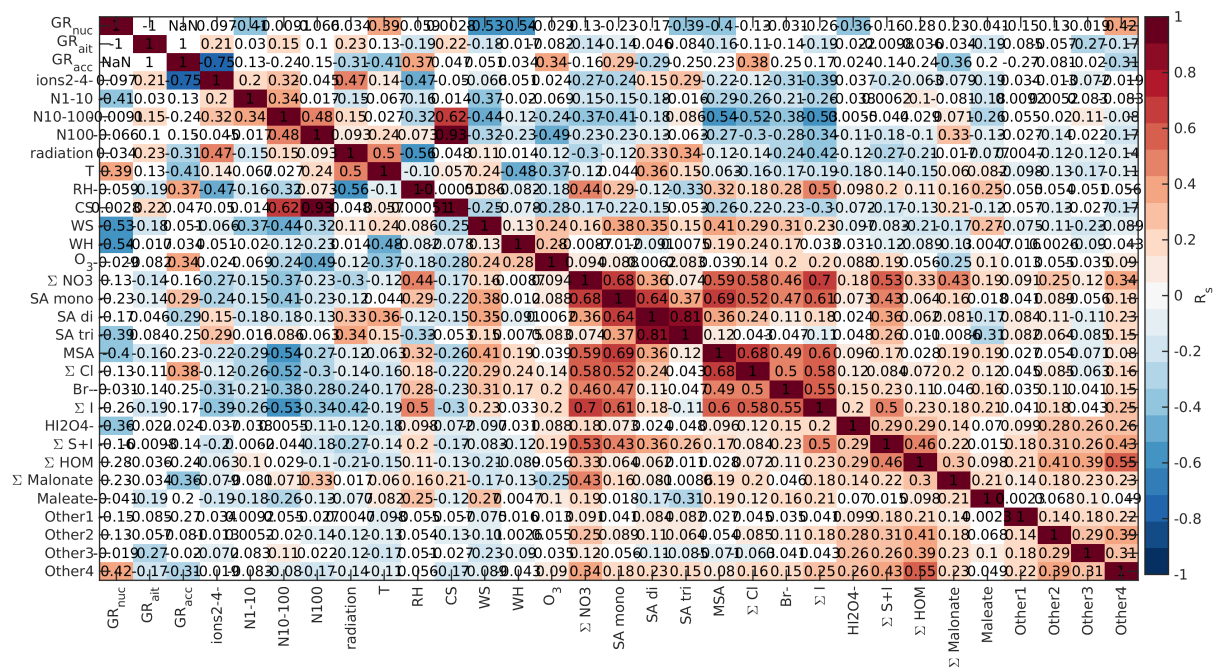


Figure 6.9: Correlations in land-influenced air during the day (10-15 h). Each square corresponds to the correlation coefficient between the variables on the x- and y-axes and the colour indicates the strength of the correlations with the square being white if p-value was above 0.05. In addition to growth rates (GR), ion and particle number concentrations (N), and the different chemical species, the figure includes global radiation, temperature (T), relative humidity (RH), condensation sink (CS), wind speed (WS), wave height (WH) and ozone.

modes have negative correlations with chloride. This is opposite to what was seen during the day for accumulation mode growth rates. Chloride ion signal was typically higher during the night and higher in marine air masses, so negative correlations with chloride likely show that nighttime growth was faster when the air had spent more time over land and the concentrations of marine species had decreased. Similar effects can be observed for bromide and MSA. For particle concentrations, most of the correlations are again negative, showing the effect of ion losses to the particle population.

If we look into the correlations of different species in marine air, we have fewer significant correlations since there are less data. During the day (Fig. 6.11), nucleation and Aitken mode growth rates have positive correlations with malonate, showing that it or photochemistry of organic species in general could grow sub-100 nm particles. In nucleation mode, we also observe negative correlations with iodine oxides and species containing both iodine and sulfur. One possible explanation for this is that these species are consumed when particles grow.

For Aitken mode, we also have positive correlations with bisulfate, chloride and the Other4 group whereas in accumulation mode all of these ions have negative correlations with the growth rates. While the exact reason for the opposite behaviour is not clear, this shows that different mechanisms are important for the growth of particles in different sizes.

When looking at the correlation between particle concentrations and different chemical species, we can observe positive correlations for sub-100 nm particles and SA. This means that more particles are produced when more SA is produced, showing that during daytime, SA can participate in NPF in marine air. On the other hand, since sulfuric acid can partly mask the signals of other species, this can also be an indication of the importance of other photochemistry.

During the day we can also observe positive correlation between N1-10 and S+I group as was seen for the whole data set. This shows that potentially both iodine and sulfur species can be important for daytime marine particle formation. With N100, we can only observe negative

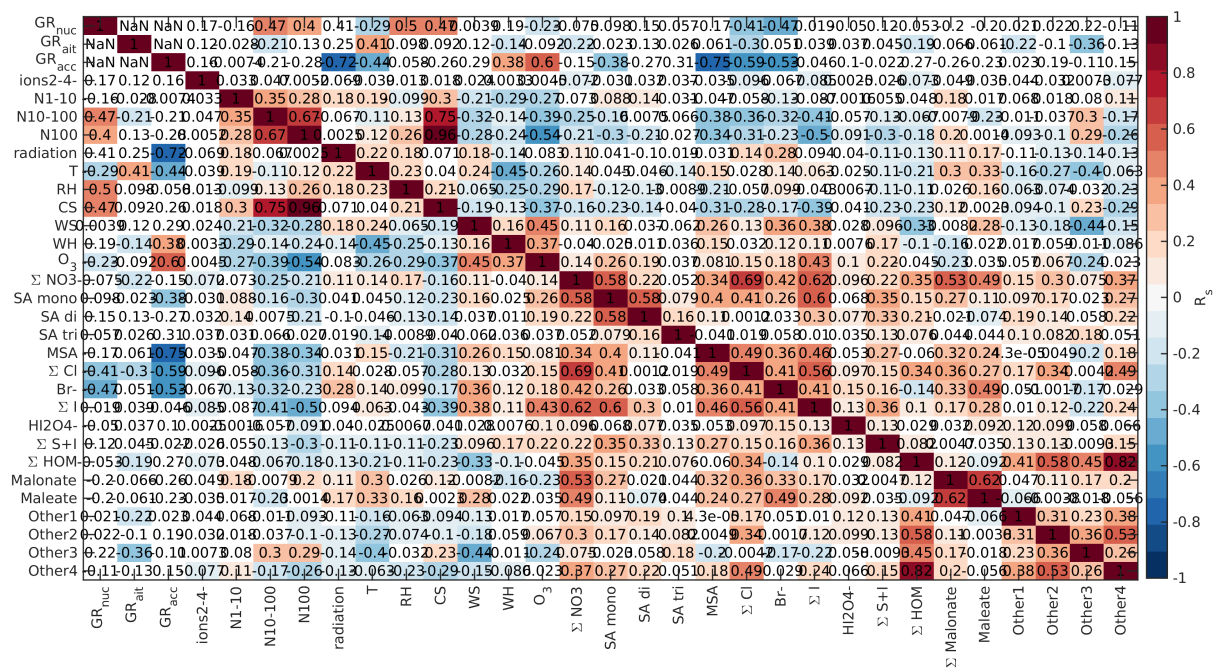


Figure 6.10: Correlations in land-influenced air during the night (0-5 h). See Figure 6.13 for full explanation.

correlation with iodine oxides. The most likely explanation is that N100 acts as a sink for iodine oxides.

During the night (Fig. 6.12) we have no significant correlations with any of the growth rates, but N1-10 has relatively strong correlations with some of the APi-TOF data groups. The most interesting are correlations with the iodine oxide group and S+I, which show that iodine could be related to the nighttime particle formation we observed in marine air. Interestingly, bromide and the Other4 group also have positive correlations with N1-10, but for MSA the correlation is negative. While bromide can have an important effect on atmospheric chemistry, iodine oxides are better known for their particle production capacity. This is why the fact that bromide is also correlating with N1-10, can be more related to it having similar sources as iodine oxides rather than bromide itself forming particles. For N10-100 there are no significant correlations with the chemical groups and for N100, we have only negative correlations with the chemical species, which is logical since N100 can act as a sink for the ions.

As shown in this section, interpreting these data is complicated and this is why next we take a look into some case studies to see if the interpretations that we made so far are valid for the selected cases.

6.6.2 Land-influenced new particle formation

To gain a deeper understanding of the role of different chemical species in particle formation, we look at case studies for both land-influenced and marine air. As an example for land-influenced air we use October 10th, 2020. This was a Class I event and the particle size distribution for this day is shown in Figure 6.13a. The 72 h air mass back trajectories show that the air masses originated from the ocean south of New Zealand, likely from the free troposphere, but later passed over the North Island of New Zealand before arriving at the station (Fig. 6.13b). The particle formation event that we observe likely occurred during the time that the air mass spent over land. At the beginning of the day we can see an Aitken mode that was formed by NPF during the previous day. Around 11 we see a new mode appearing and growing past 25 nm by early afternoon. The Aitken mode from the previous day eventually merges with the new

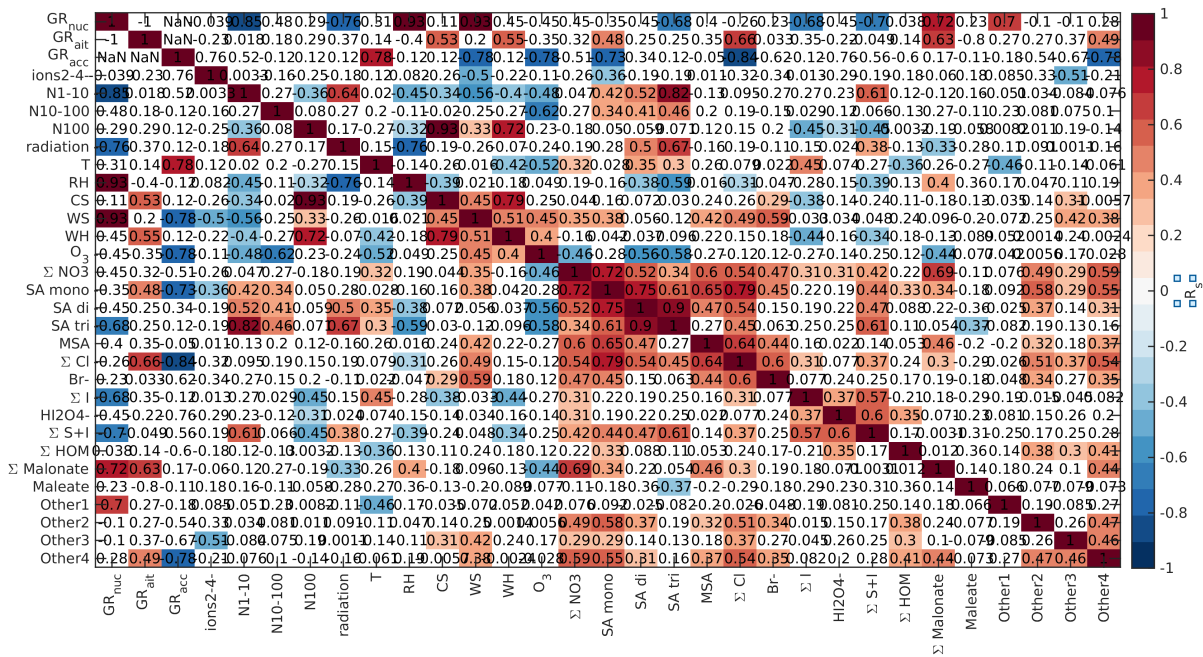


Figure 6.11: Correlations in marine air during the day (10-15 h). See Figure 6.13 for full explanation.

mode. The weakening of this Aitken mode from the previous day and the slight decrease in its diameter before it merges with the new mode can be explained by air mass history. If the air has spent less than 24 h over land, the air that reaches the station in the afternoon was still over the sea when the event of the previous day started. This means that particles in this air mass only started forming later and they have had less time to grow than the particles that formed earlier.

Figure 6.14 shows the time evolution of ion signals of different species on the same day. When new particle formation starts and the new particle mode appears, the overall ion signal decreases, likely because ions are consumed by the new particles. During the most intense particle formation period, when we can see particles around 10 nm and below, the ions are largely dominated by sulfuric acid. The fraction of sulfuric acid trimers compared to the dimer and monomer also seems to be higher than before the start of the event. This indicates that sulfuric acid could play a role in land-influenced particle formation.

The mode continues to grow until the end of the day although there are some fluctuations in the mean mode diameter. This shows that sulfuric acid is not the only species growing the particles. In the evening Other3 and different organic groups (e.g. HOM, malonate) show an increase after sulfuric acid concentrations decrease. The fact that concentrations of HOMs are observable both during the morning, which is after a different particle formation event and in the evening of this particle formation day, shows that HOMs were formed during the particle formation days and it is likely that they played a role in particle formation and nighttime growth over New Zealand.

The fraction of species other than sulfuric acid could be increased either because their sources increased, they were mixed into a shallower boundary layer, there was less sulfuric acid taking the charge, or a combination of these phenomena. The concentrations of sub-10 nm particles started decreasing around 15 h and around this time the concentration of nitrates started to increase. This could mean that the concentrations of other species started to lower or photochemistry started to weaken.

As this example shows, the data are complex to interpret since it is hard to know for example whether SA was lost due to condensation or if it helped form more particles. It is also hard

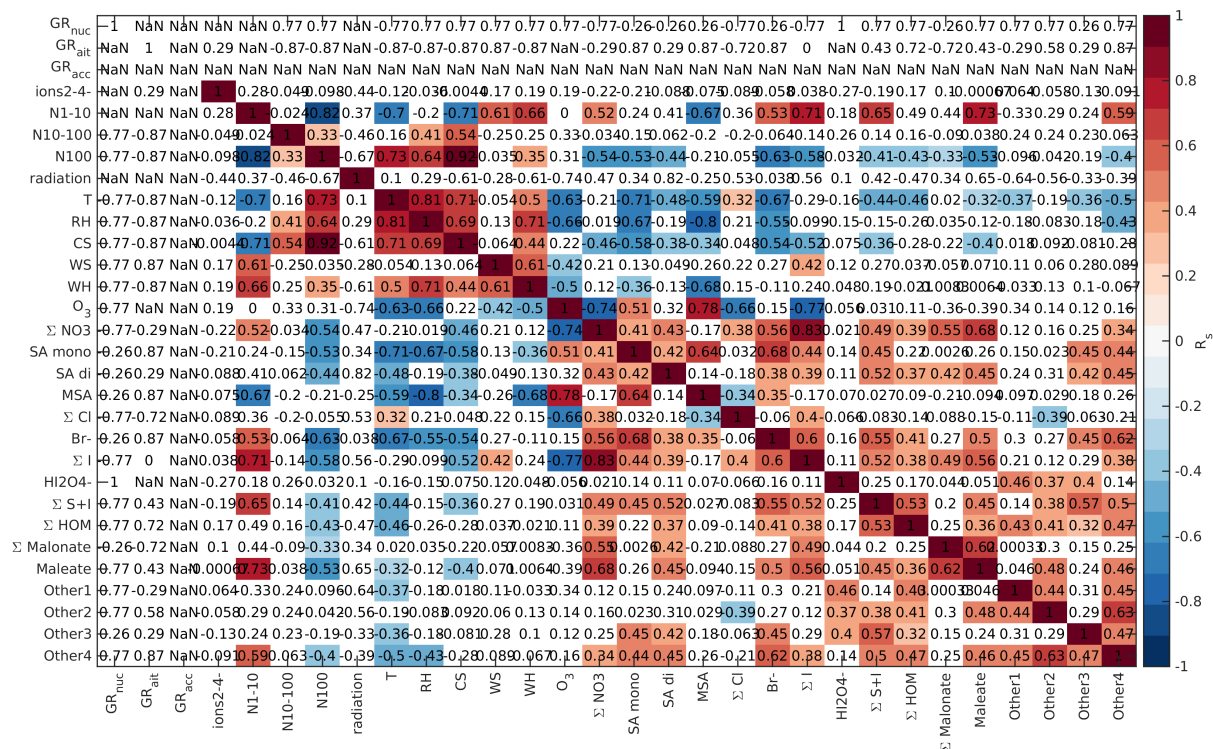


Figure 6.12: Correlations in marine air during the night (0-5 h). See Figure 6.13 for full explanation.

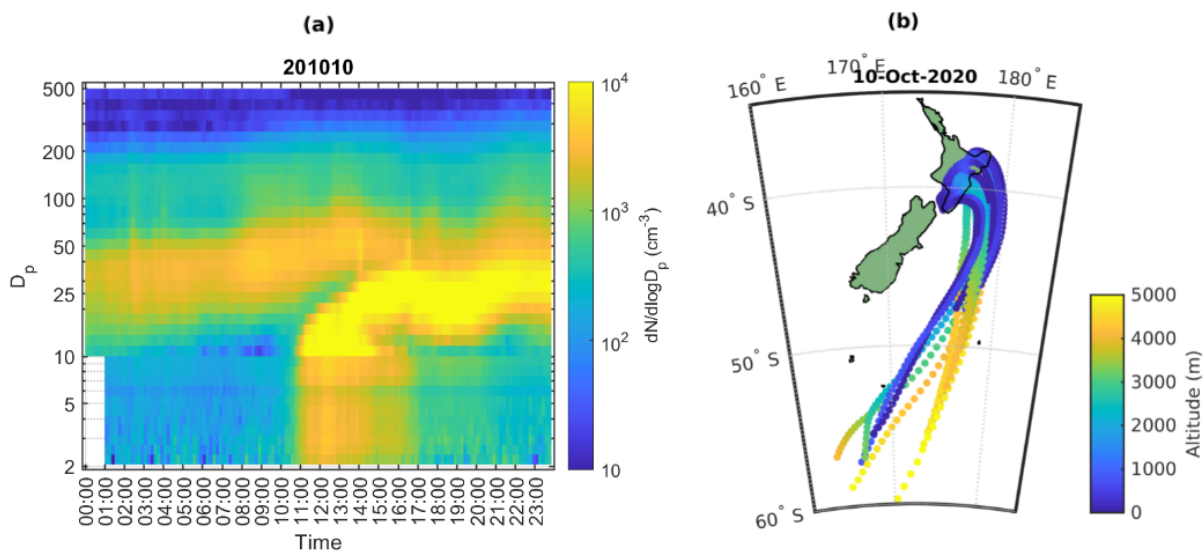


Figure 6.13: a) Particle number size distribution with combined NAIS and SMPS data during October 10th 2020. b) Air mass back trajectories coloured with altitude for the same day.

to know whether the fraction of other observable ions only increased because there was less sulfuric acid to take up the charge. In the future we would need to know the concentrations of neutral species and preferably know the chemical composition of larger chemical clusters and the particles themselves.

To get a better overview of how the chemistry affects particle formation, Figure 6.15 shows the average diurnal patterns of ion signals for new particle formation event and non-event days. Event days contain Class I and Class II days as defined by the Dal Maso et al. (2005) criteria.

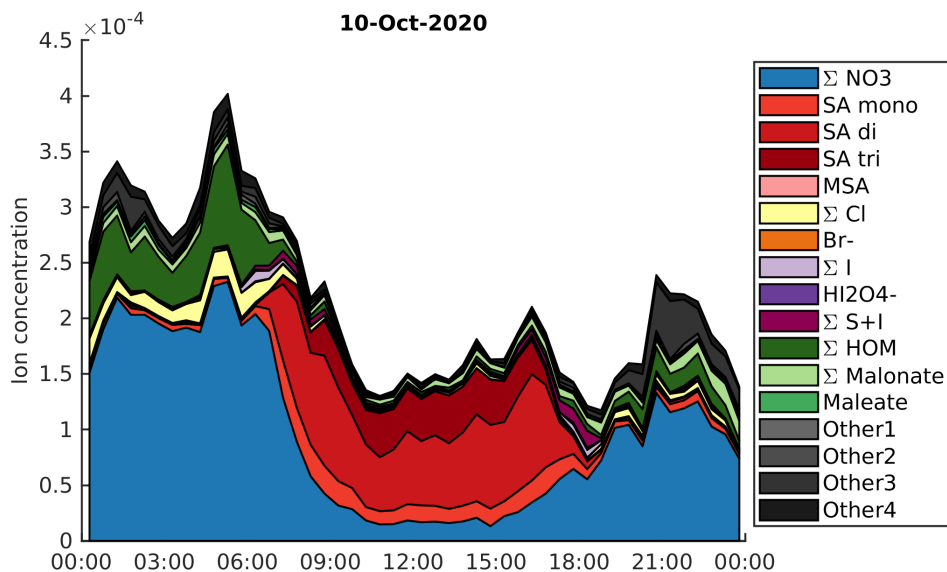


Figure 6.14: Time evolution of different ion groups during October 10th 2020.

The total ion signal reaches higher values on non-event days, which is expected as the work in the previous chapter showed that the condensation sink is slightly higher on event days and this increases the losses of ions. Other differences between event and non-event days include more variable chloride signals and higher signals of organic species on event days and higher iodine oxide signals on non-event days and different relations of different sulfuric acid ions. On event days, chloride signals are relatively high in the morning and low in the evening while on non-event-days the signal is relatively similar during the mornings and evenings. Events are likely favoured by clean chloride containing air coming from the sea in the morning and the air crossing over land during the day. During the events the condensation sink increases and air masses age, leading to loss of the chloride signal.

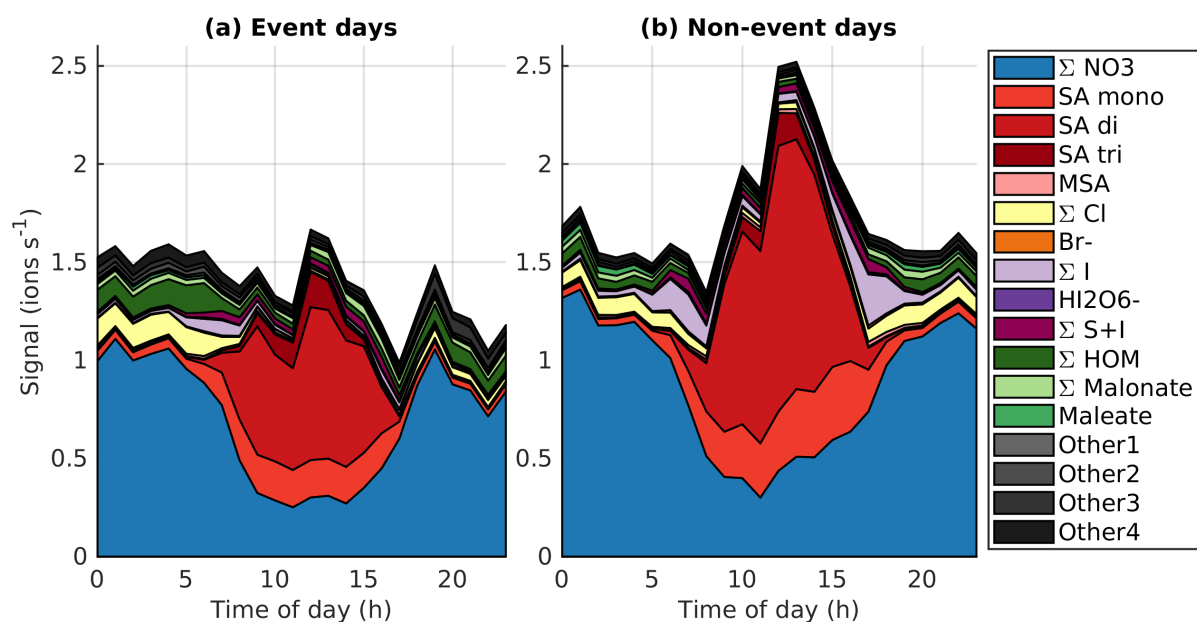


Figure 6.15: Average diurnal cycles of different chemical species on a) event days and b) non-event days.

The signal of HOMs is higher on event days compared to non-event days especially in the evening. This is similar to our example day where the precedent day had been an event day as well. Having higher HOM signals on event days supports the assumption that HOMs can play a role in land-influenced NPF at Baring Head. Even though the total signal of ions of sulfuric acid is higher on non event days, likely due to the higher condensation sink observed on NPF days, the fraction of SA dimers relative to monomers is higher on event days (median $\frac{SA_{dimer}}{SA_{monomer}} = 0.52$ (25th-75th percentiles 0.16-2.58)) than on non-event days ($\frac{SA_{dimer}}{SA_{monomer}} = 0.43$ (0.15-1.95)). Dimer formation has been shown to be an indicator of NPF in at least polluted environments (Cai et al., 2021) and having more dimers and trimers relative to monomers also indicates higher total sulfuric acid levels (Beck et al., 2021a). This confirms the results of our case study that indicated that sulfuric acid is likely to play a role in NPF at Baring Head.

6.6.3 Marine new particle formation

For marine air, we chose as an example day October 15th 2020. Almost all of this day was classified as clean marine air masses and in the particle size distribution, we can see several growth events (Fig. 6.16a). Here we show PSM data for sub-10 nm particles instead of NAIS data, since NAIS seemed to underestimate particle concentrations which is especially problematic in the clean marine air. We can see that sub-10 nm particle concentrations are also elevated in the morning between 9-12 h. A peak can be observed in N1-10 also in the evening around 21 h, but this could be related to pollution. The air mass back trajectories for this day all come from the south and considering that for most of the time their altitudes are well below 1000 m, the air has likely been within the marine boundary layer.

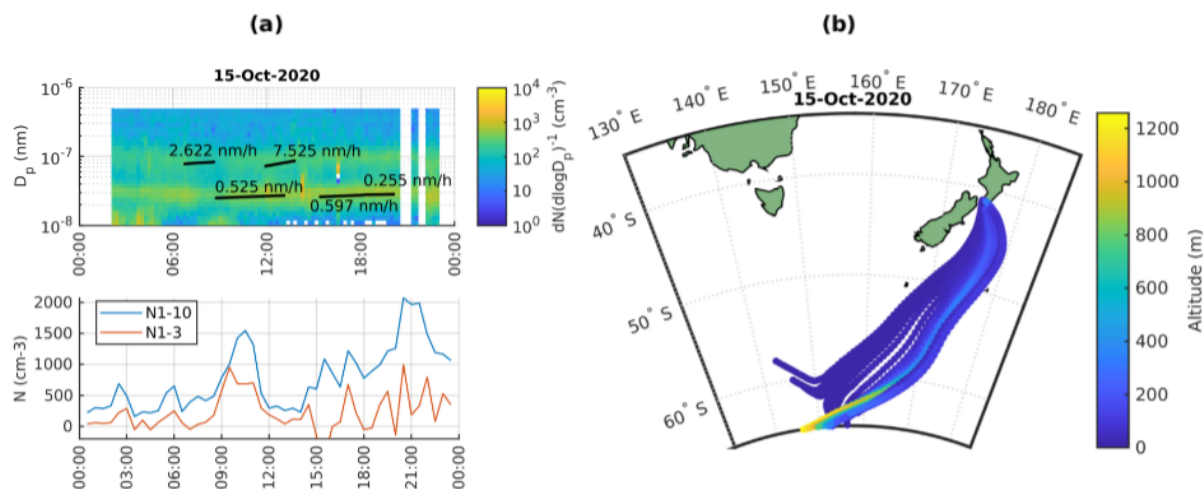


Figure 6.16: a) Upper panel shows the time evolution of particle size distribution in clean marine air and the lower panel shows the time evolution of N1-3 and N1-10 on October 15th 2020. b) Air mass back trajectories coloured by altitude for the same day.

Figure 6.17 shows the time evolution of the grouped chemical species during one day during which we observed particle growth in clean marine air. The particle growth, as observed by the automatic method, started after 6 h and it can be observable in two different modes, one around 20-30 nm and another around 100 nm (Fig. 6.16). Around the start of the first growth episode, we can observe nitrates, sulfuric acid, MSA, chloride and iodine oxides. Apart from lower iodine oxide concentrations between 9-15 h, the observable species remain the same through out the day even though their concentrations vary.

SA is the most abundant ion group, through 6 to 18 h. Already 30 years ago, Tanner and Eisele (1991) explained that both SA and MSA are formed during the day by photochemistry, but the concentrations of MSA ions increase only during the evening when SA starts decreasing,

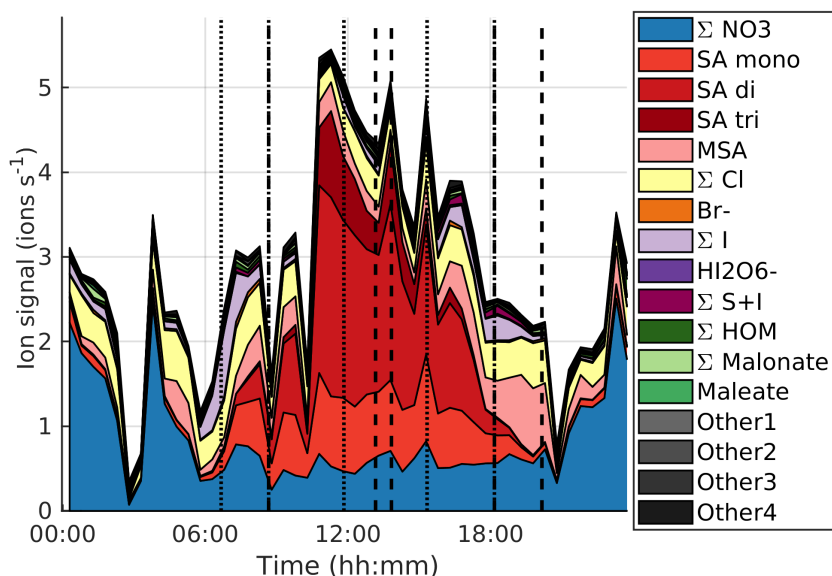


Figure 6.17: Variation of concentrations of different ions during one marine growth event on October 15th 2020. The dotted vertical line shows the start time of the growth events and the dashed lines show their end times.

because during the day SA is more likely to take up the charge. In our data, we can see some MSA also during the day, but its concentration does increase clearly in the evening when SA decreases. SA concentrations decay faster than MSA concentrations, because SA is less volatile and has thus a shorter lifetime than MSA. The fact that MSA is visible already during the day and this fraction clearly increases when SA decreases, shows that its concentrations were likely high already during the day. When the last growth episode stops around 21 h, the ion signals decrease and there is a short period of polluted air. At night, nitrates dominate the ion signal.

Even though no definite conclusions can be made based on this one day, it is likely that SA and MSA participated in the growth that we observe. They were both abundant through out the day and are both known to be able to grow particles by condensation. Iodine oxides were also observable during part of the growth and their potential to grow particles cannot be ruled out.

If we focus on the sub-10 nm particle concentrations (lower panel of Fig. 6.16), which were higher between 9-12 h and started to increase again in the evening, it is hard to say for sure which chemical species formed these particles. In the morning, sulfuric acid is the only clearly observable species that is known to participate in nucleation and in the evening SA concentrations decrease, but on the other hand we can observe iodine oxides which could participate in forming these particles.

To further relate the observed chemical species to aerosol formation, Figure 6.18 shows the diurnal variations of grouped ions in marine air when the number concentration of 1-10 nm particles is either below or above 500 cm^{-3} at a given moment. Here we use a lower particle concentration limit than for the land-influenced air since the aerosol concentrations were in general lower. Despite this lower limit, we have no APi-TOF data during which N1-10 would have been above the 500 cm^{-3} in the early morning hours or around midday.

The most notable differences between high and low N1-10 days seems to be higher concentrations of iodine oxide ions in the morning and higher SA trimer concentrations during the day when N1-10 is high. During high N1-10 days we also see relatively high concentrations of compounds with both iodine and sulfur. Malonate seems more common during low N1-10 days although even then its average concentrations are low. While the data are still not straightforward to understand, these results indicate that iodine oxides, sulfuric acid or species with both

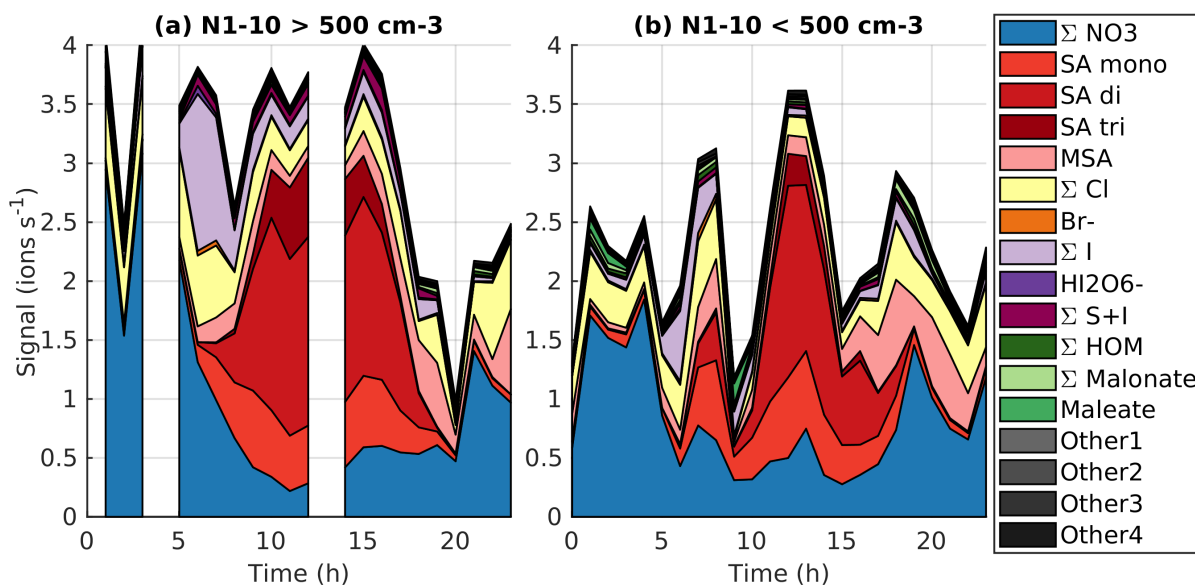


Figure 6.18: Average diurnal cycles in marine air when the number concentration of 1-10 nm particles is over (a) or below (b) 500 cm^{-3} .

iodine and sulfuric acid could play a role in marine nucleation.

6.7 Conclusions

Concentrations of different ions are determined not only by the availability of the chemical species, but also the availability of charge and the magnitude of ion sinks. The most dominant ions at Baring Head were nitrates during the night and sulfuric acid during the day. Sulfuric acid influences the diurnal cycles of many other ions as it has a low proton affinity and is prone to be negatively charged leaving other compounds neutral. Ions with marine origins such as methanesulfonic acid and compounds containing different halogens were also common. Most of the identified organic compounds had higher concentrations in land-influenced air and the forests of New Zealand seem to be a source of monoterpenes which could oxidise into highly oxygenated organic molecules.

While these data are complicated and with this data set we cannot quantitatively study the exact nucleation and growth mechanisms, we were able to identify species likely responsible for particle formation at Baring Head. In clean marine air masses, iodine oxides and sulfuric acid seemed to play an important role in particle formation, while MSA, sulfuric acid and potentially organic acids were important for particle growth. In land-influenced air, sulfuric acid and organic compounds were important for particle formation.

In the future it would be good to expand the measurements to include measurements of the neutral concentrations of gases and chemical clusters using for example bromide chemical ionisation which is suitable for detection of not only sulfuric acid and key organic compounds but also iodine oxides, which can all be important for NPF at Baring Head. Simultaneous measurements of particle chemical composition in different sizes could further clarify the chemical processes controlling aerosol formation at Baring Head.

Chapter 7

Conclusions

Marine aerosols are important for the climate because they influence the formation and properties of clouds and can interact directly with radiation. Aerosols and their interactions with clouds comprise one of the largest uncertainties in predicting future climate. Aerosol measurements are needed to constrain climate models, but so far they are scarce in marine environments and especially in the Southern Hemisphere. The goal of this thesis was to better understand marine aerosol formation. This was studied with both laboratory studies and field work. The laboratory studies aimed to identify how marine microbiology and seawater chemical properties are related to aerosol formation. With long-term ambient aerosol measurements at Baring Head, in coastal New Zealand, we could study these processes in ambient conditions and their seasonal cycle.

The first lab studies, which were part of the so-called ME3 campaign, used three mesocosms and measured the aerosol particle number concentrations in the mesocosm headspaces down to 1 nm and characterised the seawater chemical and microbiological properties extensively. The seawater used in the mesocosms was real coastal New Zealand seawater and the mesocosms were kept in different conditions with one mesocosm serving as a control mesocosm and the other two having increased temperature and lowered pH to mimic predicted future climate conditions. The smallest 1-3 nm particles displayed a clear diurnal cycle with low nighttime and high daytime concentrations. The particle concentrations varied over the experiment time and were in general higher in the mesocosms for which the water temperature and pH were altered. The 1-3 nm particles had a positive correlation with the abundance of eukaryotic nanoplankton in the morning, indicating that this type of plankton could be a possible emitter of aerosol precursor vapours.

The mesocosms used in the ME3 campaign were limited by the small headspaces of the mesocosms and the lack of measurements of different chemical species in air. This is why during my thesis, we built so-called Air-Sea-Interaction Tanks (ASIT). The ASITs were specifically designed for studying air-sea interactions and their headspaces were over five times larger than the mesocosm headspaces. This allowed us to do more extensive air measurements than during the ME3 campaign. Another major advantage of the ASIT experiments was that we were able to take the tanks out to sea on board RV Tangaroa, which meant that we could use them with open-ocean seawater.

The experiments with the ASITs showed that this is a promising way to study new particle formation directly from marine emissions. During our experiments on RV Tangaroa, we observed particle formation within the tanks' headspaces and explored possible chemical pathways of particle formation. One potential formation pathway was the formation of HOMs from monoterpenes. Other promising chemical species included dimethyl sulfide, isoprene and some volatile organic compounds that are typically thought to originate from anthropogenic sources. A preliminary look into the plankton data showed that nanophytoplankton could produce chemical species that can form aerosols. Promisingly, this was in line with the results from the ME3

campaign. Another result that was in line with the work from the ME3 campaign was negative correlations between 1-3 nm particle concentrations and ozone when combining data from both tanks. This shows that ozone could be important for marine particle formation.

One of the drawbacks of these experiments was that our time at sea was limited due to the pandemic. This limited the amount of available data, which is problematic especially when it comes to connecting the atmospheric data to seawater data since seawater samples were taken only once a day. To compensate for this, we performed additional experiments with coastal seawater, but the plankton data for these experiments is still not available.

In time to come, the data from the ASIT experiments has to be analysed further to fully understand new particle formation and chemical reactions occurring in the tanks. If we would have had the chance, we should have conducted blank experiments at sea with full instrumentation instead of doing them with less instrumentation in a different environment. Especially during the additional experiments we had many technical difficulties, which limited the available data. While the additional experiments were interesting, the technical issues and the likely low biological activity and limited photochemistry in the winter resulted in us not obtaining all the results we expected. Conducting more complementary experiments would be useful for future campaigns.

More experiments could be done for example with different plankton monocultures to characterise the emissions from single phytoplankton species. While similar studies have been done in the past, they have typically focused on emissions of one single chemical species such as DMS or a limited group of species such as halocarbons. Measuring the whole range of volatile organic compounds, other volatile species, their oxidation products, and aerosol production like we did would give a more complete picture of the relative importance of different aerosol formation pathways. Conducting more longer lasting experiments where the plankton cells have time to degrade would also be interesting.

To understand how important the processes we studied with the mesocosms are in the real atmosphere, we conducted ambient air measurements at Baring Head, in coastal New Zealand. Our measurements consisted of extensive aerosol measurements and determining the chemical composition of ambient ions. Baring Head was chosen for the field measurements because of its unique location. The station regularly receives air masses that come from the Southern Ocean and have not been in touch with land for several days, making it an ideal spot for studying clean marine air masses.

The field work at Baring Head showed that new particle formation is frequent at the site. During our 10 month measurement period, the average event frequency, determined by a traditional method, was 23 %, with the least events observed during the winter. These events were favoured by sunny conditions with low relative humidity and wind speeds. The strongest events occurred when the air mass had spent time over land and aerosol number concentrations in all size ranges increased as a function of time spent over land with the concentration of particles with diameters above 100 nm doubling in a day. This can be explained by a combination of new particle formation and primary particle emissions and these phenomena are likely to have an effect on regional cloud properties around New Zealand. It is likely that other islands in the Southern Hemisphere experience similar phenomena, since clean marine air masses crossing over land are likely to favour particle formation.

One of the key findings of this study was that while NPF events, as defined by the traditional event classification methods designed for continental sites, occurred primarily over land, new particle formation is likely to happen in open ocean air masses as well. This is supported both by observations of sub 3-nm and sub-10 nm particles and particle growth starting from nucleation mode in clean marine air. During the spring sub-10 nm particle contributed on average 29% of the total 1-500 nm particle concentration. Growth starting from nucleation mode occurred 16 % of the measurement time in clean marine air and growth starting from Aitken mode was even more common. Observing both sub-3 nm particles and particle growth starting from the nucleation

mode in air masses that had only spent time within the marine boundary layer, shows that nucleation can happen within the marine boundary layer. Whilst particle formation in marine air does occur, the formation is weaker than during terrestrially influenced NPF events. Unlike at some other coastal sites, coastal sources did not seem to play a significant role in aerosol formation at Baring Head. Formation of sub-10 nm particles in clean marine air was favoured by low temperatures, relative humidity and wind speeds. Our results highlight the need to study marine NPF with different criteria than continental NPF.

To characterise the chemical properties of the atmosphere and to relate this information to new particle formation, we also measured the chemical composition of ambient ions at Baring Head. Nitrate ions were the most abundant ions during the night whereas sulfuric acid dominated the ions during the day. We also observed many different chemical species that had likely marine origins such as methane sulfonate, iodate, chloride, and bromide. Over land, on the other hand, organic species such as highly oxygenated organic compounds were common. The concentrations of different ions are determined not only by the availability of the chemical species, but also by the availability of charge and the magnitude of ion sinks. This makes the data complicated to interpret. Our interpretations were also limited by the fact that the air at Baring Head is very clean and hence the concentrations of many of the species we observed were low and peaks were only observable until around masses of 400 amu. This means that we were not able to track cluster formation all the way up to sizes observable with aerosol instrumentation.

Despite these factors complicating our analysis, we were able to identify chemical species that were likely to contribute to aerosol formation and growth at Baring Head. In land-influenced air highly oxygenated organic compounds likely derived from monoterpene oxidation and sulfuric acid appear to be important for particle formation and growth. In clean marine air, particle formation was more likely when concentrations of iodine oxides and during the day sulfuric acid were high. For particle growth, methane sulfonic acid was also likely to play a role.

During our measurements at Baring Head, only 7.3 % of the data could be classified as clean marine air. In the future, it would be good to continue the measurements over longer periods to obtain more information on the importance of new particle formation in open ocean air and study trends over longer time periods. It would be also useful to expand the measurements to include measurements of the neutral concentrations of gases and chemical clusters using for example bromide chemical ionisation which is suitable for detection of not only sulfuric acid and key organic compounds but also iodine oxides, which can all be important for NPF at Baring Head. Simultaneous measurements of particle chemical composition in different sizes could further clarify the chemical processes controlling aerosol formation at Baring Head.

When comparing the results from the lab experiments and Baring Head, some similarities can be observed. We were able to detect sub-3 nm particles in both of the lab experiments and in clean ambient marine air at Baring Head. While some nighttime particle formation was observed both in the ME3 experiment and during the ambient measurements at Baring Head, during the day radiation is likely to play a role in particle formation. Cold temperatures seemed to also favour particle formation both in the ASITs and at Baring Head. Even though the role of different chemical precursor species in marine particle formation is still not fully clear, both the ASIT experiments and ambient measurements at Baring Head supported the potential role of iodine and sulfur species in particle formation. With the ASIT experiments, the formation of HOMs from monoterpenes seemed also like a possible aerosol formation pathway, but at Baring Head, the concentrations of HOMs were low in marine air. Further measurements would be useful to fully understand marine aerosol formation.

Apart from expanding the measurements, one important aspect for future work is incorporating measurement results with modelling. By modelling work, one could study the effect of aerosol formation from sea surface emissions on clouds and the radiative balance of the Earth, this way closing the CLAW feedback loop. The laboratory work could be used to calculate fluxes

of relevant chemical species or to estimate aerosol production from seawater with given properties. These estimates could then be used as model inputs. The ambient aerosol measurements could be used to constrain climate models and evaluate their accuracy. Collaboration between people running the measurements and modellers is important so that both measurements and models can be designed to best reduce uncertainties in predicting future climatic conditions.

It could be also interesting to combine our ambient results with satellite data to see if the new particle formation that we observed at ground level has an impact on aerosol optical depth and cloud properties around New Zealand. Satellite data could be also used to evaluate the effects of marine biological activity on marine particle formation and the concentrations of chemical species such as MSA observed at Baring Head.

To summarise, in this thesis I studied marine new particle formation extensively by both laboratory and field work. With the laboratory work, I was able to connect aerosol formation to marine phytoplankton species and study emissions of different chemical species and aerosol formation from the sea surface. With the field measurements, I could characterise aerosol size distributions and new particle formation at the Baring Head station for the first time. Furthermore, I was able to identify chemical species likely responsible for particle formation and growth, both in open ocean air masses and over land. These measurements are unique and very valuable, because marine aerosol measurements are scarce even though marine aerosols play a key role in regulating climate and better understanding of marine aerosols is needed to reduce uncertainties in climate predictions.

Bibliography

- Alexander, S. and Protat, A. (2019). “Vertical Profiling of Aerosols With a Combined Raman-Elastic Backscatter Lidar in the Remote Southern Ocean Marine Boundary Layer (43–66 S, 132–150 E)”. In: *Journal of Geophysical Research: Atmospheres* 124.22, pp. 12107–12125.
- Allen, A. G. et al. (1997). “Sources of atmospheric methanesulphonate, non-sea-salt sulphate, nitrate and related species over the temperate South Pacific”. In: *Atmospheric Environment* 31.2, pp. 191–205.
- Alpert, P. A. et al. (2017). “Fatty acid surfactant photochemistry results in new particle formation”. In: *Scientific reports* 7.1, p. 12693.
- Arar, E. J. and Collins, G. B. (1997). *Method 445.0: In vitro determination of chlorophyll a and pheophytin a in marine and freshwater algae by fluorescence*. United States Environmental Protection Agency, Office of Research and . . .
- Archer, S. et al. (2013). “Contrasting responses of DMS and DMSP to ocean acidification in Arctic waters”. In: *Biogeosciences (BG)* 10, pp. 1893–1908.
- Arnold, S. R. et al. (2009). “Evaluation of the global oceanic isoprene source and its impacts on marine organic carbon aerosol”. In: *Atmospheric Chemistry and Physics* 9.4, pp. 1253–1262.
- Avgoustidi, V. et al. (2012). “Decreased marine dimethyl sulfide production under elevated CO₂ levels in mesocosm and in vitro studies”. In: *Environmental Chemistry* 9.4, pp. 399–404.
- Ayers, G. et al. (1992). “Evidence for photochemical control of ozone concentrations in unpolluted marine air”. In: *Nature* 360.6403, pp. 446–449.
- Baccarini, A. et al. (2020). “Frequent new particle formation over the high Arctic pack ice by enhanced iodine emissions”. In: *Nature Communications* 11.1, pp. 1–11.
- Baccarini, A. et al. (2021). “Low-volatility vapors and new particle formation over the Southern Ocean during the Antarctic Circumnavigation Expedition”. In: *Earth and Space Science Open Archive*, p. 31.
- Bates, T. et al. (1992). “Sulfur emissions to the atmosphere from natural sources”. In: *Journal of Atmospheric Chemistry* 14.1-4, pp. 315–337.
- Beck, L. J. et al. (2021a). “Estimation of sulfuric acid concentrations using ambient ion composition and concentration data obtained by ion mass spectrometry measurements (APi-TOF)”. In: *Atmospheric Measurement Techniques Discussions* 2021, pp. 1–10.
- Beck, L. J. et al. (2021b). “Differing mechanisms of new particle formation at two Arctic sites.” In: *Geophysical Research Letters* 48.4, e2020GL091334.
- Bermudez, J. R. et al. (2016). “Effect of ocean acidification on the structure and fatty acid composition of a natural plankton community in the Baltic Sea”. In: *Biogeosciences (BG)* 13.24, pp. 6625–6635.
- Bermudez, R. et al. (2015). “Long-term conditioning to elevated pCO₂ and warming influences the fatty and amino acid composition of the diatom *Cylindrotheca fusiformis*”. In: *PLoS One* 10.5, e0123945.
- Bernard, F. et al. (2016). “Photosensitized formation of secondary organic aerosols above the air/water interface”. In: *Environmental science & technology* 50.16, pp. 8678–8686.

- Berresheim, H. et al. (2002). “Gas-aerosol relationships of H₂SO₄, MSA, and OH: Observations in the coastal marine boundary layer at Mace Head, Ireland”. In: *Journal of Geophysical Research: Atmospheres* 107.D19, PAR–5.
- Bianchi, F. et al. (2017). “The role of highly oxygenated molecules (HOMs) in determining the composition of ambient ions in the boreal forest”. In: *Atmospheric Chemistry and Physics* 17.22, pp. 13819–13831.
- Bianchi, F. et al. (2019). “Highly oxygenated organic molecules (HOM) from gas-phase autoxidation involving peroxy radicals: A key contributor to atmospheric aerosol”. In: *Chemical reviews* 119.6, pp. 3472–3509.
- Bigg, E. et al. (1984). “Origin of Aitken particles in remote regions of the Southern Hemisphere”. In: *Journal of Atmospheric Chemistry* 1.2, pp. 203–214.
- Bikkina, S. et al. (2014). “High abundances of oxalic, azelaic, and glyoxylic acids and methylglyoxal in the open ocean with high biological activity: Implication for secondary OA formation from isoprene”. In: *Geophysical Research Letters* 41.10, pp. 3649–3657.
- Boulon, J. et al. (2010). “New particle formation and ultrafine charged aerosol climatology at a high altitude site in the Alps (Jungfraujoch, 3580 m a.s.l., Switzerland)”. In: *Atmospheric Chemistry and Physics* 10.19, pp. 9333–9349.
- Brailsford, G. W. et al. (2012). “Long-term continuous atmospheric CO₂ measurements at Baring Head, New Zealand”. In: *Atmospheric Measurement Techniques* 5.12, pp. 3109–3117.
- Brean, J. et al. (2021). “Open ocean and coastal new particle formation from sulfuric acid and amines around the Antarctic Peninsula”. In: *Nature Geoscience*, pp. 1–6.
- Breider, T. et al. (2010). “Impact of BrO on dimethylsulfide in the remote marine boundary layer”. In: *Geophysical Research Letters* 37.2.
- Brüggemann, M. et al. (2017). “Interfacial photochemistry of biogenic surfactants: a major source of abiotic volatile organic compounds”. In: *Faraday discussions* 200, pp. 59–74.
- Brüggemann, M. et al. (2018). “Interfacial photochemistry at the ocean surface is a global source of organic vapors and aerosols”. In: *Nature communications* 9.1, p. 2101.
- Bruyn, W. J. de et al. (2002). “DMS and SO₂ at Baring Head, New Zealand: Implications for the yield of SO₂ from DMS”. In: *Journal of atmospheric chemistry* 41.2, pp. 189–209.
- Burkart, J. et al. (2017). “Organic condensation and particle growth to CCN sizes in the summertime marine Arctic is driven by materials more semivolatile than at continental sites”. In: *Geophysical Research Letters* 44.20, pp. 10–725.
- Burkholder, J. et al. (2004). “Laboratory studies of the homogeneous nucleation of iodine oxides”. In: *Atmospheric Chemistry and Physics* 4.1, pp. 19–34.
- Cai, R. et al. (2021). “An indicator for sulfuric acid–amine nucleation in atmospheric environments”. In: *Aerosol Science and Technology*, pp. 1–11.
- Cainey, J. M. et al. (2007). “Flux chamber study of particle formation from *Durvillaea* potato-rum”. In: *Environmental Chemistry* 4.3, pp. 151–154.
- Cainey, J. and Harvey, M. (2002). “Dimethylsulfide, a limited contributor to new particle formation in the clean marine boundary layer”. In: *Geophysical Research Letters* 29.7, pp. 32–1.
- Cappellin, L. et al. (2019). “A mechanism for biogenic production and emission of MEK from MVK decoupled from isoprene biosynthesis”. In: *Atmospheric Chemistry and Physics* 19.5, pp. 3125–3135.
- Carpenter, L. J. et al. (2021). “Marine iodine emissions in a changing world”. In: *Proceedings of the Royal Society A* 477.2247, p. 20200824.
- Carpenter, L. J. et al. (2000). “Novel biogenic iodine-containing trihalomethanes and other short-lived halocarbons in the coastal east Atlantic”. In: *Global Biogeochemical Cycles* 14.4, pp. 1191–1204.
- Carpenter, L. J. et al. (2013). “Atmospheric iodine levels influenced by sea surface emissions of inorganic iodine”. In: *Nature Geoscience* 6.2, p. 108.

- Chambers, S. et al. (2014). “A radon-only technique for characterising baseline constituent concentrations at Cape Grim”. In:
- Charlson, R. J. et al. (1987). “Oceanic phytoplankton, atmospheric sulphur, cloud albedo and climate”. In: *Nature* 326.6114, p. 655.
- Ciuraru, R. et al. (2015). “Photosensitized production of functionalized and unsaturated organic compounds at the air-sea interface”. In: *Scientific reports* 5, p. 12741.
- Coulson, G. et al. (2016). “Aerosol size distributions in Auckland”. In: *Air Quality and Climate Change* 50.1, p. 23.
- Cravigan, L. (2019). “The role of marine biota on the composition and concentration of potential cloud condensation nuclei”. PhD thesis. Queensland University of Technology.
- Croft, B. et al. (2019). “Arctic marine secondary organic aerosol contributes significantly to summertime particle size distributions in the Canadian Arctic Archipelago”. In: *Atmospheric Chemistry and Physics* 19.5, pp. 2787–2812.
- Croft, B. et al. (2021). “Factors controlling marine aerosol size distributions and their climate effects over the northwest Atlantic Ocean region”. In: *Atmospheric Chemistry and Physics* 21.3, pp. 1889–1916.
- Cui, T. et al. (2019). “Chemical Characterization of Isoprene-and Monoterpene-Derived Secondary Organic Aerosol Tracers in Remote Marine Aerosols over a Quarter Century”. In: *ACS Earth and Space Chemistry*.
- Dada, L. et al. (2020). “Sources and sinks driving sulfuric acid concentrations in contrasting environments: implications on proxy calculations”. In: *Atmospheric Chemistry and Physics* 20.20, pp. 11747–11766.
- Dada, L. et al. (2018). “Refined classification and characterization of atmospheric new-particle formation events using air ions”. In: *Atmospheric Chemistry and Physics*.
- Dal Maso, M. et al. (2005). “Formation and growth of fresh atmospheric aerosols: eight years of aerosol size distribution data from SMEAR II, Hyttiala, Finland”. In: *Boreal Environment Research* 10.5, p. 323.
- Dall’Osto, M. et al. (2011). “A statistical analysis of North East Atlantic (submicron) aerosol size distributions”. In: *Atmospheric Chemistry and Physics* 11.24, pp. 12567–12578.
- Dani, K. S. et al. (2017). “Relationship between isoprene emission and photosynthesis in diatoms, and its implications for global marine isoprene estimates”. In: *Marine Chemistry* 189, pp. 17–24.
- Edtbauer, A. et al. (2020). “A new marine biogenic emission: methane sulfonamide (MSAM), DMS and DMSO₂ measured in air over the Arabian Sea”. In: *Atmospheric Chemistry and Physics Discussions* 2020, pp. 1–20.
- Ehn, M. et al. (2010). “Composition and temporal behavior of ambient ions in the boreal forest”. In: *Atmospheric Chemistry and Physics* 10.17, pp. 8513–8530.
- Ehn, M. et al. (2012). “Gas phase formation of extremely oxidized pinene reaction products in chamber and ambient air”. In: *Atmospheric chemistry and physics* 12.11, pp. 5113–5127.
- Eisele, F. (1989). “Natural and anthropogenic negative ions in the troposphere”. In: *Journal of Geophysical Research: Atmospheres* 94.D2, pp. 2183–2196.
- Eisele, F. and Tanner, D. (1990). “Identification of ions in continental air”. In: *Journal of Geophysical Research: Atmospheres* 95.D12, pp. 20539–20550.
- (1993). “Measurement of the gas phase concentration of H₂SO₄ and methane sulfonic acid and estimates of H₂SO₄ production and loss in the atmosphere”. In: *Journal of Geophysical Research: Atmospheres* 98.D5, pp. 9001–9010.
- Forestieri, S. et al. (2018). “Temperature and Composition Dependence of Sea Spray Aerosol Production”. In: *Geophysical Research Letters*.
- Fossum, K. N. et al. (2018). “Summertime Primary and Secondary Contributions to Southern Ocean Cloud Condensation Nuclei”. In: *Scientific reports* 8.1, p. 13844.

- Fossum, K. N. et al. (2020). “Sea-spray regulates sulfate cloud droplet activation over oceans”. In: *npj Climate and Atmospheric Science* 3.1, pp. 1–6.
- Frege, C. et al. (2017). “Chemical characterization of atmospheric ions at the high altitude research station Jungfraujoch (Switzerland)”. In: *Atmospheric Chemistry and Physics* 17.4, pp. 2613–2629.
- Freney, E. et al. (2021). “Mediterranean nascent sea spray organic aerosol and relationships with seawater biogeochemistry”. In: *Atmospheric Chemistry and Physics* 21.13, pp. 10625–10641.
- Furneaux, K. et al. (2010). “Measurements of iodine monoxide at a semi polluted coastal location”. In: *Atmospheric Chemistry and Physics* 10.8, pp. 3645–3663.
- Gomez Martin, J. C. et al. (2020). “A gas-to-particle conversion mechanism helps to explain atmospheric particle formation through clustering of iodine oxides”. In:
- Gomez Martin, J. C. et al. (2021). “Spatial and temporal variability of iodine in aerosol”. In: *Journal of Geophysical Research-Atmospheres* 126, e2020JD034410.
- Gordon, H. et al. (2017). “Causes and importance of new particle formation in the present-day and pre-industrial atmospheres”. In: *Journal of Geophysical Research: Atmospheres*.
- Goutx, M. and Saliot, A. (1980). “Relationship between dissolved and particulate fatty acids and hydrocarbons, chlorophyll a and zooplankton biomass in Villefranche Bay, Mediterranean Sea”. In: *Marine Chemistry* 8.4, pp. 299–318.
- Gras, J. L. and Keywood, M. (2017). “Cloud condensation nuclei over the Southern Ocean: wind dependence and seasonal cycles”. In: *Atmospheric Chemistry and Physics* 17.7, pp. 4419–4432.
- Gras, J. L. et al. (2009). “Postfrontal nanoparticles at Cape Grim: observations”. In: *Environmental Chemistry* 6.6, pp. 508–514.
- Grose, M. R. et al. (2007). “Coastal marine methyl iodide source and links to new particle formation at Cape Grim during February 2006”. In: *Environmental Chemistry* 4.3, pp. 172–177.
- Guenther, A. B. et al. (1993). “Isoprene and monoterpene emission rate variability: model evaluations and sensitivity analyses”. In: *Journal of Geophysical Research: Atmospheres* 98.D7, pp. 12609–12617.
- Hall, J. A. and Safi, K. (2001). “The impact of in situ Fe fertilisation on the microbial food web in the Southern Ocean”. In: *Deep Sea Research Part II: Topical Studies in Oceanography* 48.11-12, pp. 2591–2613.
- Hamed, A. et al. (2011). “The role of relative humidity in continental new particle formation”. In: *Journal of Geophysical Research: Atmospheres* 116.D3.
- Harvey, M. et al. (1993). “Dimethylsulphide measurements at Baring Head, New Zealand”. In: *Dimethylsulphide, Oceans, Atmosphere and Climate, edited by: Restelli, G., and Angeletti, G., Kluwer Academic, Dordrecht*, pp. 143–151.
- He, X.-C. et al. (2021). “Role of iodine oxoacids in atmospheric aerosol nucleation”. In: *Science* 371.6529, pp. 589–595.
- Hepach, H. et al. (2020). “Senescence as the main driver of iodide release from a diverse range of marine phytoplankton”. In: *Biogeosciences* 17.9, pp. 2453–2471.
- Hernáiz-Izquierdo, M. et al. (2019). “Direct quantification of inorganic iodine in seawater by mixed-mode liquid chromatography-electrospray ionization-mass spectrometry”. In: *Journal of Chromatography A* 1588, pp. 99–107.
- Hodshire, A. L. et al. (2019). “The potential role of methanesulfonic acid (MSA) in aerosol formation and growth and the associated radiative forcings”. In: *Atmospheric Chemistry and Physics* 19.5, pp. 3137–3160.
- Hoffmann, E. H. et al. (2016). “An advanced modeling study on the impacts and atmospheric implications of multiphase dimethyl sulfide chemistry”. In: *Proceedings of the National Academy of Sciences* 113.42, pp. 11776–11781.

- Humphries, R. S. et al. (2021). “Southern Ocean latitudinal gradients of Cloud Condensation Nuclei”. In: *Atmospheric Chemistry and Physics Discussions*, pp. 1–35.
- Hussein, T. et al. (2008). “Observation of regional new particle formation in the urban atmosphere”. In: *Tellus B* 60.4, pp. 509–521.
- Jokinen, T. et al. (2012). “Atmospheric sulphuric acid and neutral cluster measurements using CI-API-TOF”. In: *Atmospheric Chemistry and Physics* 12.9, pp. 4117–4125.
- Jokinen, T. et al. (2021). “Measurement report: Long-term measurements of aerosol precursor concentrations in the Finnish sub-Arctic boreal forest”. In: *Atmospheric Chemistry and Physics Discussions* 2021, pp. 1–22.
- Jonkers, L. et al. (2019). “Global change drives modern plankton communities away from the pre-industrial state”. In: *Nature*, p. 1.
- Junninen, H. et al. (2010). “A high-resolution mass spectrometer to measure atmospheric ion composition”. In: *Atmospheric Measurement Techniques* 3.4, pp. 1039–1053.
- Kangasluoma, J. et al. (2016). “Heterogeneous nucleation onto ions and neutralized ions: insights into sign-preference”. In: *The Journal of Physical Chemistry C* 120.13, pp. 7444–7450.
- Kattner, G. and Brockmann, U. H. (1990). “Particulate and dissolved fatty acids in an enclosure containing a unialgal *Skeletonema costatum* (Greve.) Cleve culture”. In: *Journal of experimental marine biology and ecology* 141.1, pp. 1–13.
- Kawamura, K. and Sakaguchi, F. (1999). “Molecular distributions of water soluble dicarboxylic acids in marine aerosols over the Pacific Ocean including tropics”. In: *Journal of Geophysical Research: Atmospheres* 104.D3, pp. 3501–3509.
- Kerminen, V.-M. et al. (2012). “Cloud condensation nuclei production associated with atmospheric nucleation: a synthesis based on existing literature and new results”. In: *Atmospheric Chemistry and Physics* 12.24, pp. 12037–12059.
- Kerminen, V.-M. et al. (2000). “Low-molecular-weight dicarboxylic acids in an urban and rural atmosphere”. In: *Journal of Aerosol Science* 31.3, pp. 349–362.
- Kerminen, V.-M. et al. (2018). “Atmospheric new particle formation and growth: review of field observations”. In: *Environmental Research Letters* 13.10, p. 103003.
- Korhonen, H. et al. (2008). “Influence of oceanic DMS emissions on CCN concentrations and seasonality over the remote Southern Hemisphere oceans: A global model study”. In: *J. Geophys. Res* 113, p. D15204.
- Kremser, S. et al. (2020). “Southern Ocean Cloud and Aerosol data: a compilation of measurements from the 2018 Southern Ocean Ross Sea Marine Ecosystems and Environment voyage”. In: *Earth System Science Data Discussions* 2020, pp. 1–56.
- Kulmala, M. et al. (2001). “On the formation, growth and composition of nucleation mode particles”. In: *Tellus B: Chemical and Physical Meteorology* 53.4, pp. 479–490.
- Kulmala, M. et al. (2004). “Formation and growth rates of ultrafine atmospheric particles: a review of observations”. In: *Journal of Aerosol Science* 35.2, pp. 143–176.
- Law, C. S. et al. (2017). “Overview and preliminary results of the Surface Ocean Aerosol Production (SOAP) campaign”. In: *Atmospheric Chemistry and Physics* 17.22, pp. 13645–13667.
- Law, C. S. et al. (2018). “Climate change projections for the surface ocean around New Zealand”. In: *New Zealand Journal of Marine and Freshwater Research* 52.3, pp. 309–335.
- Lawler, M. et al. (2014). “Observations of I 2 at a remote marine site”. In: *Atmospheric Chemistry and Physics* 14.5, pp. 2669–2678.
- Li, J. et al. (2021a). “Enhanced secondary organic aerosol formation from the photo-oxidation of mixed anthropogenic volatile organic compounds”. In: *Atmospheric Chemistry and Physics* 21.10, pp. 7773–7789.
- Li, J. et al. (2018). “Investigating Source Contributions of Size-Aggregated Aerosols Collected in Southern Ocean and Baring Head, New Zealand Using Sulfur Isotopes”. In: *Geophysical Research Letters* 45.8, pp. 3717–3727.

- Li, J. et al. (2021b). “Nitrogen isotopes in nitrate aerosols collected in the remote marine boundary layer: Implications for nitrogen isotopic fractionations among atmospheric reactive nitrogen species”. In: *Atmospheric Environment* 245, p. 118028.
- Lopez-Hilfiker, F. D. et al. (2016). “Constraining the sensitivity of iodide adduct chemical ionization mass spectrometry to multifunctional organic molecules using the collision limit and thermodynamic stability of iodide ion adducts”. In: *Atmospheric Measurement Techniques*.
- MacDonald, S. et al. (2014). “A laboratory characterisation of inorganic iodine emissions from the sea surface: dependence on oceanic variables and parameterisation for global modelling”. In: *Atmospheric Chemistry and Physics* 14.11, pp. 5841–5852.
- Mahajan, A. S. (2009). “Reactive halogen species in the marine boundary layer”. PhD thesis. University of Leeds.
- Mahajan, A. et al. (2010). “Measurement and modelling of tropospheric reactive halogen species over the tropical Atlantic Ocean”. In: *Atmospheric Chemistry and Physics* 10.10, pp. 4611–4624.
- Mahfouz, N. G. A. and Donahue, N. M. (2020). “Technical note: the enhancement limit of coagulation scavenging of small charged particles”. In: *Atmospheric Chemistry and Physics Discussions* 2020, pp. 1–8.
- Manninen, H. E. et al. (2016). “How to reliably detect molecular clusters and nucleation mode particles with Neutral cluster and Air Ion Spectrometer (NAIS)”. In: *Atmospheric Measurement Techniques*.
- Mardyukov, A. and Schreiner, P. R. (2018). “Atmospherically Relevant Radicals Derived from the Oxidation of Dimethyl Sulfide”. In: *Accounts of chemical research* 51.2, pp. 475–483.
- Mayer, K. J. et al. (2020). “Secondary Marine Aerosol Plays a Dominant Role over Primary Sea Spray Aerosol in Cloud Formation”. In: *ACS central science* 6.12, pp. 2259–2266.
- McCoy, I. L. et al. (2020). “The hemispheric contrast in cloud microphysical properties constrains aerosol forcing”. In: *Proceedings of the National Academy of Sciences* 117.32, pp. 18998–19006.
- McDonald, A. et al. (1999). “Monoterpene composition of radiata pine (*Pinus radiata* D. Don) sapwood from a 13 year old progeny trial”. In: *European Journal of Wood and Wood Products* 57.4, pp. 301–302.
- McFiggans, G. et al. (2004). “Direct evidence for coastal iodine particles from *Laminaria* macroalgae—linkage to emissions of molecular iodine”. In: *Atmospheric Chemistry and Physics* 4.3, pp. 701–713.
- Merikanto, J. et al. (2009). “Impact of nucleation on global CCN”. In: *Atmospheric Chemistry and Physics* 9.21, pp. 8601–8616.
- Mesarchaki, E. et al. (2015). “Measuring air–sea gas-exchange velocities in a large-scale annular wind–wave tank”. In: *Ocean Science* 11.1, pp. 121–138.
- Meskhidze, N. and Nenes, A. (2006). “Phytoplankton and cloudiness in the Southern Ocean”. In: *science* 314.5804, pp. 1419–1423.
- Meskhidze, N. et al. (2015). “Quantifying environmental stress-induced emissions of algal isoprene and monoterpenes using laboratory measurements”. In: *Biogeosciences* 12.3, pp. 637–651.
- Mirme, S. and Mirme, A. (2013). “The mathematical principles and design of the NAIS—a spectrometer for the measurement of cluster ion and nanometer aerosol size distributions”. In: *Atmospheric Measurement Techniques* 6.4, p. 1061.
- Miyazaki, Y. et al. (2020). “New index of organic mass enrichment in sea spray aerosols linked with senescent status in marine phytoplankton”. In: *Scientific reports* 10.1, pp. 1–9.
- Modini, R. L. et al. (2009). “New particle formation and growth at a remote, sub-tropical coastal location”. In: *Atmospheric Chemistry and Physics* 9.19, pp. 7607–7621.
- Molloy, S. et al. (2009). “Identification of a suitable baseline definition of tropospheric ozone at Cape Grim, Tasmania”. In: *Baseline Atmospheric Program Australia* 2010, pp. 7–16.

- Molteni, U. et al. (2018). “Formation of highly oxygenated organic molecules from aromatic compounds”. In: *Atmospheric Chemistry and Physics* 18.3, pp. 1909–1921.
- Muller, E. et al. (2019). “Hypobromous acid as an unaccounted sink for marine dimethyl sulfide?” In: *Environmental Science & Technology*.
- Mungall, E. L. et al. (2017). “Microlayer source of oxygenated volatile organic compounds in the summertime marine Arctic boundary layer”. In: *Proceedings of the National Academy of Sciences* 114.24, pp. 6203–6208.
- Nayar, K. et al. (2014). “Surface tension of seawater”. In: *Journal of Physical and Chemical Reference Data* 43.4, p. 043103.
- Nicovich, J. et al. (2006). “Kinetics, mechanism, and thermochemistry of the gas phase reaction of atomic chlorine with dimethyl sulfoxide”. In: *The Journal of Physical Chemistry A* 110.21, pp. 6874–6885.
- Nieminen, T. et al. (2018). “Global analysis of continental boundary layer new particle formation based on long-term measurements”. In: *Atmospheric Chemistry and Physics Discussions* 2018, pp. 1–34.
- Ning, A. et al. (2021). “Molecular-level evidence for marine aerosol nucleation of iodic acid and methanesulfonic acid”. In: *Atmospheric Chemistry and Physics Discussions* 2021, pp. 1–20.
- Noble, S. R. and Hudson, J. G. (2019). “Effects of continental clouds on surface Aitken and accumulation modes”. In: *Journal of Geophysical Research: Atmospheres* 124.10, pp. 5479–5502.
- O’Dowd, C. D. et al. (2002). “Marine aerosol formation from biogenic iodine emissions”. In: *Nature* 417.6889, p. 632.
- O’Dowd, C. et al. (2010). “On the occurrence of open ocean particle production and growth events”. In: *Geophysical Research Letters* 37.19.
- Paasonen, P. et al. (2018). “Comprehensive analysis of particle growth rates from nucleation mode to cloud condensation nuclei in boreal forest”. In: *Atmospheric Chemistry and Physics* 18.16, pp. 12085–12103.
- Passananti, M. et al. (2019). “How well can we predict cluster fragmentation inside a mass spectrometer?” In: *Chemical Communications* 55.42, pp. 5946–5949.
- Peltomaa, E. et al. (2019). “Comparison of Diatoms and Dinoflagellates from Different Habitats as Sources of PUFAs”. In: *Marine drugs* 17.4, p. 233.
- Quinn, P. and Bates, T. (2011). “The case against climate regulation via oceanic phytoplankton sulphur emissions”. In: *Nature* 480.7375, p. 51.
- Quinn, P. et al. (2017). “Small fraction of marine cloud condensation nuclei made up of sea spray aerosol”. In: *Nature Geoscience* 10.9, p. 674.
- Regayre, L. A. et al. (2020). “The value of remote marine aerosol measurements for constraining radiative forcing uncertainty”. In: *Atmospheric Chemistry and Physics* 20.16, pp. 10063–10072.
- Ren, L. et al. (2015). “Observation and modeling of tide-and wind-induced surface currents in Galway Bay”. In: *Water Science and Engineering* 8.4, pp. 345–352.
- Rocco, M. et al. (2021). “Oceanic phytoplankton are a potentially important source of benzenoids to the remote marine atmosphere”. In: *Communications Earth & Environment* 2.1, pp. 1–8.
- Röhl, A. and Lammel, G. (2001). “Low-molecular weight dicarboxylic acids and glyoxylic acid: seasonal and air mass characteristics”. In: *Environmental science & technology* 35.1, pp. 95–101.
- Rolph, G. et al. (2017). “Real-time environmental applications and display system: READY”. In: *Environmental Modelling & Software* 95, pp. 210–228.
- Rosati, B. et al. (2021). “New Particle Formation and Growth from Dimethyl Sulfide Oxidation by Hydroxyl Radicals”. In: *ACS Earth and Space Chemistry*.
- Rose, C. et al. (2015a). “Frequent nucleation events at the high altitude station of Chacaltaya (5240 m asl), Bolivia”. In: *Atmospheric Environment* 102, pp. 18–29.

- Rose, C. et al. (2015b). “Major contribution of neutral clusters to new particle formation at the interface between the boundary layer and the free troposphere”. In: *Atmospheric Chemistry and Physics*.
- Rose, C. et al. (2018). “Observations of biogenic ion-induced cluster formation in the atmosphere”. In: *Science advances* 4.4, eaar5218.
- Rosenfeld, D. et al. (2019). “Aerosol-driven droplet concentrations dominate coverage and water of oceanic low level clouds”. In: *Science*, eaav0566.
- Safi, K. A. et al. (2007). “Microzooplankton composition, biomass and grazing rates along the WOCE SR3 line between Tasmania and Antarctica”. In: *Deep Sea Research Part I: Oceanographic Research Papers* 54.7, pp. 1025–1041.
- Saint-Macary, A. D. et al. (2021). “The Influence of Ocean Acidification and Warming on DMSP & DMS in New Zealand Coastal Water”. In: *Atmosphere* 12.2.
- Saiz-Lopez, A. et al. (2008). “On the vertical distribution of boundary layer halogens over coastal Antarctica: implications for O₃, HO_x, NO_x and the Hg lifetime”. In: *Atmospheric Chemistry and Physics* 8.4, pp. 887–900.
- Salter, M. et al. (2011). “Impact of an artificial surfactant release on air-sea gas fluxes during Deep Ocean Gas Exchange Experiment II”. In: *Journal of Geophysical Research: Oceans* 116.C11.
- Sanchez, K. J. et al. (2018). “Substantial Seasonal Contribution of Observed Biogenic Sulfate Particles to Cloud Condensation Nuclei”. In: *Scientific reports* 8.1, p. 3235.
- Schmale, J. et al. (2019). “Overview of the Antarctic circumnavigation expedition: Study of preindustrial-like aerosols and their climate effects (ACE-SPACE)”. In: *Bulletin of the American Meteorological Society* 100.11, pp. 2260–2283.
- Schneider, S. R. et al. (2019). “Formation of Secondary Organic Aerosol from the Heterogeneous Oxidation by Ozone of a Phytoplankton Culture”. In: *ACS Earth and Space Chemistry* 3.10, pp. 2298–2306.
- Schwier, A. N. et al. (2015). “Primary marine aerosol emissions from the Mediterranean Sea during pre-bloom and oligotrophic conditions: correlations to seawater chlorophyll a from a mesocosm study”. In: *Atmospheric Chemistry and Physics* 15.14, pp. 7961–7976.
- Schwinger, J. et al. (2017). “Amplification of global warming through pH dependence of DMS production simulated with a fully coupled Earth system model”. In: *Biogeosciences* 14.15, p. 3633.
- Sellegri, K. et al. (2016). “Evidence of atmospheric nanoparticle formation from emissions of marine microorganisms”. In: *Geophysical Research Letters* 43.12, pp. 6596–6603.
- Sellegri, K. et al. (2021). “Surface ocean microbiota determine cloud precursors”. In: *Scientific reports* 11.1, pp. 1–11.
- Sellegri, K. et al. (2005). “Quantification of coastal new ultra-fine particles formation from in situ and chamber measurements during the BIOFLUX campaign”. In: *Environmental Chemistry* 2.4, pp. 260–270.
- Shaw, S. L. et al. (2010). “Production and emissions of marine isoprene and monoterpenes: a review”. In: *Advances in Meteorology* 2010.
- Sievering, H. et al. (2004). “Aerosol non-sea-salt sulfate in the remote marine boundary layer under clear-sky and normal cloudiness conditions: Ocean-derived biogenic alkalinity enhances sea-salt sulfate production by ozone oxidation”. In: *Journal of Geophysical Research: Atmospheres* 109.D19.
- Simon, M. et al. (2020). “Molecular understanding of new-particle formation from α -pinene between -50 and +25 C”. In: *Atmospheric Chemistry and Physics* 20.15, pp. 9183–9207.
- Sipilä, M. et al. (2016). “Molecular-scale evidence of aerosol particle formation via sequential addition of HIO₃”. In: *Nature* 537.7621, p. 532.
- Six, K. D. et al. (2013). “Global warming amplified by reduced sulphur fluxes as a result of ocean acidification”. In: *Nature Climate Change* 3.11, p. 975.

- Stark, H. et al. (2007). “Influence of nitrate radical on the oxidation of dimethyl sulfide in a polluted marine environment”. In: *Journal of Geophysical Research: Atmospheres* 112.D10.
- Stein, A. et al. (2015). “NOAA’s HYSPLIT atmospheric transport and dispersion modeling system”. In: *Bulletin of the American Meteorological Society* 96.12, pp. 2059–2077.
- Stephens, B. et al. (2013). “Analysis of a 39-year continuous atmospheric CO₂ record from Baring Head, New Zealand”. In: *Biogeosciences* 10.4, p. 2683.
- Stocker, T. F. et al. (2013). “Climate change 2013: the physical science basis. Intergovernmental panel on climate change, working group I contribution to the IPCC fifth assessment report (AR5)”. In: *New York*.
- Sulo, J. et al. (2021). “Long-term measurement of sub-3 nm particles and their precursor gases in the boreal forest”. In: *Atmospheric Chemistry and Physics* 21.2, pp. 695–715.
- Takashima, H. et al. (2021). “Full latitudinal marine atmospheric measurements of iodine monoxide”. In: *Atmospheric Chemistry and Physics Discussions* 2021, pp. 1–24.
- Tanner, D. and Eisele, F. (1991). “Ions in oceanic and continental air masses”. In: *Journal of Geophysical Research: Atmospheres* 96.D1, pp. 1023–1031.
- Tinel, L. et al. (0). “The influence of the sea surface microlayer on oceanic iodine emissions”. In: *Environmental Science & Technology* 0.ja. PMID: 32975119, null.
- Tremblay, S. et al. (2019). “Characterization of aerosol growth events over Ellesmere Island during the summers of 2015 and 2016”. In: *Atmospheric Chemistry and Physics* 19.8, pp. 5589–5604.
- Vanhanen, J. et al. (2011). “Particle size magnifier for nano-CN detection”. In: *Aerosol Science and Technology* 45.4, pp. 533–542.
- Veres, P. R. et al. (2020). “Global airborne sampling reveals a previously unobserved dimethyl sulfide oxidation mechanism in the marine atmosphere”. In: *Proceedings of the National Academy of Sciences*.
- Wang, M. et al. (2020). “Photo-oxidation of aromatic hydrocarbons produces low-volatility organic compounds”. In: *Environmental science & technology* 54.13, pp. 7911–7921.
- Wang, M. et al. (2021). “Measurement of iodine species and sulfuric acid using bromide chemical ionization mass spectrometers”. In: *Atmospheric Measurement Techniques* 14.6, pp. 4187–4202.
- Wan, Y. et al. (2020). “Probing key organic substances driving new particle growth initiated by iodine nucleation in coastal atmosphere”. In: *Atmospheric Chemistry and Physics* 20.16, pp. 9821–9835.
- Wang, S. C. and Flagan, R. C. (1990). “Scanning electrical mobility spectrometer”. In: *Aerosol Science and Technology* 13.2, pp. 230–240.
- Wang, H. et al. (2006). “Water-soluble dicarboxylic acids, ketoacids and dicarbonyls in the atmospheric aerosols over the Southern Ocean and western Pacific Ocean”. In: *Journal of Atmospheric Chemistry* 53.1, pp. 43–61.
- Wang, S. et al. (2018). “Impacts of shifts in phytoplankton community on clouds and climate via the sulfur cycle”. In: *Global Biogeochemical Cycles* 32.6, pp. 1005–1026.
- Willis, M. D. et al. (2017). “Evidence for marine biogenic influence on summertime Arctic aerosol”. In: *Geophysical Research Letters* 44.12, pp. 6460–6470.
- Wollesen de Jonge, R. et al. (2021). “Secondary aerosol formation from dimethyl sulfide – improved mechanistic understanding based on smog chamber experiments and modelling”. In: *Atmospheric Chemistry and Physics* 21.13, pp. 9955–9976.
- Woodhouse, M. et al. (2013). “Sensitivity of cloud condensation nuclei to regional changes in dimethyl-sulphide emissions”. In: *Atmospheric Chemistry and Physics* 13.5, pp. 2723–2733.
- Wayne, R. P. et al. (1991). “The nitrate radical: Physics, chemistry, and the atmosphere”. In: *Atmospheric Environment. Part A. General Topics* 25.1, pp. 1–203.

- Yan, C. et al. (2018). “The role of H₂SO₄-NH₃ anion clusters in ion-induced aerosol nucleation mechanisms in the boreal forest”. In: *Atmospheric Chemistry and Physics* 18.17, pp. 13231–13243.
- Yan, C. et al. (2016). “Source characterization of highly oxidized multifunctional compounds in a boreal forest environment using positive matrix factorization”. In: *Atmospheric Chemistry and Physics* 16.19, pp. 12715–12731.
- Yan, J. et al. (2020a). “Uptake selectivity of methanesulfonic acid (MSA) on fine particles over polynya regions of the Ross Sea, Antarctica”. In: *Atmospheric Chemistry and Physics* 20.5, pp. 3259–3271.
- Yan, J. et al. (2020b). “Influence on the conversion of DMS to MSA and SO₄²⁻ in the Southern Ocean, Antarctica”. In: *Atmospheric Environment* 233, p. 117611.
- Zheng, G. et al. (2021). “New particle formation in the remote marine boundary layer”. In: *Nature communications* 12.1, pp. 1–10.